The Catalytic Mechanics of Dynamic Surfaces: Stimulating Methods for Promoting Catalytic Resonance

Manish Shetty[1,2†], Amber Walton[1†], Sallye R. Gathmann[1†], M. Alexander Ardagh[1,2], Joshua Gopeesingh[4], Joaquin Resasco[3], Turan Birol[1], Qi Zhang[1], Michael Tsapatsis[2,6,7], Dionisios G. Vlachos[2,5], Phillip Christopher[2,3], C. Daniel Frisbie[1], Omar A. Abdelrahman[2,4], Paul J. Dauenhauer[1,2*]

[1] University of Minnesota, Department of Chemical Engineering and Materials Science, 421 Washington Ave. SE, Minneapolis, MN 55455, USA
[2] Catalysis Center for Energy Innovation, 150 Academy Street, Newark, DE 19716, USA
[3] University of California Santa Barbara, Engineering II Building, University of California, Santa Barbara, CA 93106, USA
[4] University of Massachusetts Amherst, 686 N. Pleasant Street, Amherst, MA 01003, USA
[5] University of Delaware, Department of Chemical and Biomolecular Engineering, 150 Academy Street, Newark, DE 19716, USA
[6] Applied Physics Laboratory, Johns Hopkins University, Laurel, MD 20723, USA
[7] Department of Chemical and Biomolecular Engineering & Institute for NanoBioTechnology, Johns Hopkins University, Baltimore, MD, 21218, USA
* Corresponding author: hauer@umn.edu
† Authors contributed equally

Abstract. Transformational catalytic performance in rate and selectivity is obtainable through catalysts that change on the time scale of catalytic turnover frequency. In this work, dynamic catalysts are defined in the context and history of forced and passive dynamic chemical systems, with classification of unique catalyst behaviors based on temporally-relevant linear scaling parameters. The conditions leading to catalytic rate and selectivity enhancement are described as modifying the local electronic or steric environment of the active site to independently accelerate sequential elementary steps of an overall catalytic cycle. These concepts are related to physical systems and devices that stimulate a catalyst using light, vibrations, strain, and electronic manipulations including electrocatalysis, back-gating of catalyst surfaces, and introduction of surface electric fields via solid electrolytes and ferroelectrics. These catalytic stimuli are then compared for capability to improve catalysis across some of the most important chemical challenges for energy, materials, and sustainability.

1.0 Introduction. The history of synthetic heterogeneous catalysts has been a quest to find the optimal material to accelerate and control surface reactions. The best catalytic site for any chemistry has specific physical and electronic structure, which has frequently been found through exploratory research, high throughput screening, directed evolution, and experimental serendipity[1,2,3,4,5]. This search has led to entirely new classes of inorganic materials for catalytic applications including single metal atoms and alloys[6,7,8,9], metal-organic frameworks[10,11], hierarchical zeolites[12,13], multi-metallic[14,15] and intermetallic surfaces[16,17], all of which provide structural and electronic control in the design of catalytic active sites. However, the challenge of improving catalytic performance for some more mature applications by continued optimization of catalyst structure has led to an open question in catalysis; do undiscovered catalysts still exist that can provide *transformational* control of surface chemistry? More importantly, is the pursuit solely of optimal catalytic *structure* via materials discovery or optimization even the right approach to further improve catalyst design?

The pursuit of 'better' catalysts relies on the design philosophy that refined structures will always provide faster and more selective catalysts[18,19,20,21]; however, this strategy eventually approaches the fundamental limitations on *static* catalytic sites. The most restrictive catalytic limitation is the Sabatier principle, which posits that optimal catalysts exhibit intermediate surface binding energies to balance the kinetic rates of two or more reaction phenomena including surface reactions, desorption, or adsorption[22]. Since first

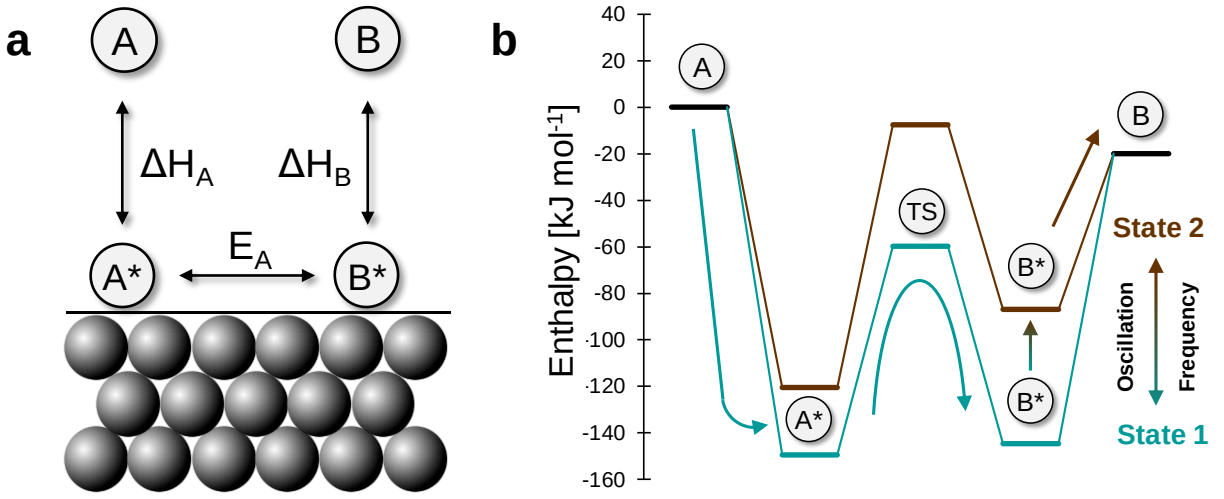

Figure 1. Dynamic heterogeneous catalysis. (a) A catalytic surface reaction is comprised of independent steps of adsorption, surface reaction(s), and desorption. **(b)** Forced variation of the energetic surface states including intermediates (e.g., A*, B*) and the transition state (TS) yields conditions favorable to adsorption and surface reaction (state 1) and desorption (state 2).

proposed by Sabatier that the optimal catalyst forms a 'surface complex' that readily forms and desorbs[23], the principle was demonstrated decades later as kinetic plots referred to as 'Sabatier volcanoes' with the optimal catalyst existing at the conditions of peak turnover frequency[24,25,26]. Lower catalytic rate on either side of the volcano derives from the catalyst favoring one elementary step over the others, resulting in lower overall turnover frequency through the whole sequence of steps. This concept has since been demonstrated across a broad range of chemistries and even extended into 'volcano surfaces' or 'maps' for multicomponent reactions[27,28,29,30,31,32,33,34,35] and dual site catalysts[36,37].

The selective capability of *static* catalysts for many important chemistries has also achieved a performance status quo. Though a theoretical limitation does not exist for catalytic selectivity in parallel, series, or more complicated network reaction mechanisms, many commercial chemical processes with the best available static catalysts only achieve ~80-90% selectivity to desired products, including large-scale reactions such as ethylene epoxidation[38] and propane dehydrogenation,[39] in addition to technologies such as methanol-to-olefins that produce a distribution of products[40,41]. For catalysts under kinetic control, 80% selectivity indicates that the desired reaction is only four times faster than undesired pathways. Moreover, there exist hundreds of potential catalytic technologies such as direct methane oxidation to methanol[42], CO_2 conversion to methanol or ethylene[43,44], and hydrogen peroxide formation from oxygen and hydrogen[45,46,47] that are not yet sufficiently selective for economic feasibility. Increasing the kinetic ratio of desirable-to-side-reaction rates by orders of magnitude to achieve nearly perfect product selectivity (>99%) for most chemicals will require a completely different approach to catalyst design.

A complementary catalysis strategy to active site design derives from the nature of catalytic mechanisms. Surface reactions are multiple sequential steps each with unique energetic and temporal characteristics.[48] From this perspective, an effective *static* catalytic active site is designed to balance the needs of two-or-more elementary phenomena. The ideal active site for product desorption is unlikely to also be ideal for surface reaction and reactant adsorption. However, a *dynamic* catalytic active site that changes on the time scale of the turnover frequency of the reaction could evolve over the catalytic cycle, providing an optimal energetic environment for each step and the overall progression of the reaction sequence[49]. A single active site can be modulated to alternate between ideal characteristics for product desorption, reactant adsorption, and surface reaction. A *dynamic* catalyst could manipulate surface coverages and dictate the dominant

pathways of complex surface mechanisms. Moreover, a catalyst that changes surface enthalpy and entropy of adsorbates can impart work (i.e., input energy) to a catalytic reaction, manipulating the extent of overall conversion.

The operation of a dynamic catalyst reflects the natural frequencies of surface chemistry. As depicted in **Figure 1a**, the sequence of surface chemistry is comprised of steps of adsorption, surface reaction, and desorption, each with their own kinetics, described by elementary kinetic rate expressions and associated constants, k_i. As the catalyst changes, the energies of the surface-bound intermediates also vary and shift the energetic favorability between each elementary step in the sequence. As depicted with a conceptual catalyst in **Figure 1b**, a catalyst oscillating between two states switches between favorability to adsorption and surface reaction (state 1) and a second condition favorable to desorption of B* (state 2). This simple two-stage catalyst has overall kinetics of combined yet temporally-independent steps that are faster than the static catalyst, provided that the frequency of switching between catalyst conditions is comparable to the natural frequencies of the independent surface reaction phenomena.

The paradigm of a dynamic catalysis changes the philosophy for catalyst synthesis and discovery and the strategy for utilizing a new temporal dimension for catalyst design. It has already been experimentally demonstrated that oscillating catalysts break the limits of static catalysts in the rate acceleration of electro-oxidation of formic acid[50]. But it is also possible that dynamic catalysts can change the mechanism for selecting individual reactions in a network[51], while also altering catalyst operation in equilibrium-controlled reactions[52]. Dynamic catalysts are common materials with *physical* design parameters including composition (e.g., metals, metal oxides), size, and structure, but they also have new *dynamic* parameters including surface oscillation frequency, amplitude, and applied waveform shape (e.g. square or sinusoidal). These parameters provide new opportunity for tuning catalyst performance but also double the complexity of system design. Physical catalyst design will likely require simultaneous knowledge of the impact of different parameters, as materials and oscillatory behavior are not independent.

In this perspective, we outline the emerging field of dynamic catalysis and establish the principles, opportunities, and general strategy for designing catalytic surfaces that change with time to achieve new performance in rate and selectivity. This includes the taxonomy of systems describing dynamic catalysts, reactors, and process systems, both forced and passive. It also requires definition of the new parameters that define changing surfaces and can be quantified across different methods of surface control and variation (e.g., electronic, mechanic). The following methods of implementing surface dynamics are amenable to different materials and chemistries, and a comparison of the ability to modulate surfaces at frequencies relevant to catalysis (i.e., near and above Sabatier volcano peaks) to selective surface intermediates provides a foundation for pursuing catalyst dynamics for any surface chemistry.

2.0 Overview of chemical dynamics. Although chemical oscillators pervade our natural world, the systematic study of chemical oscillators and the broader field of nonlinear chemical dynamics is more recent in the last century.[53,54] Non-linear chemical transient systems pertain to nonlinear spatiotemporal changes in chemical variables, such as bulk or surface concentration and temperature.[55] The breadth of systems and behaviors requires classification based on both the origin of transient behavior as well as the scale and mechanism of the transient component(s). In **Figure 2**, chemical dynamics divide between passively changing systems (spontaneously occurring) and chemically reacting systems under forced variation/oscillation (external stimulus). This division is further defined as occurring at the catalyst active site, throughout the reactor, or within a chemical reaction process. The focus of this perspective is the forced dynamics of catalysts (blue box in top left of **Figure 2**), which is discussed in detail following this section. However, the opportunity for the forced oscillatory catalytic mechanism is apparent in the context of other chemical systems (remaining boxes of **Figure 2**), which have been extensively pursued and evaluated as follows.

Process system dynamics affecting chemical reactor behavior are readily identifiable as the varying or oscillating interaction between the reactor(s) and other unit operations. In chemical processes, oscillations can emerge from the

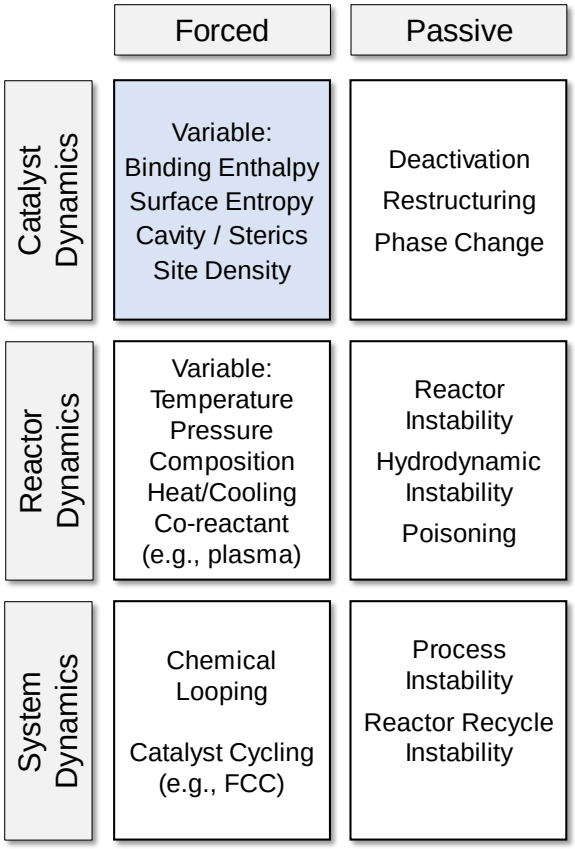

Figure 2. Taxonomy of chemical dynamics includes passive and forced oscillations at catalyst, reactor, and process system scales.

inherent characteristics of the system design at multiple frequencies and are identified when measured across multiple unit operations[56,57]; dampening and eliminating these oscillations to maintain steady, efficient operation is the goal of both system design and an effective process control algorithm[58,59,60]. In contrast, processes are also designed to force variation of a unit operation or component such as a catalyst between unit operations, including internal zeolite catalyst regeneration in fluid catalytic cracking[61] or catalyst recovery in propane dehydrogenation[62]. Another variation is the process technology of chemical looping[63,64], where materials are moved between unit operations of varying conditions (e.g., reduction/oxidation).

Within a single unit operation, the sub-field of *chemical reactor dynamics* has extensive history for implementation across variables including pressure, temperature, catalyst loading, and concentration of reactants, solvents, and diluents[65,66,67]. While one of the best known models for dynamic oscillating systems called the Lotka-Volterra model is used to describe predator-prey systems,[68,69] many chemical reaction systems exist with similar oscillatory behavior including the Belousov-Zhabotinsky (BZ) reaction[70], the Bray reaction[71,72], and the Briggs-Rauscher reaction[73], among many others. A key factor in these oscillating systems is *autocatalysis*, where the rate of growth of a species increases with its population.[53] The spatio-temporal variations on many such homogeneous catalytic systems have been described by Epstein and coworkers.[55,74]

In the context of reactor dynamics, *passive* chemical oscillations also exist on the surfaces of heterogeneous catalysts. Under isothermal and isobaric conditions, especially at low concentrations of reactants, such chemical oscillations occur for reactions where the dynamic change in surface composition of the reaction intermediates, frequently blocking and unblocking active sites, match the turn-over frequency (TOF) of the reaction.[75,76] For example, chemical oscillations for CO oxidation on Pd, Ir, Rh, CuO, and Pt surfaces are well documented. Due to the competitive adsorption of CO and oxygen, the metal catalysts transition sharply between two reactive states, a highly-active saturated oxygen phase followed by a relatively inactive saturated CO phase.[76,77,78] Other examples include hydrogen oxidation on Ni, Pd, Pt, and Rh, nitrogen oxide reduction on Pd, Pt, and Rh, and CO hydrogenation on Fe and Pd, among many other passively oscillatory catalytic systems summarized by Schmidt, Schüth, and Henry[79] and Ertl and Imbihl[80]. These dynamic systems exhibit significant complexity such as the emergence of Hopf bifurcations[81,82], the coexistence of limit cycles and multiple steady states[81,83], and the possibility for chaotic chemical behavior[84].

The complexity of chemical reactor dynamics further increases in response to *forced oscillations* in pressure, temperature, flow, or composition yielding periodic, quasi-periodic, or chaotic chemical reactor response. As described by Rutherford Aris[85], the behaviors of reacting forced oscillators have common features that derive from the shape, frequency, and forcing amplitude of the oscillation(s) and are further determined by the characteristics and parameters of the responsive chemical system. These include phase locking between the applied and response frequency, as

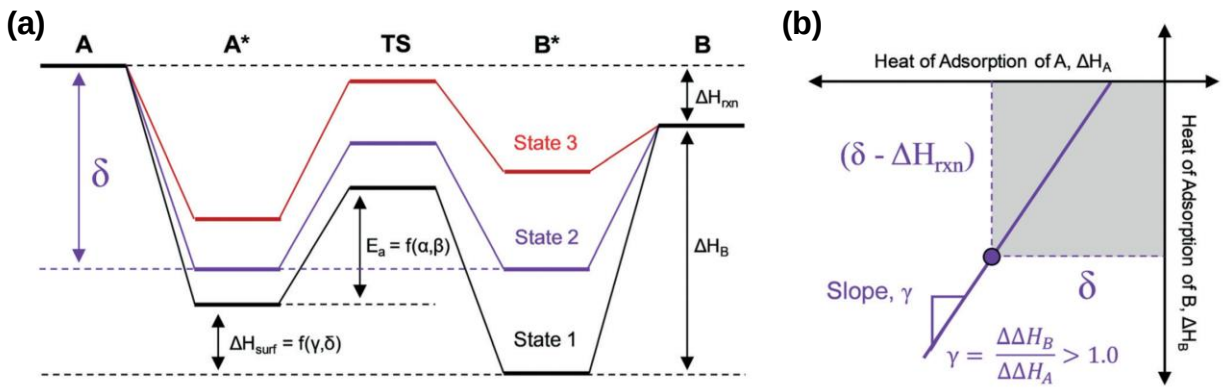

Figure 3. Parameters of dynamic heterogeneous catalysis. **(a)** State-energy diagram of oscillating heterogeneous catalyst. **(b)** Variation of the binding energy of B* linearly scales with the binding energy of A* with slope, $\gamma_{B/A}$, and common point, δ.

well as the emergence of multi-peaked oscillations[86] and unstable cycles in the system response. The prevalence of these behaviors has been experimentally observed by many forced oscillations as summarized by Silverton[87]. While oscillatory reactor behavior is generally undesired due to the challenges of safe control and steady operation, forced reactor oscillations can have significant performance benefit. For example, Veser and co-workers demonstrated significant enhancement in both conversion and selectivity to synthesis gas from methane by oscillating the direction of flow of feed gas under authothermal reactor conditions[88,89,90]. Reactor temperature oscillations were also shown to enhance catalytic rate[65,91] and improve control of selectivity to products in both parallel[60] and series reactions[92].

At the molecular level, catalysts exhibit *passive* dynamics that include common behaviors such as deactivation as well as more complex restructuring, phase change, or change in oxidation state. While not always oscillatory, catalyst restructuring can include the spontaneous redistribution of atoms either in clusters[93], single atoms[94], or layers at the exposed surface[95]. Changes in oxidation state can occur as entire materials, layers, or even single atoms such as the case in many homogeneous catalyst redox cycles[96] or in the example of N_2O decomposition on Cu-ZSM-5[75], where copper oscillates between Cu^+ and Cu^{2+}. These changes occur passively as a result of the reaction; they do not drive the reaction and are often problematic for long-term operation.

2.1 Forced Catalytic Dynamics – Tunable Surface Species. Forced catalytic dynamics by deliberate manipulation of the energy of surface species on a catalyst introduces new opportunities and behaviors not previously accessible by process or reactor dynamics. Under forced variation, catalysts stimulated by light, electricity, or mechanical energy will modify the enthalpy of adsorption (ΔH_{ads} = -ΔBE, binding energy) and/or the entropy of adsorption (ΔS_{ads}) for each surface species. For flat surfaces such as metal facets, variation of the binding energy across different materials has been shown to exhibit linear relationships with the *d*-band center with scaling parameters of slope, γ, and intercept, δ[97,98]. However, for dynamic catalysts exposed to different stimuli, the key metric is the *relative* change in binding energy between any two species connected via a transition state; the ratio of these two binding energies can then be defined as a linear relationship between two generic surface species A* and B* with parameter[52],

$$\gamma_{B/A} = \frac{\Delta\Delta H_{ads,B}}{\Delta\Delta H_{ads,A}} \qquad (1)$$

A second parameter, $\delta_{A\text{-}B}$, defines the condition of external catalytic stimulus resulting in equal surface enthalpy for the two components A* and B*; as depicted in **Figure 3a**, this energy delta is visually identified as equal energy in the gamma-delta plot **Figure 3b**. The importance of the scaling parameter, $\gamma_{B/A}$, is also apparent in the extent of relative change in A* and B*; in the depicted enthalpy diagram with $\gamma_{B/A} > 1$, B* changes in enthalpy of adsorption more than A* for identical stimulating conditions.

The implication for changing surface adsorption enthalpies is the ability to also control rate-limiting elementary steps in the reaction sequence. For surface species capable of desorption, weakening the binding energy via external stimuli enables faster desorption. Variation of the surface enthalpy between any two surface species with interconnecting transition states also permits tuning of the activation energy, and thereby the rate of the surface reaction. For surface reactions obeying linear Brønsted–Evans–Polanyi (BEP) relationships[99], the transition state is manipulated since the applied stimuli also vary the relative enthalpy of the surface reaction species (ΔH_{rxn}). Forward surface reactions can be accelerated with lower transition state energies by stronger overall binding for systems with $\gamma_{B/A} > 1$, while a surface reaction with $\gamma_{B/A} < 1$ will accelerate for weaker overall binding.

Dynamic catalysts will also manipulate the entropy of chemical species at the active site. For example, chemical species adsorbed on a flat metal facet will retain up to two degrees of translational motion and some of degrees of rotation[100], but stronger enthalpies of adsorption will further restrict the surface motion and entropy of adsorbed molecules. Despite independent contribution to the overall free energy of adsorption, entropy and enthalpy are known to correlate by the 'compensation effect'[101,102]. As such, tunable enthalpy of adsorption of surface chemical species by external stimuli can potentially also tune the entropy of bound species and change the pre-exponential factor of surface reactions. This can be further controlled by the design of tunable binding cavities, where spatial characteristics (e.g., pore size, cavity diameter) are adjusted with time via external stimuli; as relevant to these systems, tunable spatial parameters have also been shown to reduce the entropy of adsorbed surface species by reducing the extent of rotation on the surface[103]. Manipulating these surface interactions in controlled oscillatory fashion with the optimal parameters guides adsorbates along the preferred reaction pathway leading to catalytic enhancement.

2.2 Forced Catalytic Dynamics – Rate Enhancement. Forced oscillation of catalyst characteristics and associated surface intermediates provides profound new capability for controlling catalytic rate, selectivity to products, and extent of conversion as recently shown via microkinetic modeling. Dauenhauer and coworkers demonstrated that a dynamic heterogeneous catalyst oscillating between two electronic states has the potential to exhibit three to four orders of magnitude (1,000x-10,000x) increase in turnover frequency above the Sabatier maximum for the conversion of a generic reactant A(g), to product B(g) in the gas phase (**Figure 1a**).[15-17] First A(g) associatively adsorbs to the catalyst surface (A*), followed by a surface unimolecular reaction to form B*, and finally desorption to form B(g). The surface thermochemistry of A* and B* and the activation energies for the surface reaction for A* to form B* are inherently linked through the Brønsted-Evans-Polanyi (BEP) relationship with linear parameters α and β.[15]

In dynamic catalysis, surface reaction(s) and/or desorption are kinetically decoupled. The catalyst switches between surface states of high and low binding energy of B*. In the initial state 1, adsorbed A* converts to B* and forms a thermodynamic distribution on the surface. When the surface flips to a weaker binding state 2, B* readily desorbs with lower activation energy to B(g) (**Figure 1b**). Catalytic performance then depends on the selection of dynamic parameters of frequency, *f*, amplitude, ΔU, amplitude endpoint, *U*, and waveform shape (e.g., sinusoidal, square).

Interpretation of dynamic catalysis follows from the Sabatier volcano diagram (**Figure 4a**). As either side of the volcano of the generic A-to-B surface reaction is described by an elementary rate limitation, these independent rates can be extended above the Sabatier peak (dashed lines). For the selected amplitude, in this case ΔU_B of 0.6 eV, the minimum (green) and maximum (purple) achievable rates for independent elementary steps are then identified at the amplitude endpoints (U_B of -0.1 eV and 0.5 eV). The time-averaged turnover frequency response of the dynamic system is then determined by the shape and frequency of the applied surface energy waveform.

Oscillating dynamic catalysts exhibit activity response with resonance behavior similar to other complex forced oscillator systems. As the energy of the catalytic surface changes, the surface coverages and instantaneous turnover frequency also exhibit oscillatory response. By time averaging the turnover frequency for a range of applied square waveforms ($10^{-4} < f < 10^{12}$ Hz, **Figure 4b**), the

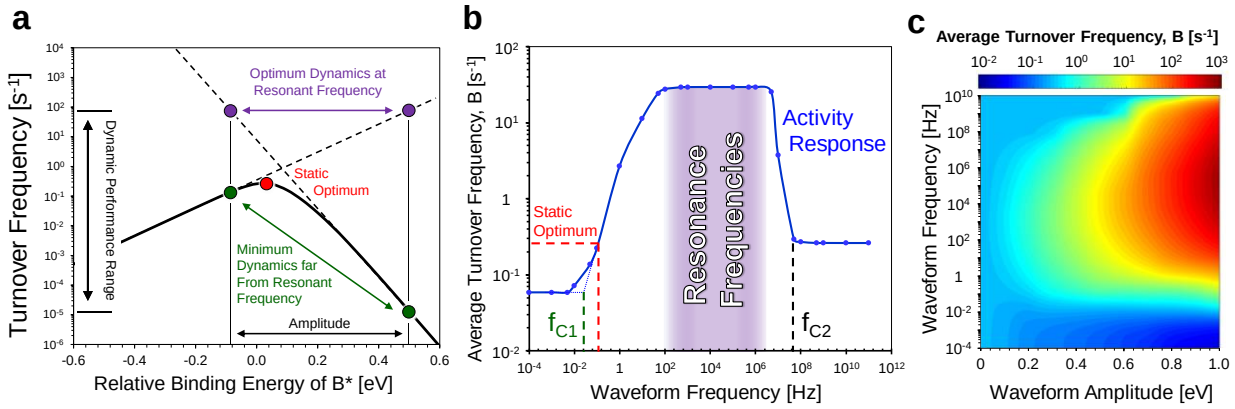

Figure 4. Dynamic catalysis for rate enhancement. **(a)** Oscillating state energy diagram for A reacting on a catalytic surface to B product (−0.1 to 0.5 eV of B*). **(b)** Average catalytic turnover frequency to product B at waveform amplitude of 0.6 eV at 150 °C and 100 bar; resonance frequencies identified in purple. **(c)** Average turnover frequency to B at 150 °C and 100 bar for variable square waveform amplitude and frequency. (reprinted with permission from reference 49). System parameters: $\gamma_{B/A}$ = 2.0, δ = 1.4 eV.

oscillating dynamic catalyst exhibits dynamic rate enhancement at a band of frequencies that lead to 'surface resonance' conditions (e.g., 10^3-10^7 s^{-1}). At these frequencies, the kinetics of the applied electronic stimulus were comparable to kinetics of the individual elementary steps identified in the Sabatier plot (**Figure 4a**, purple), and the resulting overall catalytic rate exists up to several orders of magnitude above the Sabatier maximum. Surface resonance can therefore be defined as the condition where forced oscillations lead to overall catalytic turnover frequencies comparable to natural frequencies of the surface chemistry. These natural frequencies change for each value of the binding energy descriptor in the independent axis of a Sabatier volcano plot (e.g., **Figure 4a**). For a square wave oscillation, the catalytic system switches between two natural frequencies of the elementary steps, one of which is favorable for surface reaction and the other which is favorable for desorption. Thus, larger waveform amplitudes (**Figure 4c**) produce faster resonance conditions.

2.3 Forced Catalytic Dynamics – Surface Work. Another implication of tunable and/or oscillating catalysts is the energetic contribution arising from forcibly reducing the binding energy of surface adsorbates. This directly addresses a grand challenge in catalytic reaction engineering to overcome chemical equilibrium that limits many chemical conversion strategies/technologies.[52] Important chemical conversions including ammonia synthesis, water-gas shift, dry reforming of methane, and alkane dehydrogenation suffer from mildly exergonic Gibbs free energy of reaction at industrially relevant conditions that limit overall conversion for reactions.[104,105,106,107,108] Strategies to address equilibrium limitations include operation at high pressure for ammonia or in staged reactors with varying temperature for water-gas shift reaction[109,110], tandem reactions, or separation to deprive the system of either reactants or products (i.e., Le Chatelier's principle).[111,112] A third strategy is the application of work; added work to a system can perturb to a steady state away from equilibrium.[113,114,115,116]

A dynamic catalyst surface with oscillating binding energies provides work to adsorbates to move the steady-state reaction away from equilibrium.[52] As depicted in **Figure 5a**, the simulated A-to-B surface-catalyzed reaction in a batch reactor operating under dynamic conditions approaches a steady state different from equilibrium, independent of the starting composition of the batch reactor. This offset from equilibrium disappears when the catalyst switches from dynamic to static conditions, and the reactor rapidly converts to equilibrium as required by thermodynamics. A broader evaluation of contributed work via dynamic catalysis is depicted in **Figure 5b**, where a range of frequencies with amplitude of 1.0 eV in BE_{B*} produces three distinct regions as the waveform oscillation moves from higher to lower binding energies in a batch reactor. For this reaction, green depicts a 50/50% A/B mixture at equilibrium, and two red and blue lobes identify regions of high and low conversion to B,

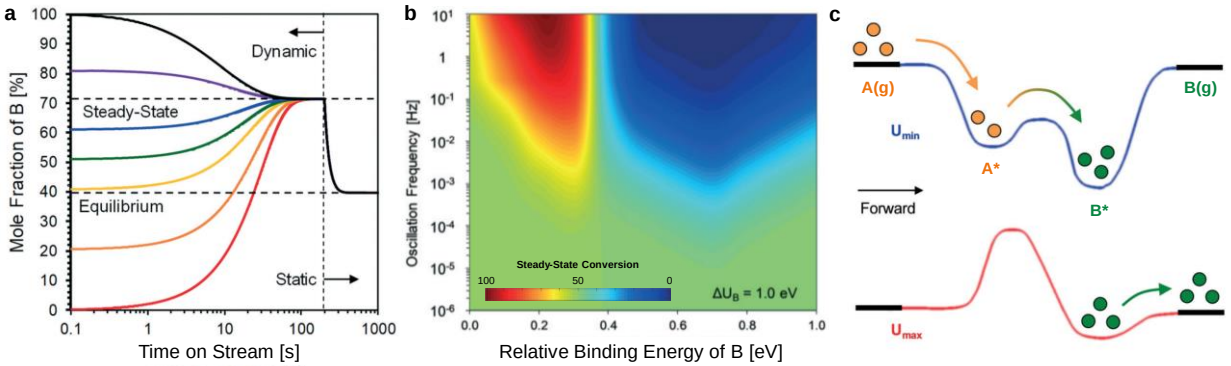

Figure 5. Dynamic catalysis of A-to-B reaction at high conversion (X > 10%) in a batch reactor. **(a)** Seven initial concentrations of B converge on steady state product composition of 70% B but return to equilibrium of 40% B under static catalyst conditions. **(b)** Dynamic catalytic conversion of A to B for low gamma ($\gamma_{B/A} \sim 0.5$, $\delta \sim 1.4$ eV). Steady-state average conversion of A-to-B in a batch reactor (equilibrium at 50% – green) for varying square wave amplitude high binding energy state [eV] and oscillation frequency [Hz] for fixed amplitudes ΔU_B of 1.0 eV. **(c)** Free energy diagram of a dynamic catalyst switching between two states, U_{min} and U_{max}. The catalytic molecular pump moves molecules of A in orange through adsorption to A* and then reaction to B* at U_{min}; subsequent oscillation moves molecules of B* to product B in the gas phase at U_{max}. (reprinted with permission from reference 52).

respectively, at oscillatory steady state (i.e., a dynamic catalytic system that achieves a stable limit cycle). In this specific example, dynamic catalysts can push a reaction to any steady state conversion, depending on the selected oscillation parameters.

Catalytic reactions progressing away from equilibrium emerge in dynamic catalysis from the asymmetry of the reaction energy profile. As depicted in **Figure 5c**, a catalyst oscillating between two binding conditions fills the surface with B* at U_{min}, since B* is lower in energy than A*; subsequent flipping of the catalyst to U_{max} then desorbs B* to B(g) in the forward direction. At U_{max}, B* prefers desorption as opposed to converting back to A* given the relative activation energies ($E_{a,des} << E_{a,rxn}$). To promote the reverse reaction, A* must be lower in energy (i.e., stronger binding) than B* at U_{min}; this transition in directionality occurs at delta energy, $\delta_{A\text{-}B}$, where both A* and B* have identical adsorption enthalpy. This transition at $\delta_{A\text{-}B}$ is visible in **Figure 5b** as the distinct transition between the red/blue directional lobes of steady state conversion at relative binding energy of B* of 0.4 eV.

Returning to the concept of surface work, the effects of dynamic catalysis on conversion was measured by calculating the apparent change in the Gibbs free energy for the overall reaction A-to-B ($\Delta\Delta G_{rxn}$). Thermodynamic efficiency can be defined by comparing this value with the oscillation amplitude, ΔU. Note that $\Delta\Delta G_{rxn}$ can be positive or negative depending on the direction that conversion changes under dynamic conditions, so the thermodynamic efficiency can also be positive or negative.

$$Thermodynamic\ efficiency\ (\%) = \frac{\Delta\Delta G_{rxn}}{\Delta U} \quad (2)$$

Efficiency was calculated for varying oscillation amplitudes of 0.0-1.0 eV at 10 Hz frequency using square, sine, and triangle waveforms [44]. Square waveform dynamics were again most efficient, and efficiencies of 30-40% were achieved once amplitudes of >0.2 eV were applied. In addition, the effects of varying waveform position (i.e., oscillation endpoints) and amplitude on efficiency were studied over a range of 0-1.5 eV. Waveform position has significant effects on both the magnitude and sign of the efficiency parameter, due to changing the directionality of the reaction, and efficiencies from -15% to 15% were measured.

While the behavior of dynamic catalysts disagree with the maxim that catalysts only accelerate reactions to equilibrium, their behavior is consistent with other dynamic chemical devices including molecular pumps, rotors, and walkers[117]. The commonality is the 'ratchet' mechanism with asymmetric shape and motion that selectively transfers energy into the chemical system. These mechanisms meet the requirements of the principle

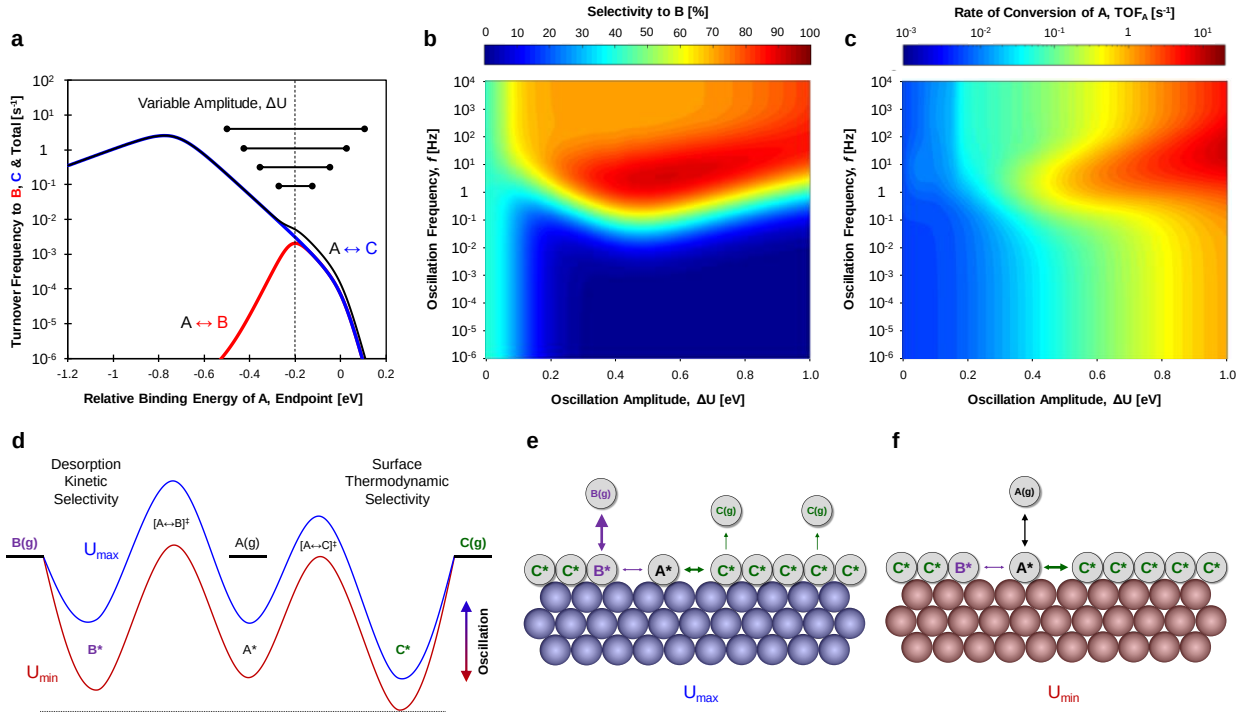

Figure 6. Dynamic heterogeneous catalysis, using a variable amplitude square waveform, for a parallel reaction system with A-to-B and A-to-C chemistry. **(a)** Volcano plots for reactant consumption (black) and product formation (red/blue) turnover frequency. Dynamic catalysis oscillations with varying oscillation amplitude are shown as black horizontal bars. **(b)** Selectivity to the production of B (mol%) with varying oscillation frequency (10^{-6} to 10^{4} Hz) and amplitude (0.0 to 1.0 eV). The oscillation midpoint was held constant at the volcano peak for product B formation. **(c)** Consumption rate of A (s^{-1}) with varying oscillation frequency and amplitude. Conditions: T ~ 150 °C, 100 bar A feed pressure, 1% conversion of A. Parameters: ΔH_{ovr} ~ 0 kJ mol^{-1} for both reactions, BEP parameters of $\alpha \sim 0.6$, $\beta \sim 100$ $kJmol^{-1}$, linear scaling parameters of $\gamma_{B/A} \sim 2.0$, $\gamma_{c/A} \sim 0.5$, and $\delta_{B-A} \sim 1.4$ eV, $\delta_{C-A} \sim 1.4$ eV. Relative binding energies of A in all panels a-c can be converted to absolute binding energies of A by adding 1.4 eV to the independent axis. Mechanisms of dynamic selectivity to products in parallel chemistry. **(d)** Oscillation of surface binding energies of A*, B*, and C* between strong (U_{min}, red) and weak (U_{max}, blue) enthalpy of adsorption occurs through two transition states. Two general behaviors can produce high selectivity to specific products: weak surface binding permitting reaction surface resonance to product B(g), or strong surface binding that leads to a C* dominated surface. **(e)** The surface turnover state, U_{max}. **(f)** The surface filling state, U_{min}. Chemical dynamic parameters: $\gamma_{B/A} = 1.3$, $\gamma_{C/A} = 0.6$, and $\delta_{B-A} = 0.6$ eV, $\delta_{C-A} = 1.5$ eV, $U_L = -0.5$ eV, $\Delta U = 0.4$ eV. (adapted with permission from reference 51).

of microscopic reversibility by always permitting all chemical intermediates to pass through the same transition states at any instant in time, even when the reaction energy profiles are changing[118]. They also exist throughout biology providing capability for controlling the location and movement of chemicals, including the mobility and movement of ions against equilibrium across membranes[119,120]. In comparison with these existing ratchet-based systems, dynamic catalytic surfaces are another example of asymmetric dynamic systems but with the added benefit of manipulating surface chemistry.

2.4 Forced Catalytic Dynamics – Network Selectivity. The ability to enhance rate and provide work via dynamic catalysis raises the opportunity for controlled steering of molecules through preferred chemical pathways. The complex reaction networks of catalytic surface mechanisms that contain energetically similar pathways and comparable rate contribute to reduced selectivity towards desired products and devalued chemical processes[121,122]. Introduction of dynamics in adsorbate enthalpy or entropy to a catalyst active site provides new handles to enhance or slow particular elementary steps, each of which has unique characteristics of frequency and binding

energy variation. Selective performance then requires identifying these chemical differences, pairing the catalyst with a method of stimulating change, and optimizing the dynamic parameters (e.g., frequency) to maximize selectivity.

Simulation of parallel reaction systems (catalytic conversion of chemical A via parallel pathways to products B and C) with a broad range of chemical parameters (adsorbate linear scaling parameters γ and δ, and Brønsted Evans Polanyi parameters α and β) revealed that parallel chemistries can be highly tuned towards selectivity between either product through the manipulation of oscillation parameters (amplitude and frequency).[51] As shown in the example with opposite gamma values between parallel reactions ($\gamma_{B/A} \sim 2.0$, $\gamma_{C/A} \sim 0.5$) in the Sabatier volcano plots of **Figure 6a**, static catalysts either select for product C or a 50/50% ratio of B and C; no condition exists for selective production solely of B. However, oscillation of the binding energy of A* at varying amplitude and frequency centered at -0.2 eV relative binding energy of A* reveals complex reaction behavior. As depicted in **Figure 6b**, selectivity to B increases over 50% and becomes almost perfect at 1-10 Hz for oscillation amplitudes of 0.4-0.7 eV, concurrent with an acceleration of the overall conversion of A in **Figure 6c**.

Dynamic selectivity to products exhibits complex behavior resulting from two mechanisms as depicted in **Figure 6d-6f**. During the strong binding condition (U_{min}, red in **Figure 6d**), one of the two products (C* in this example) dominates surface coverage with stronger binding energy, leading to suppression of the other pathway(s) as shown in **Figure 6f**. Alternatively, under the catalyst condition U_{max}, the other reaction pathway (B* in this example) more readily desorbs due to weaker binding energy and can achieve 'catalytic resonance' behavior in the resonance band of frequencies; higher rates lead to higher time-averaged turnover frequency and higher selectivity, as shown in **Figure 6e**. The selectivity map (**Figure 6b**) exhibits a complex pattern due to the multiple competing mechanisms leading to different reaction products. Although not shown here, sampling of a wider range of both chemical and dynamic catalyst parameters indicates significant potential for controlling the selectivity to products for a wide range of catalytic chemistries.[51]

2.5 Forced Catalytic Dynamics – Real Surface Mechanisms. While progress has been made on simulating the enhancement of reactivity and selectivity of dynamic systems of simple model systems for the conversion of a generic reactant to product (A to B) in the gas phase, further exploration is required to understand complex systems reflective of real catalytic mechanisms important to energy, materials, and sustainability applications. The dynamics of real catalytic systems will need to account for bimolecular reactions, the evolution of poisons, and more complex mechanisms such as Eley-Rideal. Surfaces will also contain more than one type of active site, such as metals with different facets, edges, and defects; each of these sites will potentially have unique dynamic parameters for each elementary reaction. However, this complexity is matched by the addition of several controlling parameters; dynamic catalysis could be conducted via several superimposed waveforms or even exist as a single complex periodic function. These could be custom designed for each chemistry-material-stimulus combination, offering an entirely new way to think and implement catalyst design and optimization.

The scale of complexity in dynamic catalysis limits the ability to computationally evaluate real chemical systems. Even 'simple' surface chemical mechanisms such as water-gas-shift, formic acid decomposition, and methanol decomposition contain 2-to-8 elementary steps in series and parallel[123,124,125]. More complicated chemistries can contain 10-to-100 or more elementary steps including cracking chemistries, reforming, and catalytic combustion[126,127,128]. These surface mechanisms are already computationally expensive, and the introduction of dynamics more than doubles the number of required parameters. This is further challenged by the computational difficulty in identifying stable limit cycle solutions at oscillatory steady state for every parameter set of interest. Evaluation of these challenging systems will require both advanced computational approaches for converging forced dynamic simulations as well as parameter screening methods such as machine learning to optimize dynamic catalyst systems[129,130]. These efforts begin with an understanding of the different methods of dynamically stimulating catalytic surfaces.

3.0 Stimulating Methods for Dynamic Catalysis. Implementing dynamic catalysis requires physical devices with methods for controllable variation of a catalyst physical or electronic structure. The techniques to stimulate catalyst change are distinct from other reactor technologies that merely supply energy to a reactor. While techniques such as microwave irradiation[131], plasma[116], and pulsed heating[132] or pulse pressure[133] can be used continuously or dynamically with catalysts leading to unique, beneficial, reactor behavior, they do not manipulate the catalyst itself and are not the focus of this perspective.

Catalyst stimulation exists in three categories related to the general approach of mechanical, electrical, or photochemical perturbations from their resting structures. These general categories can be applied broadly to many different types of materials that are porous or non-porous, metal or non-metals, rigid or floppy, but the selected technique within each category will determine the optimal materials for implementation. The optimal materials-stimulus combination maximizes the extent of catalyst variation in physical or electronic properties leading to controllable variation in enthalpy and/or entropy of adsorbates at frequencies relevant to catalytic turnover (>0.1 s^{-1}) and preferably higher (>10 s^{-1}). The following describes nine different stimulating techniques along with a description of their implementation, their capability for manipulating adsorbates, and the performance metrics for surface oscillation speed.

3.1 Mechanical Stimuli – Dynamic Surface Strain. The use of mechanical force can take many forms with the goal of changing the catalyst physical and electronic structure. Metals under stress are known to strain and deform, yielding new behaviors in adsorption and catalysis that are interpreted via changes in band structure. As shown by Mavrikakis, the adsorption energy of molecules for changes of the lattice constant ($\Delta d/d_{eq} < 2.5\%$) due to strain was comparable to changes in metal composition; in both cases, binding energy increased with higher values of the simplest descriptor of the electronic structure of the metal, the *d*-band center[134]. The overlap of the *d* orbitals decreases as the atomic distances increase under strain, producing a narrower *d*-band with a center that shifts upward[135]. A higher *d*-band center closer to the Fermi level reduces occupation of the adsorbate-surface anti-bonding molecular orbital producing a stronger chemical bond between the adsorbate and the surface; similarly, a lower *d*-band center further from the Fermi level increases occupation of the anti-bonding state and weakens the surface bond[136]. As such, physical changes implemented by stress at the surface manifest as electronic control of adsorption and surface chemistry[137].

Strain occurs in *static* systems using materials under external stress or multi-layer materials with lattice mismatch. Stress leading to separation of atoms introduces tensile strain, while stress decreasing lattice parameters constitutes compressive strain. For example, carbon monoxide adsorption on copper overlayers on different transition metals and facets exhibited a distinct vibrational shift in infrared stretch frequency, indicating stronger adsorption under strain[138]. Similar modification of metals via strain has been experimentally demonstrated also for overlayers of Co/Cu[139], Pt/Pt-Cu[140], and Pt/Ru[141], indicating that chemisorption binding control occurs broadly across materials and substrates. The extent of adsorption enthalpy shift via strain has been calculated via DFT for many adsorbates including O_2 on Au[142], CO on Pt[143], and O_2 on Cu[144], among other systems indicating binding energy shifts as high as ~0.5 eV for large strain of 3-5%.

Similar strain effects on adsorption can also occur for nanoparticles on different supports and doped catalysts. These changes in heats of adsorption are attributed to both lattice mismatch (a geometric factor) and also to a ligand effect due to charge transfer between one material and the other (electronic effect). While calculations can freeze a supported structure and move it to vacuum to remove electronic effects, in practice there is an inherent coupling between geometric and electronic effects that is difficult to deconvolute. Despite the concept of catalyst strain being heavily studied, and in some cases, successfully directed for improved performance[145], demonstration of strain effects on kinetics is limited in part due to the aforementioned coupling and the difficulty in systematically introducing strain in experimental systems.

Physically implementing *dynamic* strain in materials for adsorption and catalysis requires a mechanism for dynamic control[146]. The concept of thin overlayers can be extended to dynamic systems if the substrate undergoes controllable physical

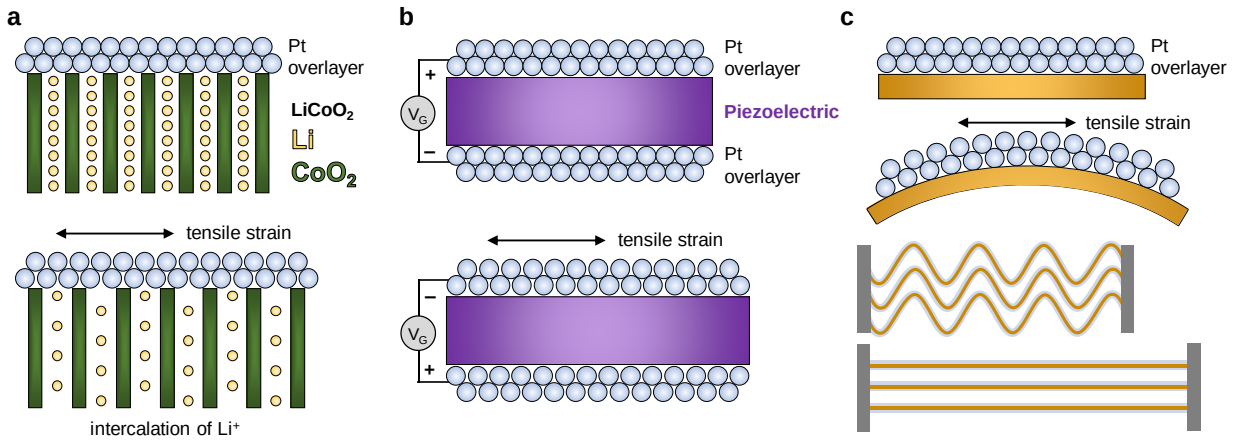

Figure 7. Mechanisms of Dynamic Strain. **(a)** Intercalation of ions such as Li^+ within a metal oxide (e.g., CoO_2) induces strain that transfers to a thin Pt overlayer. **(b)** Imposed electric field to a piezoelectric layer induces strain that transfers to a thin Pt overlayer. **(c)** Mechanical stress on a thin substrate such as poly-methyl-methacrylate (PMMA) induces strain in a thin Pt over layer.

modification. In one example depicted in **Figure 7a**, a thin Pt layer is deposited on $LiCoO_2$, which can expand and contract as much as ~3% due to Li intercalation during charge and discharge to $Li_{0.5}CoO_2$ corresponding to ~5% compressive strain in the Pt overlayer[147]. This general approach can potentially be expanded to other intercalated ions (e.g., Na^+, K^+) into materials such as carbons (e.g., graphite)[148], metal oxides (e.g., V_2O_5[149]), or metal sulfides (e.g., TiS_2)[150].

Other stress-based strategies have the common mechanism of external stimulus applied to the support to induce strain that is transferred to a catalytic overlayer such that the electronic properties can be varied with physical deformation of the active site. One variation is the piezoelectric substrate that generates polarization of charge under mechanical stress; under the converse piezoelectric effect, the application of an electric field induces compressive or tensile strain[151]. A possible multi-layer piezoelectric device in **Figure 7b** could expand to apply stress to an external thin metal overlayer, impose strain, and electronically modify the catalyst surface. In this system, the pairing and fabrication of the piezoelectric/catalyst-overlayer can select from numerous lead-based and lead-free[152] piezoelectric materials including PZT $Pb(Zr_xTi_{1-x})O_3$, $(K_xNa_{1-x})NbO_3$[153], and BCZT $(Ba(Ti_{0.8}Zr_{0.2})O_3$-$(Ba_{0.7}Ca_{0.3})TiO_3$[154]. These piezoelectric materials can introduce strain as high as ~1% with phase switching faster than 1000 Hz[155].

The substrate supporting a catalytic overlayer can also be physically stimulated with time, such as the case when thin catalyst layers are deposited on mechanically deformed surfaces[156]. In one incarnation, tungsten carbide (WC) deposited on a poly(methyl methacrylate) diaphragm was physically deformed via variation in surround gas pressure to apply tensile and compressive stress to the WC catalyst[157]; this approach achieved >3% strain in WC and a measurable shift in the *d*-band center of WC of 0.07 eV. A challenge with this approach is minimizing local variation in strain, which can produce a distribution in catalyst electronic behavior and performance.

3.2 Surface Acoustic Waves and Resonance Oscillation. The alternative to straining a substrate in contact with a catalytic material is the direct stimulation of the catalyst itself. Introducing propagating deformation waves into materials for adsorption has been extensively evaluated by the methods of both 'surface acoustic waves' (SAW) and resonance oscillation (RO) of bulk acoustic waves[158]. Dynamic lattice distortion induced either through the surface or the bulk material supporting a catalytic surface changes local interatomic distances introducing electronic variation of the local band structure and work function[159]. As described in detail by Yasunobu Inoue, these controlled variations have been implemented in a variety of materials with extensive capability for manipulating adsorption and enhancing catalysis[160].

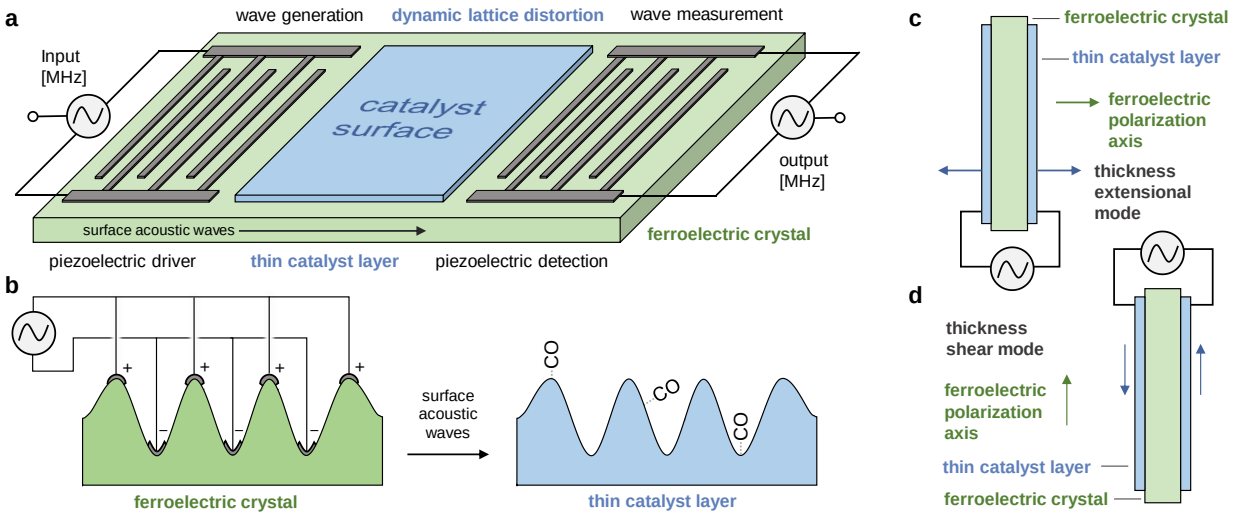

Figure 8. Surface acoustic waves and resonance oscillations of metal catalysts. **(a)** Surface acoustic waves (SAW) at megahertz frequencies are generated on ferroelectric crystal surfaces using piezoelectric interdigital transducers. Waves then propagate across the catalyst surface and can be detected by piezoelectric transducers. **(b)** Oscillating voltage [MHz] applied to interdigital transducers expands and contracts the piezoelectric surface layer to deform the ferroelectric crystal and produce surface acoustic waves. Propagated SAWs deform the thin metal or metal oxide catalyst layer creating local regions of high strain for adsorbed species. **(c)** Resonance oscillation (RO) of bulk acoustic waves by thickness-extension resonance oscillation (TERO). **(d)** Resonance oscillation by bulk acoustic waves by thickness shear resonance oscillation (TSRO).

Surface acoustic waves depicted in **Figure 8a** are generated on a ferroelectric crystal (e.g., $LiNbO_3$) that exhibits piezoelectric behavior; these lattice deformation Rayleigh waves then propagate through a thin layer of catalyst transferring dynamic strain and electronic variation to the active surface[161]. By the photolithographic deposition of interdigital transducers, oscillating voltage produces regions of both high tensile and compressive strain consistent with the applied voltage and spacing between the electrodes (**Figure 8b**). The propagation velocity of the surface wave, v, and the unit length spacing of the interdigital transducer electrodes, δ, can then be used to calculate the wave frequency, $f \sim v/\delta$. For many ferroelectric materials and electrode spacing, SAWs are commonly generated with frequencies of 1-100 megahertz.

Surface acoustic waves have been observed using a Doppler imaging method with an oscillation amplitude of several nanometers up to 200 nm normal to the surface[158, 162,163]. These dynamic deformations when propagating through films of Cu, Au, and Pd metal were observed by photoelectron emission microscopy to shift the work function of these catalytic surfaces[159]. The resulting deformation-derived electronic tuning of the material has been attributed to several unique catalytic behaviors including increased rates of CO oxidation on Pt[164,165] and ethanol oxidation to acetaldehyde on Pd[166]. While the precise mechanism(s) leading to variation in binding energy and catalytic turnover remain under discussion, definitive evidence exists of significant physical and electronic catalyst changes in the presence of Rayleigh surface acoustic waves.

Another incarnation of acoustic waves occurs via resonance oscillation of bulk ferroelectric materials with piezoelectric characteristics[158]. As depicted in **Figure 8c and 8d**, resonance oscillation occurs via the application of radio frequency electric power to electrodes on both sides of a ferroelectric. Oscillating potential induces electric field-promoted lattice distortion which propagates through the ferroelectric in the direction of polarization. Acoustic waves either promote thickness-extension mode resonance oscillation (TERO) in **Figure 8c** or thickness shear-extension mode resonance oscillation (TSRO) in **Figure 8d**, depending on the orientation of the surface electrodes relative to the ferroelectric polarization axis[160]. While any frequency can be applied to the electrodes, the resonance frequencies derive from the natural frequency of the crystal and higher

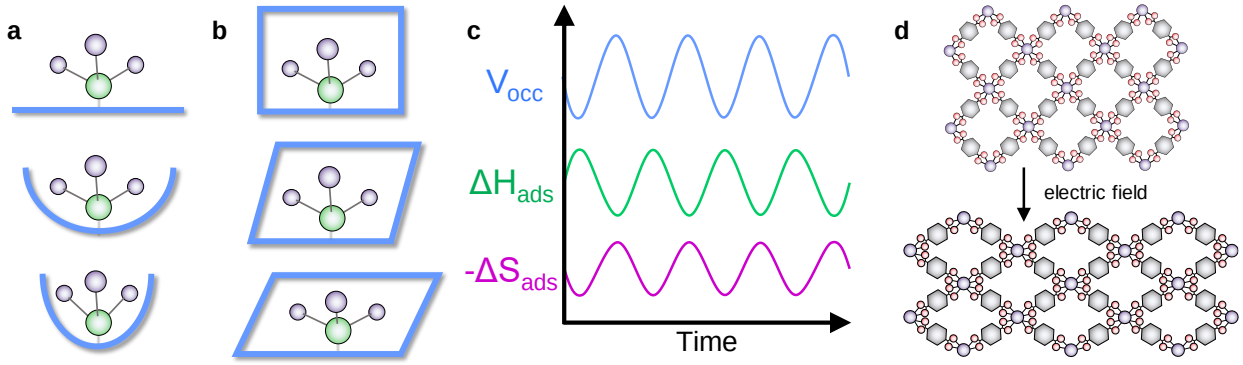

Figure 9. Dynamic Pores, Cavities, and Pockets. (a) Dynamic pockets that oscillate between open and closed conformations. **(b)** Dynamic pores that oscillate between relaxed and strained conditions. **(c)** Dynamic local occupiable volume (V_{occ}) in a porous material and associated changes in enthalpy (ΔH_{ads}) and entropy ($-\Delta S_{ads}$) of adsorption. **(d)** Structural switching of MIL-53(Cr) in the presence of an electric field.

harmonics as determined by the crystal thickness, density, and elastic constant. For the characteristics and size of many ferroelectrics, these resonant frequencies are ~1-100 megahertz[160]. Similar to surface acoustic waves, the RO waves exhibit surface distortion up to ~100 nm, especially in the TERO orientation[158]. These surface deformations have led to increases in the rate of reaction such as oxidation of methanol on Pt and Pd films[167].

Implementing dynamic catalysis using acoustic waves has the benefit of extensive characterization and methods of implementation combined with the broad range of materials that can be stimulated including both metals and metal oxides. Selection of piezoelectric/ferroelectric materials can draw from materials across the full range of chemistry-relevant temperatures (25 – 500 °C) to select acoustic supports operable relative to their Curie temperature. While these devices appear to achieve significant local strain and electronic variation, applying these devices to specific chemistries (e.g., direct methanol oxidation) will require a fundamental understanding of the acoustic wave on surface binding energies and transition states, which does not yet exist.

3.3 Dynamic cavities, pockets, and pores. Physical deformation of surfaces can also include the temporal variation of pores, cavities, and pockets within catalytic materials as depicted in **Figure 9a and 9b**. Binding sites within a porous material are surrounded by surfaces which contain additional binding sites as well as support material and non-catalytic functionalities (e.g., ligands, defects)[103]. The electronic interaction of the adsorbate and surround cavity increases as cavities and pores shrink owing to chemisorption and van der Waals interactions. Additionally, cavities and pores that approach the size of the adsorbate will stress the molecule and introduce strain and new geometry in molecular structure. For porous materials with regular shapes, cavities can be defined with pore diameter and compared with molecular descriptors such as the molecular van der Waal or kinetic diameters. More complex multi-pore and cavity-containing materials require descriptors that account for irregular shapes, such as the occupiable volume (V_{occ}), which quantifies the amount of space that can be occupied by atomic-scale (2.8 Å diameter) spheres[103,168].

In addition to increasing the enthalpy of adsorption, shrinking cavities and pores will simultaneously reduce the entropy of surface adsorbates by restricting molecular rotation, often with a linear 'compensation effect' between adsorption enthalpy and entropy[101]. Molecules on flat surfaces lose translation entropy[100], but additional modes of rotational entropy are lost as surface curvature increases to form surrounding local environments. As depicted in **Figure 9c**, an adsorbed molecule exposed to swelling and shrinking environments can be described with varying occupiable volumes; the enthalpy of adsorption (ΔH_{ads}) decreases as the environment expands due to reduced interaction with the wall and weaker binding, but the entropy of the adsorbate increases with additional space for the molecule to rotate[103]. Predicting these enthalpic and entropic effects of dynamic cavities on catalytic reactions requires simultaneous understanding of surface intermediate and transition state enthalpy

and entropy relative to at least one descriptor of the changing physical and electronic structure of the surrounding catalytic site.

Flexible dynamic materials exist as two different classes depending on their structure and time-resolved variation. As depicted in **Figure 9a**, a flexible pocket open to the environment will open and close interacting with the adsorbate through the enclosing walls. These systems exist as short chains of polymers such as enzymes, or surfaces such as metals with unreactive ligands (i.e., self-assembled monolayers) that enclose the reacting adsorbate[169]. Alternatively, an enclosed pore or cavity as depicted in **Figure 9b** exists within a repeating microstructure that compresses, expands, or shears under external stimuli to alter the local environment around a catalytic site. A significant number of microporous materials (i.e., nanometer-scale cavities) exist with sufficient flexibility to manipulate adsorbate energy, including metal organic frameworks[170,171,172] and other molecular sieves[173].

3.3.1 Dynamic MOFs and COFs. Porous frameworks that change with time are known as '4D materials' and 'third generation porous coordination polymers' with spatiotemporal variation in their physical structure and associated adsorption characteristics[174,175]. Comprising many of the examples of 4D materials, metal organic frameworks (MOFs) and covalent organic frameworks (COFs) exhibit both crystalline repeat units of definable pores and flexibility leading to significant pore deformation[176]. Of the immense number of possible MOF structures, flexibility has been predicted to occur by six mechanisms depending on the dimensionality of the material[174]. In three-dimensional materials, this includes: (i) the elongation and shortening of interlayer pillars such as in $[Cu_2(dhbc)_2(bpy)]_n$[177], (ii) the sliding of interpenetrated grids of materials such as in MOF-508 $[Zn_2(bdc)_2(bpy)]_n$ [178], and (iii) the expanding and shrinking of frameworks common to MIL materials[170,172].

Unique flexibility was first noted in the considerable expansion of MOFs upon adsorption. Referred to as 'breathing', the host framework can flex and contort substantially yielding macroscopic expansion up to 200-300% upon adsorption[175]. One insightful material is MIL-53(Cr), which has a porous structure comprised of chain-like building units with a linker of benzene dicarboxylate (bdc)[179]. Upon synthesis, the unit cell (17.34 by 12.18 Å) contains excess bdc linker, which upon post-synthesis removal widens the unit cell (16.73 by 13.04 Å); subsequent rehydration then shrinks the unit cell (19.69 by 7.85 Å)[176]. This dramatic change derives from flexibility near the chromium metal nodes, which are influenced by the interaction with water. This flexing of the framework is common to a substantial sub-class of MOFs, permitting reversible variation in the microporous structure[180].

Another example where flexibility is prominent in determining adsorption and diffusion is ZIF-8. ZIF-8 is a zeolitic-imidazolate framework (ZIF) consisting of zinc (Zn) centers bridged by 2-methyl-imidazole (2mIm) ligands[181]. In the crystal structure of ZIF-8, the 3.4 Å six-ring window is responsible for its molecular sieving ability. The imidazole rings around the window are almost parallel to the window plane, and the aperture size is defined by hydrogen atoms on the four and five positions of the imidazole rings. The imidazolate ring however swings on THz frequency relative to the six-ring plane increasing the pore aperture allowing access to molecules that would be otherwise forbidden in a rigid framework[182,183,184,185]. When guest species are present in the framework, in addition to the vibrational swinging effect, the imidazolate linkers can rotate to new equilibrium positions with a non-zero torsion angle. The linker rotation is often accompanied by expansion of the unit cell. Depending on the context, such a transition is termed interchangeably as "gate opening", "as prepared/high pressure (AP/HP)" or "low loading/high loading (LL/HL)"[186,187]. Likewise, the gate-opening transition in ZIF-7, where the 2mIm linker in ZIF-8 is replaced by benzimidazole, is called "narrow pore/large pore (NP/LP)" transition[188]. The gate opening phenomenon is strongly affected by an interplay of guest species, pressure and temperature. The structural flexibility of ZIF-8 is also dependent on crystal size, adding to the complexity of this behavior[189]. Without flexibility some of the most promising separation properties of ZIFs would not have been possible.

In addition to host-guest interactions, MOF structure can be controlled with other stimuli including temperature, pressure and acoustic waves, light, and electric and magnetic fields[176]. Photo-responsive MOFs contain additional light-

sensitive functional groups or linkers that exhibit reversible conformational changes (e.g., trans-to-cis) leading to structural variation such as pore widening/narrowing[190,191]. Thermo-responsive MOFs exhibit continuous thermal expansion (positive and negative) with substantial volume change with temperature; additional MOF phase change with temperature is an activated process leading to hysteresis in structural and pore size variation when heating or cooling[192,193]. Similarly, many pressure-sensitive MOFs exhibit pressure-induced continuous reversible conformational changes in addition to both reversible and irreversible phase changes to new high pressure structures[194,195].

A more recent stimulus is the application of electric fields to MOFs. In one example depicted in **Figure 9d**, MIL-53(Cr) with empty pores was shown to exhibit variation in unit cell volume in an electric field ($0 < E < 3$ V nm^{-1}) followed by substantial change with hysteresis associated with a phase change from the larger (8 Å) to smaller (3.5 Å) pore form[196]. More importantly, this structural transition was observed to occur continuously and without hysteresis when MIL-53(Cr) was loaded with carbon dioxide or methane, indicating that structural control can still occur in the presence of chemical reactants. An applied electric field was also used to reduce the flexibility of a ZIF-8 film and affect its gas permeation properties.[197] An explanation for electric field sensitivity has been proposed as the formation of an induced dipole, resulting from structural deformations and electronic polarization of the MOF structure[198,199]. This has led to the design of new MOFs which incorporate structures such as dipolar rotors to achieve higher dielectric permittivity[200] and structural response at lower E field strength.

Utilizing dynamic MOFs and COFs for catalysis will require the ability to select and tune porous cavities to oscillate adsorbate binding energy and entropy with time, thus manipulating the associated transition states and intermediates of reaction. Of the options for stimulating methods, electric fields, pressure, and light are all potentially viable provided physical methods exist to incorporate catalytic MOFs and COFs into a flow reactor while maintaining contact with the stimulus source. Additionally, selecting the combination of MOF, chemistry, and stimulus method requires more detailed understanding of the range of achievable changes of enthalpy and entropy within expanding and contracting pores and cavities.

3.3.2 Pockets, Polymers, and Enzymes. The alternative to a repeating porous crystal structure that exhibits dynamic behavior is the formation of a pocket or cavity on a surface. One approach for rigid confinement are nanobowls, which are surface pockets made of metals and metal oxides that surround the catalytic active site[201,202]. Surface pockets can be prepared step-wise via techniques such as ALD or be synthesized as 2D materials, as is the case with delaminated zeolite 2D sheets such as MWW[203,204]. More flexible pockets exist when soft materials are added to hard surfaces, as is the case when larger inert adsorbates are added to metal or metal oxide/sulfide surfaces to surround reacting adsorbates providing a flexible confining environment[205,206]. Implementing dynamic variation of these pocketed materials is challenging, unless the entire hard structure can be strained as previously discussed or the surface coverage of inert co-adsorbates near the active site can be controllably varied with time.

Other opportunities derive from soft materials that can spontaneously fold into shapes that naturally form pockets and cavities, the most successful of which are protein chains folded into enzyme catalysts[207]. These folded chain catalysts exhibit multiple forms of dynamics including allosteric regulation, conformal oscillation, activation (folding), and complete deactivation (unfolding)[208]. With regard to allosteric regulation, the folded protein catalyst (enzyme) has a second site where binding of an additional molecule, the 'effector', can change the conformation of the protein between 'tensed' and 'relaxed' structures[209,210]. These secondary molecules can both enable (allosteric activation) and disable enzymes (allosteric inhibition), providing on/off switching through physical changes around the catalytic active site[211].

The more complicated discussion surrounds the role of dynamic enzyme changes and their role in catalysis[212]. As stated by Kern and co-workers, "Because many enzymatic reactions occur on time scales of micro- to milliseconds, it is anticipated that the conformational dynamics of the enzyme on these time scales might be linked to its catalytic action"[213]. Protein dynamics span the range of femtoseconds to nanoseconds for local flexibility in the enzyme, while larger collective motions occur

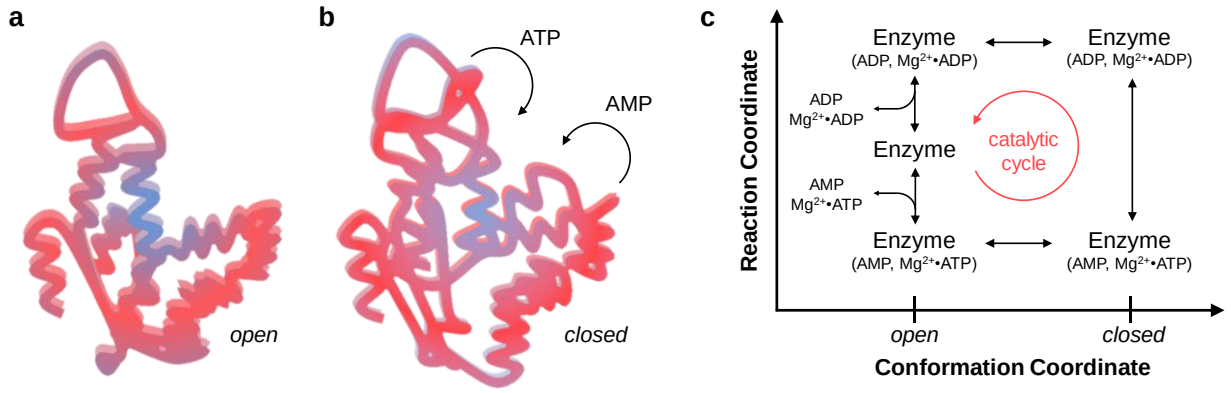

Figure 10. Catalytic dynamics of enzymes. **(a)** Open configuration of enzyme *Aquifex* Adk allowing adsorption and desorption of adenosine phosphates (ATP, ADP, and AMP). **(b)** Closed enzyme configuration leading to the reaction of ATP and AMP to two molecules of ADP. **(c)** Two dimensional reaction and conformation coordinate describing the enzymatic cycle of converting ATP and AMP to two molecules of ADP through open and closed configurations.

on the microsecond to second range[214]. These slower motions have been associated with sequential steps in a catalytic cycle, as in the case of the enzyme adenylate kinase (Adk). This enzyme adsorbs reactants (ATP and AMB, adenosine phosphates) in its open conformation (**Figure 10a**), promotes catalysis by switching to its closed conformation (**Figure 10b**), and then desorbs products (ADB) by switching back again to the open form[215,216]. These types of slower conformal changes alter the free energy landscape such that enzyme reaction pathways require description in three dimensions including a reaction coordinate and conformal coordinate[217,218], as shown in **Figure 10c**. A controversy arises from the additional question of whether faster enzyme motion can drive surface chemistry by transferring kinetic energy to the substrate; the argument against this potential secondary mechanism is the rapid dissipation rate of faster conformal changes relative to the rate of catalytic turnover[219,220].

3.4 Plasmon and Photocatalysis Dynamics. Photoexcitation of metal catalysts offers another stimulus for dynamic catalysis due to its fast time response and chemical specificity. Light excitation pulses can be applied dynamically with high frequencies since metal nanoparticles will thermally equilibrate with their surrounding environment within 100s of picoseconds following a photoexcitation pulse.[221] Thus, one could imagine a half duty-cycle photoexcitation of a working catalyst with a range of frequencies from 10^{9} Hz to 10^{-2} Hz, controlled electronically or mechanically (chopped).

Significant literature exists on the photoexcitation of adsorbate-covered extended metal surfaces, which shows that photoexcitation results in non-thermal energy exchange between the metal and adsorbates. Transient charge transfer to or from adsorbates can induce desorption and dissociation events,[222,223,224,225] as depicted in **Figure 11a**. Recent work has shown that photoexcitation of nanoparticle catalysts can increase reaction rates and induce non-thermal selectivity, even at relatively low photon fluxes (~1 W/cm^2). This is true for both coinage metal nanoparticles that support localized surface plasmon resonances and on small (few nm diameter) non-plasmonic nanoparticles[226,227,228]. Nanostructuring of the metal effectively focuses photon absorption near adsorbate-metal interfaces, rather than in the bulk of the metal. These effects of light on reactivity have been interpreted to result from charge transfer to or from adsorbates, thereby influencing elementary step energetics.[229,230,231]

In the context of using photoexcitation for dynamic control of catalysis, it is interesting to consider: (1) to what extent photoexcitation of metal surfaces modifies the effective binding energies of adsorbates, (2) what relationship exists between photon flux or wavelength and induced changes in binding energies, and (3) how the nature of the adsorbate, metal, or elementary process (dissociation, desorption, etc.) influences the relationship between the photon flux and modified elementary step energetics. Recent effort has begun to address these questions and suggests that photoexcitation has promise for dynamically

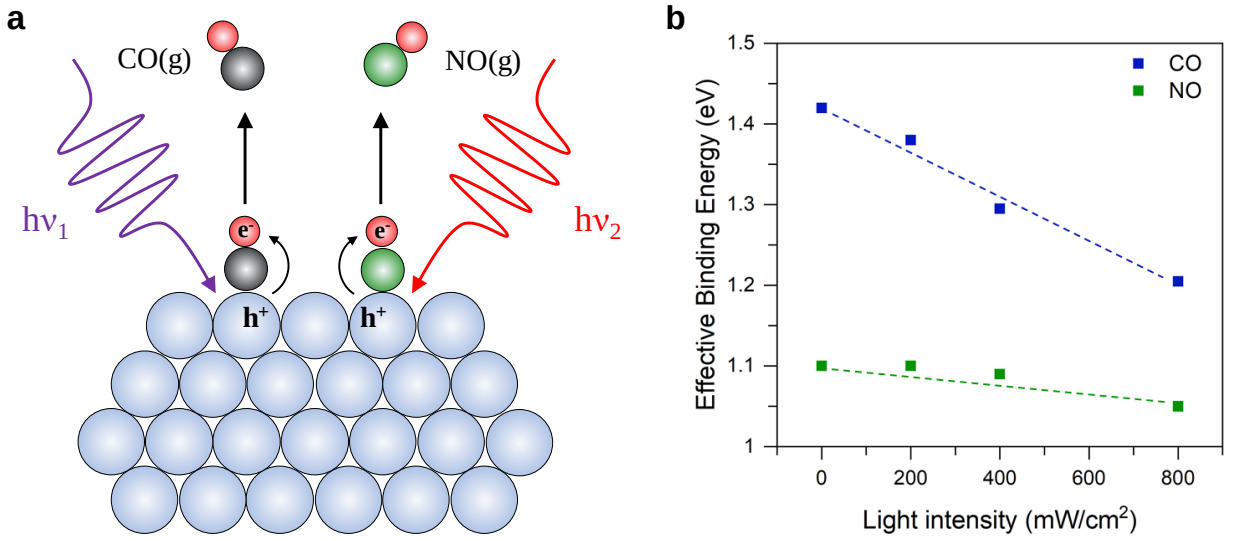

Figure 11. **(a)** Schematic illustrating specific activation of metal-adsorbate bonds using photoexcitation with targeted photon energies. **(b)** Experimental results for the effect of light (425 nm) on effective CO and NO binding energies to Pt. Catalyst consisted of 1 wt. % Pt/Al_2O_3 prepared by dry impregnation. Effective binding energies were estimated using a Redhead analysis with adsorbate surface concentrations followed by in-situ FTIR. A pre-exponential factor of 10^{13} s^{-1} was assumed, indicating a small entropy of activation for desorption. Light intensity was calibrated for specular illumination. As LED illumination onto IR cell was done at an angle, light intensities are likely an overestimate of true flux at the catalyst bed.

modulating catalyst performance. The dissociation rate of diatomic molecules such as O_2 and H_2 on Ag and Au have been shown to be promoted by photoexcitation with visible light. Extensive control experiments and chemical signatures suggest that these increased rates are not the result of thermal processes. Rather, they result primarily from photo-induced transient charge donation to the adsorbed diatomics.[227,228,232,233,234] Under illumination, the average population of antibonding orbitals of the adsorbed diatomic molecules is higher than in the dark. This results in an increase in the effective rate constant for dissociation and a decreased effective dissociation barrier.

It has analogously been shown for reactions where active sites are poisoned with adsorbates that catalytic rates are significantly enhanced under illumination. Kinetic signatures that indicate reduced coverage of poisoning species under illumination have been observed for CO-covered Pt, H-covered Pd, and N-covered Cu.[226,235,236,237] These results suggest that illumination of metal catalysts can also influence the effective rate constants and activation barriers for desorption processes. While these measurements support the notion that illumination can influence dissociation and desorption elementary step energetics, these arguments rely on kinetic signatures of overall catalytic processes. This makes insights regarding the influence of light on single elementary steps challenging to extract.

To directly assess the influence of photoexcitation of metal nanoparticles on elementary step energetics, we performed temperature programmed desorption (TPD) experiments of CO and NO from small <5 nm diameter Pt particles on an Al_2O_3 support in the dark and under illumination. The adsorbate surface concentration was measured by *in-situ* FTIR. Redhead analysis of CO and NO TPD spectra in the dark resulted in estimated desorption barriers of ~1.4 eV for CO and ~1.1 eV for NO, consistent with previous measurements.[238] When performing TPDs under illumination from continuous wave photon fluxes provided by 425 nm LED sources up to ~800 mW/cm^2, an effective decrease in CO desorption barrier of ~0.25 eV was observed as shown in **Figure 11b**. Identical experiments for NO showed only a ~0.05 eV decrease in NO desorption barrier induced by ~800 mW/cm^2 illumination. These results directly demonstrate that low intensity photon fluxes can strongly influence the

energetics of desorption processes from metal nanoparticle surfaces. This chemical specificity is inconsistent with a picture of photoexcitation simply resulting in equilibrium heating[239]; the process is adsorbate specific.

Translating photoexcitation to dynamic catalysts has unique characteristics relative to other oscillatory catalyst stimuli, since the applied wavelength can be tuned to manipulate specific adsorbates. If light is applied with dynamic fluxes, the approach may enable dynamic control over individual elementary step energetics, and thus control over reactivity or selectivity. Further, with the development of relationships between photoexcitation and energetics of elementary steps, the influence of dynamic modulation of light on catalytic performance should be predictable from microkinetic models. Finally, it is worth briefly mentioning that photon fluxes typically only penetrate tens of microns into catalytic beds of supported metal nanoparticles.[240] Thus the design of reactors to exploit any potential use of dynamic photoexcitation of catalytic processes will need to address the issue of photon penetration depth into porous catalytic beds.

3.5 Dynamic Electrocatalysis. In an electrochemical system, the electron driving force and ultimately the rate of reaction are dictated by the potential applied across the working and counter electrode. However, in addition to dictating the rate of reaction, the applied potential also controls the coverage of adsorbates on the surface of the working electrode[241,242,243]. The potential drop between the two electrodes does not occur linearly across the distance between them; most of the voltage change occurs within a few angstroms of the surface electrode[244]. Therefore, despite the typical magnitude of voltage applied in such systems (0.1 – 10 V), a relatively strong electric field (> 1.0 V nm^{-1})[245,246,247,248] is formed which can significantly alter the binding energy of adsorbates on the surface.

The most significant effect unique to electrochemical systems is the ability to readily tune the free energy of an electron-mediated process as a function of applied potential. Taking the Volmer adsorption step as a simple example,

$$H^+ + e^- + * \leftrightarrow H_* \qquad (3)$$

where * represents an active site, we can define the free energy of adsorption for the Volmer step,

$$\Delta G_{ads} = \Delta G_{ads,0} + eV \qquad (4)$$

where $\Delta G_{ads,0}$ is the free energy change of adsorption at zero applied potential. This demonstrates the linear relationship between the free energy of hydrogen adsorption via the Volmer step and applied potential; every volt of applied potential leads to ~100 kJ mol^{-1} change in the adsorption free energy. Therefore, in an aqueous electrochemical system, the coverage of hydrogen adatoms on the surface of a Pt electrode can be readily described as a function of the applied potential[241]. This is the concept of underpotential deposition (UPD), where sub-monolayer hydrogen adsorption is dictated by the applied potential. In addition to the magnitude of such effects, electrochemical systems can achieve such changes on relatively short time scales. The main temporal consideration here is the time required to form the electric double layer, characterized by a time constant that relies on the resistance and capacitance of the system (τ_{EDL} = RC), which typically occurs on the micro- to nano-second time scale. A wide range of applied potential oscillation frequencies can therefore be achieved with this approach, readily achieving frequencies as high as one megahertz.

Combining the speed and magnitude of the electric potential stimulus, an electrocatalytic system can be rapidly oscillated between two potentials at which different rate-determining limitations exist. This was recently experimentally demonstrated by Abdelrahman et al. for formic acid electro-oxidation over a platinum working electrode, where square wave oscillations in applied potential allowed for the dynamic modulation of the Faradaic rate of reaction[50]. At less oxidizing potentials, formic acid can readily adsorb and decompose to adsorbed carbon monoxide (CO*) with a kinetic rate constant varying between 1 - 100 s^{-1}, depending on the exposed platinum facet [249,250,251,252]. Despite the facile formation of CO* at lower potentials, the rate of its oxidative desorption is trivial at lower potentials because of the relatively high binding energy of CO (BE_{CO} ~ 1.9 eV). At more oxidizing potentials (> 0.6 V NHE), the rate of CO* oxidative desorption is non-trivial, but the rate of CO* formation is greatly diminished. The contribution of the CO* mediated pathway for formic acid oxidation therefore faces a kinetic disconnect; a

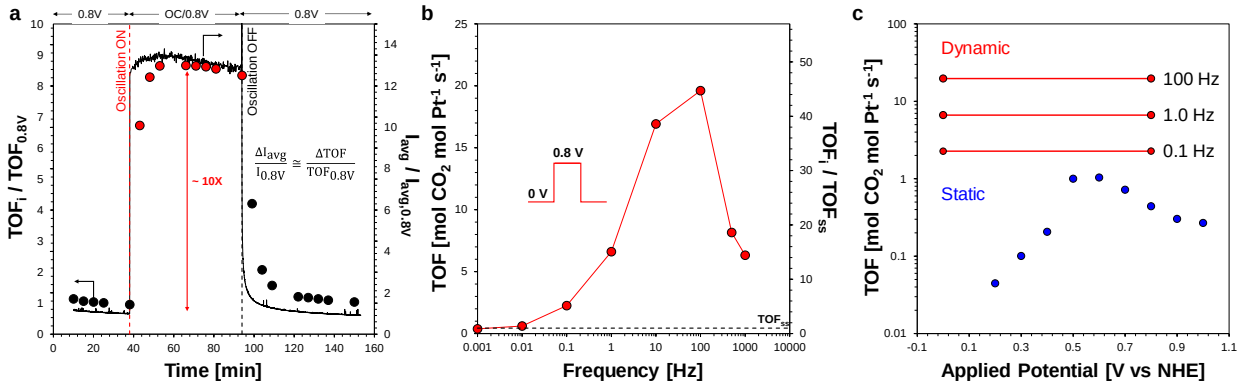

Figure 12. Resonance promoted formic acid electro-oxidation. **(a)** Initial steady applied potential of 0.8 V NHE transitions to dynamic square wave oscillation of the applied potential between open circuit (OC) and 0.8 V NHE at 0.1 Hz and 50% duty cycle. The resulting time-averaged catalytic turnover frequency exhibits a 10-fold increase as measured independently by both exchange current and CO_2 product formation rate measured by gas chromatography. **(b)** Square wave applied potentials (50% duty cycle) yield variable average catalytic turnover frequencies as a function of the oscillation frequency. The peak resonance-enhanced electrocatalytic reaction rate occurs at 100 Hz, with a maximum average TOF 20 s^{-1}, respectively. TOF_{SS} (0.44 s^{-1}) is the steady-state reaction rate at fixed applied potential of 0.8 V. **(c)** Static formation rate of CO_2 from formic acid (blue) at fixed applied potentials ($0.2 < V < 1.0$ NHE) is significantly lower than the dynamic turnover frequencies (red) varying at 0.1, 1, and 100 Hz with square waveforms at 50% duty cycle with an amplitude of zero to 0.8 V NHE applied potential. (reprinted with permission from reference 50).

single applied potential cannot optimally balance the energetic needs of both CO* formation and its subsequent oxidative desorption. Alternatively, a dynamic electrocatalytic system oscillating between applied potentials that favor either of the rate-determining processes can overcome this kinetic disconnect.

Abdelrahman et al. showed that switching from a fixed potential to an oscillation between open circuit and the same applied potential (0.8V to 0.8V/OC) rapidly increased the turnover frequency to the new dynamic level of activity, followed by a quick return to the original level of activity when the oscillation was stopped (**Figure 12a**). This demonstrates the reversible nature of dynamic catalysis, where a 0.1 Hz oscillation increases the TOF by approximately one order of magnitude. Extending the same square wave over a wide range of oscillation frequencies ($10^{-3} < f < 10^{3}$ Hz), a maximum TOF of 20 s^{-1} is achieved at a resonance oscillation frequency of 100 Hz (**Figure 12b**). This greatly exceeds both the static TOF at the oscillation endpoint (0.8 V, 0.44 s^{-1}) and the maximum achievable under any potentiostatic condition; the resonant TOF is ~ 20X larger than the static maximum TOF of ~1 s^{-1} at 0.6 V (**Figure 12c**).

3.6 Dynamic Solid Electrolytes. Another method to alter the electronic characteristics of transition metals such as Pt, Co, and Ni to the extent required for dynamic catalysis is the deposition of surface ions using electronic potential. Referred to as 'non-faradaic electrochemical modification of catalytic activity,' metal catalyst layers or clusters can be supported on metal oxide solid electrolytes that provide ions such as oxygen (O^{2-}) or sodium (Na^{+}), as shown in **Figure 13a-13d**[253,254]. Ions on metals are known to form strong local electric fields as high as ~1 V/A, as in the case of cesium on Ag[255], which can change the adsorbate and transition state energies of surface-catalyzed reactions. Application of electronic potential drives these ions out of the solid electrolyte support to form a counter-charge at the metal surface, providing time-resolved reversible capability for modifying the metal catalyst surface.

The use of solid electrolytes has been extensively evaluated for catalysis and adsorption for transition metal catalysts. When using yttrium-stabilized zirconia (YSZ) as a solid electrolyte support, oxygen ions can back-spillover onto the metal surface and desorb as O_2. Desorption energy of O_2 from Pt/YSZ was shown to vary as much as 0.6 eV for applied potentials of zero to 0.6 V[256]; similar adsorption weakening was observed for

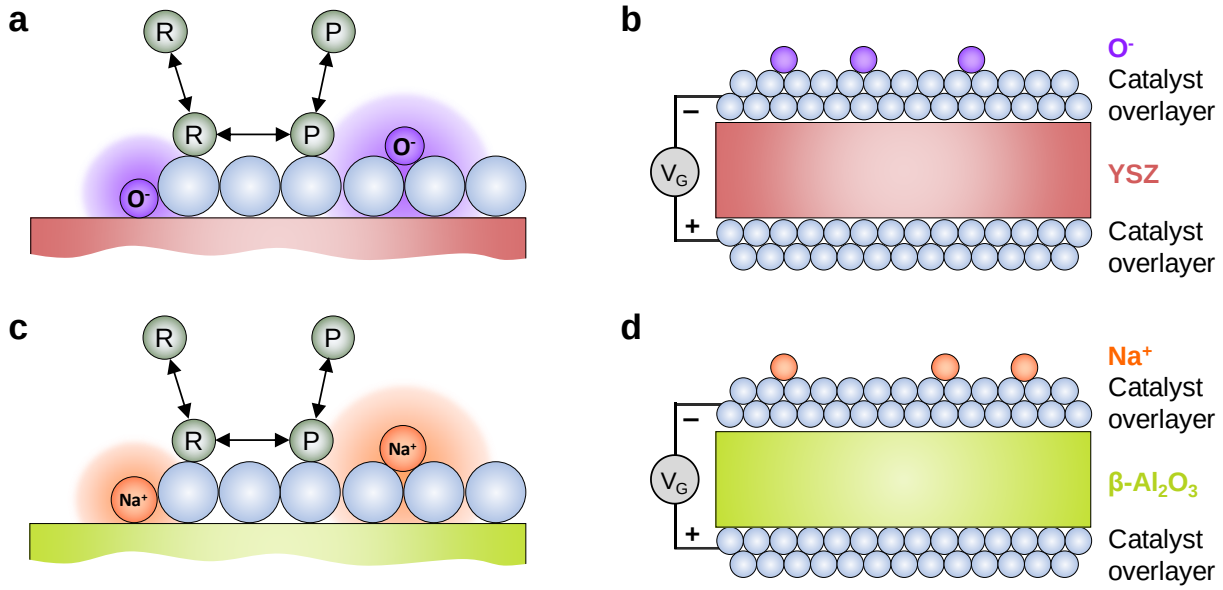

Figure 13. Non-faradaic modification of catalytic activity. **(a)** The presence of O^- atoms on a metal surface creates a local electric field and variation in the work function of the metal to alter surface binding energy and catalysis. **(b)** Oxygen atoms spill onto metal catalyst overlayers from yttrium-stabilized zirconia under electronic potential. **(c)** Sodium ions on a metal surface creates a local electric field and variation in the work function of the metal to alter surface binding energy and catalysis. **(d)** Sodium ions spill onto metal catalyst overlayers from β-Al_2O_3 under electronic potential.

other metals such as Ag[257], Rh, Pd, Ni, IrO_2, and RuO_2[258], with binding energy shifts of oxygen as high as 1.42 eV[253]. Surface modification has been shown to exhibit a significant shift in the work function of the metal catalyst (>0.5 eV)[259]. These strong surface manipulations with deposited ions at applied potential also enhance catalytic reactions, such as ethylene oxidation on Pt, which achieves a 50-fold rate increase at potentials above open circuit (no applied potential)[260].

Solid electrolytes have potential utility for dynamic catalysis due to the strength and mechanism of surface electronic modulation. Applied potential using sodium or oxygen ions produces large potentials even on metals, which are electron dense and more difficult to electronically manipulate than oxides or sulfides. Surface ions can spill onto metals over a broad range of temperature (as high as 400 °C) and strongly affect the catalyst in the gas phase, which is possible since the countercharge ions are provided to the catalytic surface from the support[259]. The breadth of choices for ions and solid electrolyte further increase the probability that they can be paired with a particular catalytic reaction. However, scaling these systems to large surface area will require new electrode design that also enhances the rate of ion transport in these solid electrolyte materials (e.g., YSZ), which are currently slower than required for dynamic catalytic resonance[259].

3.7 Catalytic Field-Effect Transistors (CATFET). Transistors are layered semiconductor devices that can amplify or switch electronic signals and electrical power using an externally controlled input voltage. These devices are typically made of selectively-doped silicon onto which three metallic contacts are deposited: a ‘gate’ to receive external input, a ‘source’ for incoming signal/power, and a ‘drain’ for outgoing signal/power. The gate voltage serves as a switch by electronically manipulating the ability of charge carriers to flow in the channel between the source and drain using a ‘field effect’, wherein the applied gate voltage induces an electric field across the device and countercharge in the channel. This accumulation of charge in the channel increases its conductivity, permitting signal or power to flow between the input and output terminals.[261,262]

The interest in using field-effect transistors (FET) beyond electronics applications arises from their ability to controllably manipulate the electronic characteristics of many different

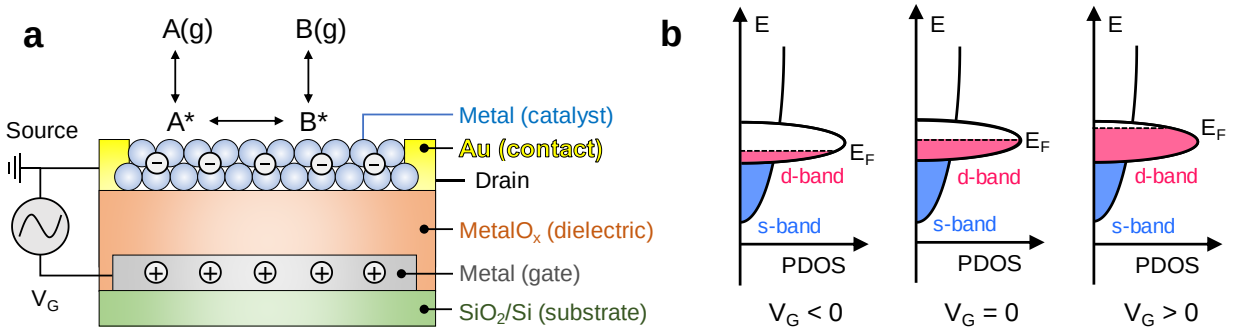

Figure 14. Catalytic Field-Effect Transistor (CATFET). **(a)** Multi-layer catalytic field-effect transistor consists of a substrate, a metal gate, metal oxide dielectric, and thin (<5 nm) catalyst layer. Catalyst layer is connected via gold electrodes to an oscillating voltage source, V_G. **(b)** Partial density of states of the thin metal catalyst layer. The application of positive or negative gate potential induces higher density of holes or electrons to raise or lower the Fermi level.

materials for catalysis and separations. Applying the field-effect transistor concept to catalysis to produce a CATFET (catalytic field effect transistor) requires altering the device geometry to expose the channel to the reacting bulk fluid. As depicted in **Figure 14a**, a multilayered CATFET is fabricated on a substrate (e.g., Si wafer), where a patterned metallic gate lies underneath an insulating dielectric layer (e.g., SiO_2). The catalytic channel, either a metal or semiconductor, is then supported on the insulating layer, and metallic contacts for the source and drain are deposited on either side of this layer. Under operation, an external voltage, V_G, is applied to the gate, resulting in capacitive charging; charge accumulation at the gate causes the dielectric to polarize *via* an internal electric field, inducing a screening countercharge (electrons or holes) in the catalytic channel. As depicted in the partial density of states of the CATFET metal layer (**Figure 14b**), changing gate voltages tunably varies the filling of the catalyst's *d*-band orbital as if changing between different catalytic materials. Thus, the gate voltage modulates the electronic occupation of the catalyst, manipulating the electron population of anti-bonding molecular orbitals between an adsorbate and the surface and thereby changing the extent of chemisorption bond strength.

Design of these devices must ultimately balance electronic and catalytic performance, thus determining the appropriate materials and their respective thickness for each layer. For example, thin, two-dimensional catalytic channels are required to ensure that the metals screening the electric field and accumulating charge are also the same metal atoms accessible for catalysis. While silicon is commonly used as the active channel in electronic applications, a wide range of metallic and semiconducting materials can be used when targeting catalytic activity for a reaction of interest; this includes many metal oxides or metal sulfides (e.g., TiO_2, ZnO, or MoS_2) and even noble metals such as Au.[263,264,265,266,267,268,269] The deposition methods for such materials includes atomic layer deposition (ALD), chemical vapor deposition (CVD), sputtering, e-beam evaporation, or conventional liquid phase techniques such as incipient-wetness impregnation (IWI) and strong electrostatic adsorption (SEA). The insulating dielectric layer can be generated as a thermal oxide or deposited using the aforementioned techniques. It is important to note that the active channel area required for catalysis will be orders of magnitude larger than that of a conventional FET, so the synthetic methods selected for preparing these devices will be critical in determining the quality, cohesion, and electronic performance of the dielectric-catalyst interface.

Further design considerations include maximizing the field-effect strength, as stronger field effects induce higher countercharge in the catalytic channel and thus stronger shifts in adsorbate binding energy. For this reason, the gate insulator material should have a large dielectric constant, *k*, to avoid dielectric breakdown and shorting of the CATFET device under high gate voltages. In terms of device design, this means replacing the conventional insulator, low *k* (~4) SiO_2, with transition metal oxides or nitrides (e.g., TiO_2, ZrO_2, and HfO_2) having much larger dielectric constants (~20); even stronger field-

effect transistors can be produced using paraelectrics and dielectrics with *k* greater than 100. The dielectric should further be as thin a layer as possible to maximize injected charge per volt of bias applied to the gate. An additional consideration is the valence electron count per atom in the catalytic channel. For CATFETs, metal oxide and metal sulfide catalytic channels are likely preferable to metallic catalysts, because they have large unit cells and thus fewer valence electrons per unit of surface area; the gate induced charge will therefore have a proportionally larger effect on the activity of metal oxides and sulfides than on pure metals or alloys. Finally, the contacts (i.e., source and drain) will ideally be inert to the chemistry of interest, or passivated (i.e., protected by an inert overlayer), to prevent unwanted additional or side reactions.

Tunable surfaces in FET devices have already shown performance benefits for applications including sensing, adsorption, and even catalysis. Several FETs with active oxide layers such as ZnO, V_2O_5, and MoS_2 have been demonstrated to respond to the chemical environment such as pH in the liquid phase and molecular gases O_2, N_2, H_2, H_2S, CH_4, and NH_3 in the vapor phase.[263,270–272] A recent publication even demonstrated that FETs can be used to detect COVID-19 in trace amounts as low as 1.0 fg/mL.[273] For reactions, these same active layers, as well as VSe_2, show tunable performance in the hydrogen evolution reaction (HER) and liquid phase redox chemistries such as ferrocene oxidation/ferrocenium reduction ($Fe \rightarrow Fe^+ + e^-$).[264,265,274,275] For these redox chemistries, the FET changes performance by varying the amount of electron density on the active surface, and thus changing the barrier for electron transfer from the FET to the reactants. Moving to electrocatalytic reactions, Frisbie, Neurock, and coworkers demonstrated a four-fold enhancement of exchange current density for HER on a two-dimensional MoS_2 CATFET; they proposed that this observed rate enhancement was caused by both lowering the barrier for electron transfer from FET to reactants and modulation of the binding energy of atomic hydrogen, which affects the Volmer and Heyrovsky steps of the HER mechanism. Performing DFT calculations to assess the change in binding energy of H* on MoS_2, they found that a -40 to 100 V range in gate voltage correlated to a 16 meV change in the binding energy of H*.[264]

Many opportunities exist for dynamic modulation of both binding energies and activation energies of surface reactions using CATFET devices. The main control of the device is through the applied gate voltage, which has ranged from -50 to 100 V in previous experiments.[265,266,274] This voltage can be modulated as high as ~1 MHz and maintain a consistent square, sinusoidal, sawtooth, or triangle waveform, allowing access to catalytically-relevant dynamic frequencies. The sensitivity of adsorbates to binding energy modulation from an applied gate voltage will also play a factor in rate enhancement. For example, while only ~4x rate enhancement has thus far been demonstrated for HER on MoS_2 using a CATFET, atomic hydrogen has been shown to be one of the less-responsive adsorbates to external electric fields on Ni(111) surfaces.[275] Other adsorbates such as CO, O, and OOH will be more sensitive to induced electric fields based on calculations for Pt(111);[276] this means that CATFETs show promise for a broad range of chemistries including the oxygen evolution reaction (OER), oxygen reduction reaction (ORR), CO oxidation, formic acid oxidation or decomposition, and methanol oxidation or decomposition.[50,277–279]

3.8 Dynamic Ferroelectrics. Ferroelectrics, such as niobates, titanates, and zirconates (for example, $BaTiO_3$, $PbTiO_3$, $SrTiO_3$ and $LiNbO_3$), are materials that have a macroscopic polarization (electric dipole moment per unit volume) that can be switched by an applied electric field.[280,281] The emergence of polarization is a consequence of the offsets in the centers of positive and negative charges in the bulk of a material along a crystallographic direction. This offset creates a charge imbalance that leads to bound surface charges on the free-standing ferroelectrics' surfaces; the surface charges can in turn modify the surface chemistry. The polarization in ferroelectrics emerge below a critical *Curie temperature*, T_c, and changes in catalytic activity at T_c of ferroelectrics were observed as early as 1952.[282] More significant effects are obtained when the ferroelectric insulators are used as catalyst supports. For example, not only are the catalytic activity of both silver and copper enhanced by a ferroelectric support,[283] but $BaTiO_3$ leads to a peak in ethylene conversion by nickel at its Curie Temperature.[284] The macroscopic polarization can be switched *by* an external electric field, allowing

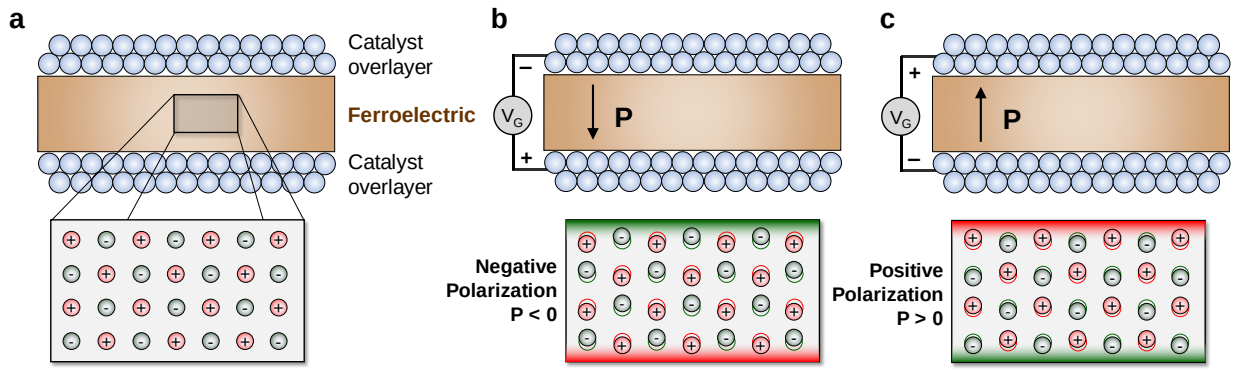

Figure 15. Ferroelectric-promoted dynamic catalysis. **(a)** Catalyst overlayers on both sides of a ferroelectric surface. **(b)** Application of an applied voltage, V_G, initiates atomic rearrangement and spontaneous polarization stabilizing charge in the catalytic overlayer. **(c)** Polarization is reversed at reverse applied voltage sufficiently strong to overcome the re-polarization energy barrier.

ferroelectrics to achieve fast switchable surface chemistry[285]. Differences in adsorption on opposing surfaces of ferroelectrics (positively or negative charged) have been shown in the adsorption of NO on Cu surfaces by the polarization direction of ferroelectric $LiNbO_3$ supports[283], or directly on the ferroelectric $PbTiO_3$ surface.[286] Therefore, rapid switching of ferroelectric polarization has the potential to quickly flip between binding states required for *dynamic* catalysis.

In addition to their spontaneous polarization, ferroelectric materials are also often used as high permittivity dielectrics for applications such as capacitors.[287] These applications exploit the enhanced dielectric constants of ferroelectrics near their Curie temperatures. While the spontaneous polarization disappears at the T_c, the proximity to the ferroelectric phase makes the material highly polarizable. This *paraelectric* mode of operation of the ferroelectric materials can also be used to obtain dynamic surface chemistry via an electric field, similar to the dielectrics discussed in the preceding section.

In the context of achieving *dynamic* catalysis, the polarization can greatly affect the charge transfer and separation in ferroelectric/semiconductor interfaces for back-gated electrochemical reactors and support catalytic active transition metals and oxides that influence the gas-surface interactions (**Figure 15**). For the former, polarization can be utilized to modulate the charge density in the catalyst layer that affects the catalytic properties.[264] This can help overcome limitations of low charge density transfer to the catalyst layer by metal oxides that inherently exhibit low dielectric constants.[264] For the latter, it has been shown through first principles calculations that the polarization can significantly affect the catalytic properties of the thin film catalysts.[288] The extent of these effects depends on the electronic structures of both the metal and the ferroelectrics.[289] For example, Kolpak et al., have shown that switching polarization direction from P^+ to P^- for $PbTiO_3$ changes the chemisorption energy for CO, C, O and N around 0.4 to 0.8 eV on a monolayer Pt film.[289] Dissociative adsorption of CO is adsorbed on ultra-thin Pt films on negatively poled $PbTiO_3$, that is otherwise not seen on bulk or supported Pt.[289] This is attributed to the availability of Pt-*d* states on negative poled surface near the Fermi level that enhance the adsorption of O, making the dissociation thermodynamically favorable.[289]

Physically implementing catalytic dynamics with ferroelectrics will first require that materials have sufficiently high T_C to enable high polarization at a catalytically relevant temperature (e.g., from a minimum of ~300 °C, to an optimal 350 °C). Multiple well-known oxide ferroelectrics with the so-called perovskite crystal structure (such as titanates, niobates, and zirconates) have T_C substantially in excess of room temperature, from $BaTiO_3$, for example (with T_C = 120 °C), to $PbTiO_3$ (with T_C ~ 500 °C) and $LiNbO_3$ (with T_C ~ 1140°C).[290,291] Second, the ferroelectric must be switchable at a reasonable working voltage, dictated by the ferroelectric thickness and the *coercive field*. The coercive field is the magnitude

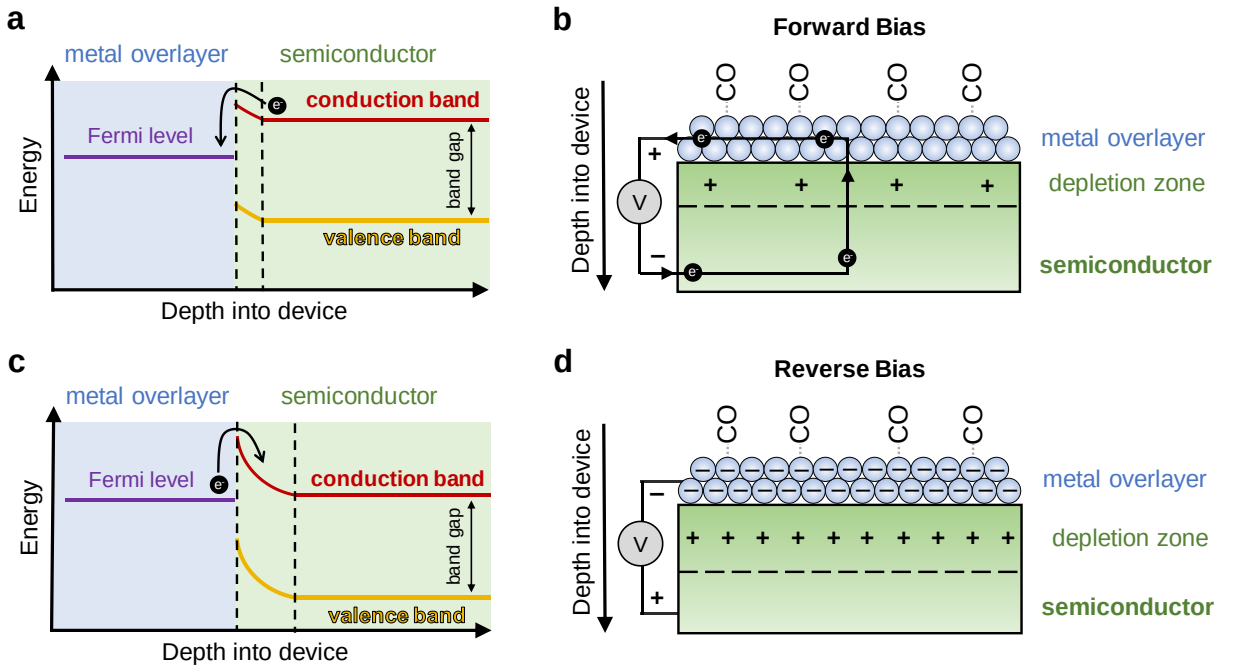

Figure 16. Schottky junctions and catalytic diodes. **(a-b)** Forward bias produces a low barrier for electrons passing from the semiconductor conduction band to the metal overlayer. **(c-d)** Reverse bias accumulates charge in the metal overlayer.

of the electric field required to switch the polarization, and it depends on the material composition, processing, as well as the operating temperature. Values of order 10-100 kV cm^{-1} are common in typical materials.[292] It is clear from DFT computations that large changes in adsorption energies can be achieved on thin film metals on ferroelectric oxides.[289] Using a dynamic approach, the surface can be oscillated between multiple polarization states where surface reaction and desorption are periodically enhanced or suppressed for specific reactions.[281] For example, such a dynamic strategy employed on CrO_2 monolayer supported on $PbTiO_3$ has been computationally shown to enhance NO_x decomposition and CO oxidation while circumventing oxygen and sulfur poisoning.[293]

3.9 Dynamic Catalytic Diodes and Schottky Junctions. The Schottky junction, named for Walter H. Schottky, describes the potential energy barrier formed at the interface between a semiconductor and metal, as depicted in **Figure 16a-16d**.[294–296,297] At this junction, the chemical potentials equilibrate, causing excess charge carriers in the semiconductor to flux into the metal; the semiconductor band edges bend until the center of the band gap matches the Fermi level of the metal[294] in a phenomenon called 'Fermi level pinning.'[298] Band bending creates a Schottky potential energy barrier at the interface; the height of this barrier can be readily manipulated by application of an external voltage, allowing for control of electron transport through the device and thus control of the electronic state of the metal. Under forward bias for the *n*-type device (**Figure 16a-16b**), the positive terminal is connected to the metal, and the negative terminal is connected to the semiconductor. The Schottky barrier height is reduced and thermally excited electrons in the semiconductor conduction band drop over the barrier and flow through the metal as a continuous current of hot electrons. Under reverse bias (**Figure 16c-16d**), band bending increases and electrons accumulate in the metal overlayer, unable to surmount the larger barrier. Both biases manipulate the interfacial electronic environment, forming a depletion zone in the semiconductor and modulating the electron density of the metal. With a thin metal layer, appreciable charge accumulation per metal active site could alter the binding energies of molecules to the metal and potentially enhance metal-catalyzed reactions.

Common Schottky diode materials include semiconductors such as ternary oxides (e.g.,

$PbTiO_3$), transition metal oxides (e.g., TiO_2), and transition metal nitrides (e.g., GaN), along with metals Pt, Pd, Ir, and Au, among others.[295,299–301] These devices have demonstrated performance in applications including sensing, adsorption, and catalysis. The most common reaction studied with these devices has been CO oxidation; CO has been used extensively to characterize the performance of Schottky diodes.[295,302–307] In one example, CO was adsorbed on a Pt/TiO_2 diode, and its adsorption was characterized using infrared spectroscopy. Various voltages were applied ranging from -2.0 to 2.0 V, and the IR wavelength of adsorbed CO was shown to shift by ~20-50 cm^{-1}.[307] Relating the IR wavelength shift directly to a change in the binding energy, the applied voltage shifted the binding energy of CO by ~2.5-6.2 meV (0.06-0.14 kcal/mol). This demonstrates that applying biases to alter the Schottky barrier height tunes the electronic occupation of the metal and thus controls the metal-adsorbate bond. Going beyond adsorption to catalysis, others have observed an increase in the oxidation rate of CO which correlated with the current through the Schottky diode. A study on a Pt/Si catalytic nanodiode observed a correlation between the turnover frequency of CO-to-CO_2 and applied bias, suggesting that the reverse bias-induced negative charge build-up on Pt enhances the reaction rate.[308]

Since the Schottky diode is modulated using an externally applied electric field, the bias voltage can be oscillated at catalytically-relevant frequencies between millihertz and megahertz with square, sinusoidal, triangular, or sawtooth waveforms depending on the capability of the waveform generator (e.g., oscilloscope). The maximum voltage amplitude is limited by the device integrity at the Schottky junction. Once the semiconductor breakdown voltage is exceeded under reverse bias, the device breaks down, sparks, and may form a persistent electric arc due to high current. The active metal layer may vaporize under these extreme conditions. Typical values for the negative breakdown voltage are in the range of -10 to -100 V, and the onset voltage for current generation under forward bias is about +0.2 to +0.5 V[294,309,310], depending on device design and construction.

In terms of device design, the material options are vast and include any *n*-type or *p*-type semiconductor and any metal. It has been observed that the metal selection has negligible effect on the Schottky barrier height, which could allow for the most catalytically-relevant metal to be used in a device.[298] These devices may be synthesized using a variety of techniques, often employing different methods to synthesize the semiconductor and the metal. Semiconductors are typically synthesized using chemical vapor deposition (CVD), colloidal nanoparticle growth, liquid phase epitaxy, and molecular beam epitaxy (MBE). Metals are then deposited or pasted onto the semiconductor using atomic layer deposition (ALD), strong electrostatic adsorption (SEA), CVD, and e-beam physical vapor deposition.[294,298] The synthesis technique is selected based on the desired thickness of the material, the desired material properties (e.g., crystallinity, defect density), and the device geometry. Moving forward, catalytic diodes are promising candidates for dynamic catalysis.

4.0 Implementing Dynamic Catalysis. Putting the mechanisms of dynamic catalysis into practice requires merging materials, chemistry, and oscillatory parameters and understanding the resulting catalytic performance. Building dynamic catalytic devices requires an understanding that different catalytic stimuli impose unique surface behavior which must be evaluated and optimized. Once in operation, oscillatory catalytic systems also require standardized performance metrics and control experiments. With these foundational concepts in place, the path forward to designing systems merges experiment, modeling, and optimization to address the most important problems in energy and materials.

4.1 Evaluating Catalytic Stimuli. To compare the different external dynamic stimuli, it is critical to quantify the sensitivity of the heat of adsorption (opposite of the binding energy) of individual adsorbates (gamma: γ parameter) towards external stimulus. The key comparison is the sensitivity of external stimuli relative to periodic trends in catalytic materials[276]; application of light, strain, or electric potential in many systems yields behavior significantly different from different catalysts. While the breadth of variability with different stimuli adds complexity to the dynamic catalyst design and selection process, it also adds opportunity for identifying a more efficient catalytic system. Development of linear scaling relationships that characterize the nature of stimuli are direct methods for making

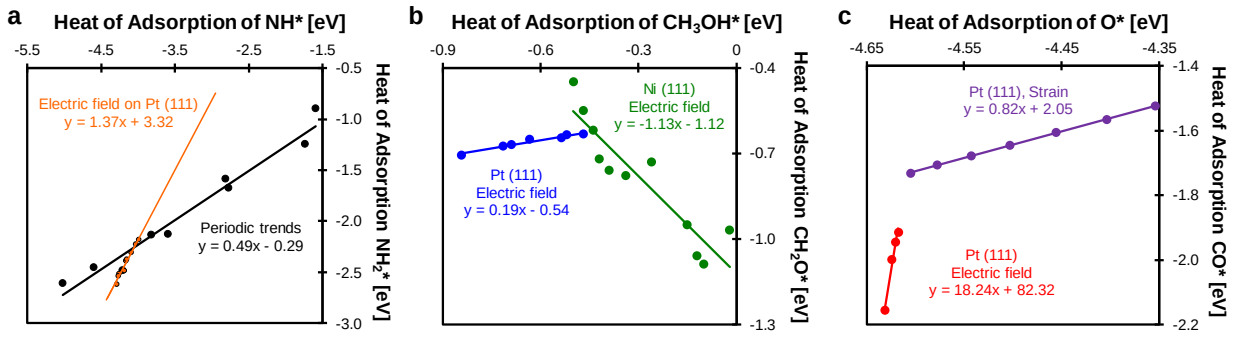

Figure 17. Linear scaling of adsorbates with catalytic stimuli. **(a)** Periodic trends with varying metals as compared to electric field on Pt (111) surface for the heat of adsorption of NH_2* versus NH*. **(b)** Adsorption with electric field on Ni (111) and Pt (111) surface for the heat of adsorption of methanol (CH_3OH*) versus formaldehyde (CH_2O**), and **(c)** Adsorption on Pt (111) surface for heat of adsorption of CO* versus O* with strain and electric field.

comparisons,[52,276,311] and microkinetic modeling (MKM) based on these relationships across different potential dynamic catalyst technologies will ultimately be the tool to predict new catalysts.[50,52]

Examples of the opportunity provided by different stimuli can already be found in the application of strain and electric fields to transition metals. As shown in **Figure 17a**, comparison of the periodic trends for the adsorption of NH_2* and NH* with the application of electric fields on Pt (111) surface both indicate positive scaling of $\gamma_{NH2*/NH*}$ of 0.49 and 1.37, respectively.[51,276,312–317] The divergence of the two linear relations indicates the potential for breaking periodic linear scaling relationships. In addition, the linear relationships (i.e., gamma parameters) are likely to be metal-dependent for the same external stimulus, as shown for distinct $\gamma_{CH2O2**/CH3OH*}$ on Ni (111) and Pt (111) surface (**Figure 17b**).[276,318] Notably, $\gamma_{CH2O2**/CH3OH*}$ has an opposite sign on Ni (111) and Pt (111) surfaces. Furthermore, gamma parameters are expected to be dependent on the nature of dynamic external stimuli, as shown for the different $\gamma_{CO*/O*}$ with strain and electric field on the Pt (111) surface (**Figure 17c**).[276,311] Interestingly, $\gamma_{CO*/O*}$ was ~22 times greater with electric field than with strain. These examples indicate that stimulus-derived linear scaling is likely to be both unique from periodic trends and catalyst-stimulus dependent, providing an optimization challenge for selecting the most effective combination.

Substantial effort is required to expand the collective base of knowledge on the different types of catalytic stimuli and their variation in surface control. For example, most calculations have been conducted on specific metal surfaces, but the dependence of scaling relationships on the different crystal facets, adsorption sites, and defects requires deeper investigation. In addition, the applicability of existing Brønsted–Evans–Polanyi (BEP) relationships under stimuli remains to be determined. Specifically, it is unknown whether such transition-state relationships under stimuli will be similar to periodic trends[318] or vary with catalyst-stimulating type/method. Understanding and predicting transition state energies and associated linear scaling relationships under catalyst stimulation remains a challenge in the next decade.

4.2. Dynamic Catalysis Metrics: Efficiency. To compare dynamic catalysis with other reaction engineering and catalyst design approaches, metrics must describe catalyst performance while accounting for the oscillatory behavior unique from static conditions. These metrics are intended to be generalizable across different reaction chemistries, catalyst systems, and reactor designs, permitting identification of oscillatory conditions that lead to the most effective use of materials and selected dynamic parameters.

In addition to the thermodynamic efficiency defined in equation 2, a second metric evaluates the ability of dynamic systems to enhance catalytic rate. For every cycle that an oscillatory catalyst turns over, an open question is the number of molecules that also catalytically turnover. A ‘turnover efficiency’ therefore compares the frequency of catalytic turnover frequency to the frequency of catalyst dynamics. This efficiency is calculated as described in equation 5, where the

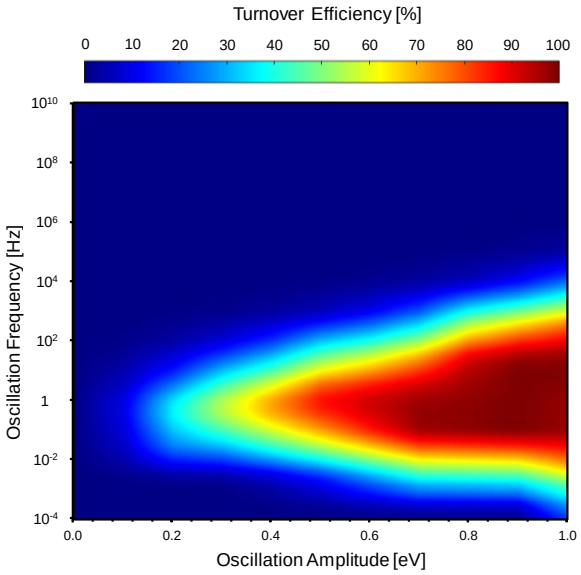

Figure 18. Turnover efficiency for the generic A-to-B reaction with varying oscillation amplitude and frequency. Dynamic conditions ranged from 0-1.0 eV and 10^{-4} to 10^{10} Hz. Reaction conditions were 150 °C, 100 bar A feed pressure, and 1% time-averaged yield of B.

turnover frequency (i.e., the apparent turnover frequency of the system) is divided by the oscillation frequency after subtracting the average steady state TOF.

$$Turnover\ efficiency\ (\%) = \frac{(Dynamic\ TOF) - (Average\ Steady\ State\ TOF)}{(Oscillation\ frequency)} \quad (5)$$

The reason for this subtractive correction of the 'average steady state TOF' arises from the mechanism of dynamic catalytic rate enhancement. As depicted in the volcano plot of **Figure 4a**, catalytic turnover frequency exists for any catalyst binding energy between the volcano plot itself (green dots in **Figure 4a**) and the extended inverted volcano plot (dashed lines with purple dots in **Figure 4a**); the actual performance depends on the applied frequency of catalytic oscillation. To determine the efficiency of the oscillation, the steady state turnover frequency consisting of the static volcano plot must be subtracted. For a catalytic system oscillating with a square waveform of 50% duty cycle (half the time spent at each endpoint), the 'average steady state TOF' is just the average of the two volcano plot points (green in **Figure 4a**).

As an example, the turnover efficiency was calculated for the dynamic catalytic system of **Figure 4** using the definition of equation 5. As depicted in **Figure 18**, the turnover efficiency of this high gamma ($\gamma_{B/A}$ ~ 2.0) A-to-B reaction exhibits the full range from completely inefficient to almost perfectly efficient dynamic performance. The band of efficient dynamic oscillation exists around ~1 Hz and widens with larger square waveform amplitude. The onset of efficient behavior occurs with the first corner frequency of **Figure 4b** and extends up to the start of the resonance band; in this region there exists an almost linear relationship between applied frequency and catalytic turnover frequency indicative of highly efficient dynamics. Inefficiency therefore derives from two sources: (i) at low oscillation frequencies, negligible rate enhancement occurs, and (ii) in the resonance band, the catalytic TOF stops increasing as the applied oscillation frequencies continue to increase.

4.3 Interpreting Dynamic Catalysis. Moving forward, discoveries for dynamic catalysis will focus on experimentally demonstrating rate, conversion, or selectivity enhancement for important reaction chemistries such as NH_3 synthesis and the partial oxidation of CH_4. Interpreting these experiments requires accounting for the observed behaviors by establishing benchmark experiments that separate dynamic catalyst behavior from experimental artifacts including deactivation, restructuring, and catalyst reduction/oxidation.[319,320] One effective experimental method is to 'bracket' experimental trials with time-on-stream as a benchmark steady state static condition. By regularly returning to this benchmark, dynamic enhancements will appear as reversible application of stimulus, while catalyst physical changes will result in failure to recover the benchmark catalytic performance.

The second suggested benchmarking experiment compares the time-averaged production rate under dynamic conditions with the static, steady state rate at both amplitude endpoints (U_{min} and U_{max}). As an example, an electrocatalysis system oscillating between 0 V and 0.6 V should compare the dynamic apparent turnover frequency with the steady state electrocatalytic rate at both 0 V and 0.6 V. This is demonstrated in **Figure 12c**, when a volcano versus applied voltage is observed for formic acid electro-oxidation on Pt with

dynamic rates observed above all fixed-voltage conditions.[50] To claim oscillatory rate enhancement, the observed time-averaged dynamic production rate needs to exceed the steady state rates obtained at either operating endpoint.

Finally, we urge caution in interpreting apparent activation energies ($E_{a,app}$) under dynamic catalytic conditions. Simulation has shown that the rate limiting step strongly depends on the oscillation frequency and endpoints, so $E_{a,app}$ will vary due to changing dynamic conditions. For simple mechanisms with only monomolecular elementary steps, the apparent activation energy equals a weighted sum of the activation energy for each elementary step, with the activation energies weighted by Campbell's degree of rate control (X_{RC}) for each step.[321] If the reaction includes bidentate surface species, bimolecular steps, or Eley-Rideal mechanisms, then this simple analysis will break down and caution is urged in interpreting the apparent activation energy without careful experiments to determine X_{RC} under various dynamic conditions.

4.4 The Path Forward for Dynamic Catalysts. The emerging challenge for catalysis dynamics is identifying the opportunities to pair surface chemistries with materials and stimulation methods and using enabling oscillation frequencies and amplitudes. While predicting behavior is possible with oscillatory microkinetic surface chemistry models, the absence of sufficient data and kinetic parameters to reliably predict permanently transient surface reactions prevents immediate progress. In particular, models require dynamic linear scaling relationships of adsorbates on different catalytic materials, sites, and stimuli, with γ and δ parameters for each combination of adsorbates in a reaction network connected by accessible transition states. The other open question for building microkinetic models remains the viability of transition state scaling relationships; do the same predictions of transition state energies based on surface reaction thermodynamics hold across different stimuli? Or will dynamic light, electricity, or stress each produce unique transition states as the adsorbed reactant and product species are bound more strongly or weakly to the surface? The breadth of information required for answering these questions and predicting dynamic catalytic enhancement requires a dedicated focus on data collection and computational prediction.

New experimental tools are also required to probe the dynamics of surfaces at the time scale of catalytic resonance (>1 Hz). While existing spectroscopic methods are able to characterize adsorbed surface species of static catalysts, new techniques are required measure changing surface coverage on the time scale of seconds or faster. This will likely require increased technique sensitivity as the sampling time will be significantly reduced, particularly if catalyst surfaces are to be evaluated above 10-100 Hz. It would also be instructive to characterize the catalyst itself under oscillatory conditions. Electronic or physical changes can already be quantified using devices like a Kelvin probe to measure the work function of a metal or techniques like adsorption to measure porosity of cavities and pores, but modifying these insightful techniques to achieve measuring rates comparable to catalytic resonance under reaction conditions will be challenging.

The integration of all of this data into dynamic predictive models is itself a challenge, as oscillatory multi-step microkinetic models are complex demanding simulations. As previously shown[52], dynamic microkinetic simulations solved using brute force conventional solvers can require orders of magnitude more computational time than conventional static microkinetic models, even for simple A-to-B surface reactions. Moreover, the introduction of dynamics approximately doubles the number of parameters to evaluate, making exhaustive evaluation of all kinetic parameter permutations impossible. Advancing predictive capability will require the use of more effective solution methods to more efficiently approach stable limit cycle solutions. Additionally, the extensive breadth of dynamic parameter space will require machine learning approaches to predict regions of operability leading to rate enhancement and selectivity control.

After promising dynamic systems are identified, the problem remains to synthesize the materials that will enable precise control of surfaces. Many of the proposed catalytic stimuli will require synthetic methods more akin to device manufacturing, potentially requiring more expensive synthetic techniques than conventional catalyst impregnation manufacturing. The challenge will be to produce these dynamic catalyst devices with sufficient surface area to supplant conventional catalytic materials (e.g., particles).

Lower surface area catalysts are potentially viable, since catalyst activity could be significantly higher, provided heat and mass transfer are controllable at these higher rates. These active surfaces must also be stable, even when operating at kilohertz frequencies continuously over their lifetime. And these surfaces must be amenable to industrial equipment, preferably with a three-dimensional active surface accessible by stimuli such as light and electricity. These added costs associated with making dynamic catalytic devices will ultimately be weighed against the new economic opportunities with improved selectivity control, new lower-cost chemical processing conditions, and utilization of currently stranded resources.

Despite these technical challenges, many of the most important catalytic chemistries exhibit behavior amenable to dynamic rate enhancement and are worth pursuing. For example, important energy reactions including the hydrogen evolution reaction (HER) and the oxygen evolution reaction (OER) both exhibit Sabatier volcanos across catalytic materials[322,323]. Faster, more efficient promotion of these reactions will enable energy storage and energy utilization as hydrogen. Additionally, the direct oxidation of methane remains a selectivity challenge, as activation of C-H bonds and subsequent oxidation to methanol competes with over-oxidation to carbon dioxide[324]. The ability to temporally control the extent of oxidation provides a new opportunity for selective, one-step utilization of abundant and distributed natural gas. And finally, the capability for both controlling surface chemistry and adding work could potentially drive thermodynamically unfavorable reactions such as ammonia synthesis. This key reaction for fertilizer, chemicals, and energy storage exhibits a distinct Sabatier maximum, which limits synthetic conditions to high temperature and expensively-high pressure[325]. Dynamic catalysts that power the reaction forward at low pressure can potentially reduce the cost of ammonia manufacture and scale down these process systems to distributed renewable wind and solar energy generation sites. Utilization of dynamic sites can address all of these problems and more in the near future.

Supporting Information. The supporting information is available containing the experimental methods and data of Figures 11 and 18.

Acknowledgements. We acknowledge financial support of the Catalysis Center for Energy Innovation, a U.S. Department of Energy - Energy Frontier Research Center under Grant DE-SC0001004. Sallye Gathmann acknowledges financial support from the National Science Foundation Graduate Research Fellowship under Grant No. CON-75851, project 00074041.

Keywords: Catalysis, dynamics, resonance

References

(1) Trapp, O.; Weber, S. K.; Bauch, S.; Hofstadt, W. High-Throughput Screening of Catalysts by Combining Reaction and Analysis. *Angew. Chemie Int. Ed.* **2007**, *46* (38), 7307–7310. https://doi.org/10.1002/anie.200701326.

(2) Ling, C.; Ouyang, Y.; Li, Q.; Bai, X.; Mao, X.; Du, A.; Wang, J. A General Two-Step Strategy–Based High-Throughput Screening of Single Atom Catalysts for Nitrogen Fixation. *Small Methods* **2019**, *3* (9), 1800376. https://doi.org/10.1002/smtd.201800376.

(3) Cho, H. J.; Ren, L.; Vattipalli, V.; Yeh, Y. H.; Gould, N.; Xu, B.; Gorte, R. J.; Lobo, R.; Dauenhauer, P. J.; Tsapatsis, M.; Fan, W. Renewable P-Xylene from 2,5-Dimethylfuran and Ethylene Using Phosphorus-Containing Zeolite Catalysts. *ChemCatChem* **2017**, *9* (3), 398–402. https://doi.org/10.1002/cctc.201601294.

(4) Beaudry, A. A.; Joyce, G. F. Directed Evolution of an RNA Enzyme. *Science (80-.).* **1992**, *257* (5070), 635 LP – 641. https://doi.org/10.1126/science.1496376.

(5) Kuchner, O.; Arnold, F. H. Directed Evolution of Enzyme Catalysts. *Trends Biotechnol.* **1997**, *15* (12), 523–530. https://doi.org/https://doi.org/10.1016/S0167-7799(97)01138-4.

(6) Darby, M. T.; Stamatakis, M.; Michaelides, A.; Sykes, E. C. H. Lonely Atoms with Special Gifts: Breaking Linear Scaling Relationships in Heterogeneous Catalysis with Single-Atom Alloys. *J. Phys. Chem.*

Lett. **2018**, *9* (18), 5636–5646. https://doi.org/10.1021/acs.jpclett.8b01888.

(7) Darby, M. T.; Réocreux, R.; Sykes, E. C. H.; Michaelides, A.; Stamatakis, M. Elucidating the Stability and Reactivity of Surface Intermediates on Single-Atom Alloy Catalysts. *ACS Catal.* **2018**, *8* (6), 5038–5050. https://doi.org/10.1021/acscatal.8b00881.

(8) Lucci, F. R.; Liu, J.; Marcinkowski, M. D.; Yang, M.; Allard, L. F.; Flytzani-Stephanopoulos, M.; Sykes, E. C. H. Selective Hydrogenation of 1,3-Butadiene on Platinum–Copper Alloys at the Single-Atom Limit. *Nat. Commun.* **2015**, *6* (1), 8550. https://doi.org/10.1038/ncomms9550.

(9) Liu, J.; Lucci, F. R.; Yang, M.; Lee, S.; Marcinkowski, M. D.; Therrien, A. J.; Williams, C. T.; Sykes, E. C. H.; Flytzani-Stephanopoulos, M. Tackling CO Poisoning with Single-Atom Alloy Catalysts. *J. Am. Chem. Soc.* **2016**, *138* (20), 6396–6399. https://doi.org/10.1021/jacs.6b03339.

(10) Yang, D.; Gaggioli, C. A.; Ray, D.; Babucci, M.; Gagliardi, L.; Gates, B. C. Tuning Catalytic Sites on Zr6O8 Metal–Organic Framework Nodes via Ligand and Defect Chemistry Probed with Tert-Butyl Alcohol Dehydration to Isobutylene. *J. Am. Chem. Soc.* **2020**, *142* (17), 8044–8056. https://doi.org/10.1021/jacs.0c03175.

(11) Dorneles de Mello, M.; Kumar, G.; Tabassum, T.; Jain, S. K.; Chen, T.-H.; Caratzoulas, S.; Li, X.; Vlachos, D. G.; Han, S.; Scott, S.; Dauenhauer, P. J.; Tsapatsis, M. Phosphonate-Modified UiO-66 Brønsted Acid Catalyst and Its Use in Dehydra-Decyclization of 2-Methyltetrahydrofuran to Pentadienes. *Angew. Chemie Int. Ed.* **2020**, *59* (2–9). https://doi.org/10.1002/anie.202001332.

(12) Verboekend, D.; Pérez-Ramírez, J. Design of Hierarchical Zeolite Catalysts by Desilication. *Catal. Sci. Technol.* **2011**, *1* (6), 879–890. https://doi.org/10.1039/c1cy00150g.

(13) Zhang, X.; Liu, D.; Xu, D.; Asahina, S.; Cychosz, K. A.; Agrawal, K. V.; Al Wahedi, Y.; Bhan, A.; Al Hashimi, S.; Terasaki, O.; Thommes, M.; Tsapatsis, M. Synthesis of Self-Pillared Zeolite Nanosheets by Repetitive Branching. *Science (80-.).* **2012**, *336* (6089), 1684 LP – 1687. https://doi.org/10.1126/science.1221111.

(14) Hunt, S. T.; Román-Leshkov, Y. Principles and Methods for the Rational Design of Core-Shell Nanoparticle Catalysts with Ultralow Noble Metal Loadings. *Acc. Chem. Res.* **2018**, *51* (5), 1054–1062. https://doi.org/10.1021/acs.accounts.7b00510.

(15) Alonso, D. M.; Wettstein, S. G.; Dumesic, J. A. Bimetallic Catalysts for Upgrading of Biomass to Fuels and Chemicals. *Chem. Soc. Rev.* **2012**, *41* (24), 8075–8098. https://doi.org/10.1039/c2cs35188a.

(16) Furukawa, S.; Komatsu, T. Intermetallic Compounds: Promising Inorganic Materials for Well-Structured and Electronically Modified Reaction Environments for Efficient Catalysis. *ACS Catal.* **2017**, *7* (1), 735–765. https://doi.org/10.1021/acscatal.6b02603.

(17) Dasgupta, A.; Rioux, R. M. Intermetallics in Catalysis: An Exciting Subset of Multimetallic Catalysts. *Catal. Today* **2019**, *330*, 2–15. https://doi.org/https://doi.org/10.1016/j.cattod.2018.05.048.

(18) Lanzafame, P.; Perathoner, S.; Centi, G.; Gross, S.; Hensen, E. J. M. Grand Challenges for Catalysis in the Science and Technology Roadmap on Catalysis for Europe: Moving Ahead for a Sustainable Future. *Catal. Sci. Technol.* **2017**, *7* (22), 5182–5194. https://doi.org/10.1039/c7cy01067b.

(19) Stassen, I.; De Vos, D.; Ameloot, R. Vapor-Phase Deposition and Modification of Metal–Organic Frameworks: State-of-the-Art and Future Directions. *Chem. - A Eur. J.* **2016**, *22* (41), 14452–14460. https://doi.org/10.1002/chem.201601921.

(20) Karim, W.; Tschupp, S. A.; Herranz, J.; Schmidt, T. J.; Ekinci, Y.; Van Bokhoven, J. A. State-of-the-Art Nanofabrication in Catalysis. *Chimia (Aarau).* **2017**, *71* (4), 160–169. https://doi.org/10.2533/chimia.2017.160.

(21) Iglesia, E. Consequences of Confinement for Catalysis Within Voids of Molecular Dimensions. In *Catalysis in Chemistry and Biology, Proceedings of the 24th International Solvany Conference on Chemistry*; Belgium, 2018; pp 148–155. https://doi.org/10.1142/9789813237179_0023.

(22) Sabatier. *La Catalyse En Chimie Organique*; Paris et Liege, 1920. https://doi.org/10.14375/np.9782369430186.

(23) Lipkowitz, K. B.; Boyd, D. B. *Reviews in Computational Chemistry*; John Wiley & Sons, Ltd, 2006; Vol. 12. https://doi.org/10.1002/9780470125892.

(24) Balandin, A. A.; Ferapontov, V. A.; Tolstopyatova, A. A. The Activity of Cadmium Oxide as a Catalyst for Hydrogen Dehydrogenation. *Bull. Acad. Sci. USSR Div. Chem. Sci.* **1960**, *9* (10), 1630–1636. https://doi.org/10.1007/BF00906559.

(25) Balandin, A. A. The Multiplet Theory of Catalysis - Energy Factors in Catalysis. *Russ. Chem. Rev.* **1964**, *33* (5), 258–275. https://doi.org/10.1070/rc1964v033n05abeh001407.

(26) Rootsaert, W. J. M.; Sachtler, W. M. H. Interaction of Formic Acid Vapour with Tungsten. *Zeitschrift fur Phys. Chemie* **1960**, *26* (1–2), 16–26. https://doi.org/10.1524/zpch.1960.26.1_2.016.

(27) Medford, A. J.; Vojvodic, A.; Hummelshøj, J. S.; Voss, J.; Abild-Pedersen, F.; Studt, F.; Bligaard, T.; Nilsson, A.; Nørskov, J. K. From the Sabatier Principle to a Predictive Theory of Transition-Metal Heterogeneous Catalysis. *J. Catal.* **2015**, *328*, 36–42. https://doi.org/https://doi.org/10.1016/j.jcat.2014.12.033.

(28) Vijh, A. K. Sabatier-Balandin Interpretation of the Catalytic Decomposition of Nitrous Oxide on Metal-Oxide Semiconductors. *J. Catal.* **1973**, *31* (1), 51–54. https://doi.org/https://doi.org/10.1016/0021-9517(73)90269-8.

(29) Vijh, A. K. Interpretation of Some Aspects of Catalytic Oxidation of Ammonia and Propylene by Semiconducting Oxides in Terms of Volcano-Shaped Plots. *J. Chim. Phys.* **1973**, *70*, 1444–1447. https://doi.org/10.1051/jcp/1973701444.

(30) Toulhoat, H.; Raybaud, P.; Kasztelan, S.; Kresse, G.; Hafner, J. Transition Metals to Sulfur Binding Energies Relationship to Catalytic Activities in HDS: Back to Sabatier with First Principle Calculations. *Catal. Today* **1999**, *50* (3–4), 629–636. https://doi.org/10.1016/S0920-5861(98)00497-0.

(31) Chianelli, R. R.; Berhault, G.; Raybaud, P.; Kasztelan, S.; Hafner, J.; Toulhoat, H. Periodic Trends in Hydrodesulfurization: In Support of the Sabatier Principle. *Appl. Catal. A Gen.* **2002**, *227* (1–2), 83–96. https://doi.org/10.1016/S0926-860X(01)00924-3.

(32) Ichikawa, S. Volcano-Shaped Curves in Heterogeneous Catalysis. *Chem. Eng. Sci.* **1990**, *45* (2), 529–535. https://doi.org/10.1016/0009-2509(90)87039-U.

(33) Logadottir, A.; Rod, T. H.; Nørskov, J. K.; Hammer, B.; Dahl, S.; Jacobsen, C. J. H. The Brønsted-Evans-Polanyi Relation and the Volcano Plot for Ammonia Synthesis over Transition Metal Catalysts. *J. Catal.* **2001**, *197* (2), 229–231. https://doi.org/10.1006/jcat.2000.3087.

(34) Vijh, A. Volcano Relationships in Catalytic Reactions on Oxides. *J. Catal.* **1974**, *33* (3), 385–391. https://doi.org/10.1016/0021-9517(74)90285-1.

(35) Barteau, M. A. Linear Free Energy Relationships for C1-Oxygenate Decomposition on Transition Metal Surfaces. *Catal. Letters* **1991**, *8* (2), 175–183. https://doi.org/10.1007/BF00764114.

(36) Kumar, G.; Nikolla, E.; Linic, S.; Medlin, J. W.; Janik, M. J. Multicomponent Catalysts: Limitations and Prospects. *ACS Catal.* **2018**, *8* (4), 3202–3208. https://doi.org/10.1021/acscatal.8b00145.

(37) Andersen, M.; Medford, A. J.; Nørskov, J. K.; Reuter, K. Scaling-Relation-Based Analysis of Bifunctional Catalysis: The Case for Homogeneous Bimetallic Alloys. *ACS Catal.* **2017**, *7* (6), 3960–3967. https://doi.org/10.1021/acscatal.7b00482.

(38) van den Reijen, J. E.; Versluis, W. C.; Kanungo, S.; d'Angelo, M. F.; de Jong, K. P.; de Jongh, P. E. From Qualitative to Quantitative Understanding of Support Effects on the Selectivity in Silver Catalyzed Ethylene Epoxidation. *Catal. Today* **2019**, *338*, 31–39. https://doi.org/10.1016/j.cattod.2019.04.049.

(39) Nawaz, Z. Light Alkane Dehydrogenation to Light Olefin Technologies: A Comprehensive Review. *Rev. Chem. Eng.* **2015**, *31* (5), 413–436. https://doi.org/10.1515/revce-2015-0012.

(40) Gogate, M. R. Methanol-to-Olefins Process Technology: Current Status and Future Prospects. *Pet. Sci. Technol.* **2019**, *37* (5), 559–565. https://doi.org/10.1080/10916466.2018.1555589.

(41) Hwang, A.; Bhan, A. Deactivation of Zeolites and Zeotypes in Methanol-to-Hydrocarbons Catalysis: Mechanisms and Circumvention. *Acc. Chem. Res.* **2019**, *52* (9), 2647–2656. https://doi.org/10.1021/acs.accounts.9b00204.

(42) Ravi, M.; Ranocchiari, M.; van Bokhoven, J. A. The Direct Catalytic Oxidation of Methane to Methanol—A Critical Assessment. *Angew. Chemie - Int. Ed.* **2017**, *56* (52), 16464–16483. https://doi.org/10.1002/anie.201702550.

(43) Saeidi, S.; Amin, N. A. S.; Rahimpour, M. R. Hydrogenation of CO2 to Value-Added Products - A Review and Potential Future Developments. *J. CO2 Util.* **2014**, *5*, 66–81. https://doi.org/10.1016/j.jcou.2013.12.005.

(44) Lee, M. Y.; Park, K. T.; Lee, W.; Lim, H.; Kwon, Y.; Kang, S. Current Achievements and the Future Direction of Electrochemical CO2 Reduction: A Short Review. *Crit. Rev. Environ. Sci. Technol.* **2020**, *50* (8), 769–815. https://doi.org/10.1080/10643389.2019.1631991.

(45) Wilson, N. M.; Flaherty, D. W. Mechanism for the Direct Synthesis of H2O2 on Pd Clusters: Heterolytic Reaction Pathways at the Liquid-Solid Interface. *J. Am. Chem. Soc.* **2016**, *138* (2), 574–586. https://doi.org/10.1021/jacs.5b10669.

(46) Flaherty, D. W. Direct Synthesis of H2O2 from H2 and O2 on Pd Catalysts: Current Understanding, Outstanding Questions, and Research Needs. *ACS Catal.* **2018**, *8* (2), 1520–1527. https://doi.org/10.1021/acscatal.7b04107.

(47) Lewis, R. J.; Hutchings, G. J. Recent Advances in the Direct Synthesis of H 2 O 2. *ChemCatChem* **2019**, *11* (1), 298–308. https://doi.org/10.1002/cctc.201801435.

(48) J. A. Dumesic L. M. Aparicio, J. E. Rekoske, and A. A. Treviño, D. F. R. *The Microkinetics of Heterogeneous Catalysis*; American Chemical Society, 1993.

(49) Ardagh, M. A.; Abdelrahman, O. A.; Dauenhauer, P. J. Principles of Dynamic Heterogeneous Catalysis: Surface Resonance and Turnover Frequency Response. *ACS Catal.* **2019**, *9* (8), 6929–6937. https://doi.org/10.1021/acscatal.9b01606.

(50) Gopeesingh, J.; Ardagh, M. A.; Shetty, M.; Burke, S.; Dauenhauer, P. J.; Abdelrahman, O. A. Resonance-Promoted Formic Acid Oxidation via Dynamic Electrocatalytic Modulation. *ACS Catal.* **2020**. https://doi.org/10.1021/acscatal.0c02201.

(51) Dauenhauer, P. J.; Ardagh, M. A.; Shetty, M.; Kuznetsov, A.; Zhang, Q.; Christopher, P.; Vlachos, D. G.; Abdelrahman, O. A. Catalytic Resonance Theory: Parallel Reaction Pathway Control. *Chem. Sci.* **2020**, *11* (13), 3501–3510. https://doi.org/10.1039/c9sc06140a.

(52) Ardagh, M. A.; Birol, T.; Zhang, Q.; Abdelrahman, O. A.; Dauenhauer, P. J. Catalytic Resonance Theory: SuperVolcanoes, Catalytic Molecular Pumps, and Oscillatory Steady State. *Catal. Sci. Technol.* **2019**, *9* (18), 5058–5076. https://doi.org/10.1039/c9cy01543d.

(53) Epstein, I. R.; Pojman, J. A.; Nicolis, G. *An Introduction to Nonlinear Chemical Dynamics: Oscillations, Waves, Patterns, and Chaos* ; Oxford University Press, 1999; Vol. 52. https://doi.org/10.1063/1.882734.

(54) Nicolis, G.; Portnow, J. Chemical Oscillations. *Chem. Rev.* **1973**, *73* (4), 365–

384. https://doi.org/10.1021/cr60284a003.
(55) Epstein, I. R.; Showalter, K. Nonlinear Chemical Dynamics: Oscillations, Patterns, and Chaos. *J. Phys. Chem.* **1996**, *100* (31), 13132–13147. https://doi.org/10.1021/jp953547m.
(56) Duan, P.; Chen, T.; Shah, S. L.; Yang, F. Methods for Root Cause Diagnosis of Plant-Wide Oscillations. *AIChE J.* **2014**, *60* (6), 2019–2034. https://doi.org/10.1002/aic.14391.
(57) Thornhill, N. F.; Huang, B.; Zhang, H. Detection of Multiple Oscillations in Control Loops. *J. Process Control* **2003**, *13* (1), 91–100. https://doi.org/10.1016/S0959-1524(02)00007-0.
(58) Huang, R.; Harinath, E.; Biegler, L. T. Lyapunov Stability of Economically Oriented NMPC for Cyclic Processes. *J. Process Control* **2011**, *21* (4), 501–509. https://doi.org/10.1016/j.jprocont.2011.01.012.
(59) Guardabassi, G.; Locatelli, A.; Rinaldi, S. Status of Periodic Optimization of Dynamical Systems. *J. Optim. Theory Appl.* **1974**, *14* (1), 1–20. https://doi.org/10.1007/BF00933171.
(60) Horn, F. J. M.; Lin, R. C. Periodic Processes: A Variational Approach. *Ind. Eng. Chem. Process Des. Dev.* **1967**, *6* (1), 21–30. https://doi.org/10.1021/i260021a005.
(61) Bai, P.; Etim, U. J.; Yan, Z.; Mintova, S.; Zhang, Z.; Zhong, Z.; Gao, X. Fluid Catalytic Cracking Technology: Current Status and Recent Discoveries on Catalyst Contamination. *Catal. Rev. - Sci. Eng.* **2019**, *61* (3), 333–405. https://doi.org/10.1080/01614940.2018.1549011.
(62) Maddah, H. A. A Comparative Study between Propane Dehydrogenation (PDH) Technologies and Plants in Saudi Arabia. *Am. Sci. Res. J. Eng. Technol. Sci.* **2018**, *45* (1), 49.
(63) Ishida, M.; Zheng, M.; Akehta, T. Evaluation of a Chemical Looping Combustion Power Generation System by Graphic Energy Analysis. *Energy* **1987**, *12*, 147–154.
(64) Bayham, S. C.; Tong, A.; Kathe, M.; Fan, L. S. Chemical Looping Technology for Energy and Chemical Production. *Wiley Interdiscip. Rev. Energy Environ.* **2016**, *5* (2), 216–241. https://doi.org/10.1002/wene.173.
(65) Bailey, J. E. Peridic Operation Of Chemical Reactors: A Review. *Chem. Eng. Commun.* **1974**, *1* (3), 111–124. https://doi.org/10.1080/00986447408960421.
(66) Sinčić, D.; Bailey, J. E. Pat-Hological Dynamic Behavior of Forced Periodic Chemical Processes. *Chem. Eng. Sci.* **1977**, *32* (3), 281–286. https://doi.org/10.1016/0009-2509(77)80206-6.
(67) Kalz, K. F.; Kraehnert, R.; Dvoyashkin, M.; Dittmeyer, R.; Gläser, R.; Krewer, U.; Reuter, K.; Grunwaldt, J. D. Future Challenges in Heterogeneous Catalysis: Understanding Catalysts under Dynamic Reaction Conditions. *ChemCatChem* **2017**, *9* (1), 17–29. https://doi.org/10.1002/cctc.201600996.
(68) Lotka, A. J. Analytical Note on Certain Rhythmic Relations in Organic Systems. *Proc. Natl. Acad. Sci.* **1920**, *6* (7), 410–415. https://doi.org/10.1073/pnas.6.7.410.
(69) Lotka, A. J. Contribution to the Theory of Periodic Reactions. *J. Phys. Chem.* **1910**, *14* (3), 271–274. https://doi.org/10.1021/j150111a004.
(70) Zaikin, A. N.; Zhabotinsky, A. M. Concentration Wave Propagation in Two-Dimensional Liquid-Phase Self-Oscillating System. *Nature* **1970**, *225* (5232), 535–537. https://doi.org/10.1038/225535b0.
(71) Bray, W. C. A Periodic Reaction in Homogeneous Solution and Its Relation to Catalysis. *J. Am. Chem. Soc.* **1921**, *43* (6), 1262–1267. https://doi.org/10.1021/ja01439a007.
(72) Bray, W. C.; Liebhafsky, H. A. Reactions Involving Hydrogen Peroxide, Iodine and Iodate Ion. I. Introduction. *J. Am. Chem. Soc.* **1931**, *53* (1), 38–44. https://doi.org/10.1021/ja01352a006.
(73) Briggs, T. S.; Rauscher, W. C. An Oscillating Iodine Clock. *J. Chem. Educ.* **1973**, *50* (7), 496. https://doi.org/10.1021/ed050p496.

(74) Sagués, F.; Epstein, I. R. Nonlinear Chemical Dynamics. *Dalt. Trans.* **2003**, No. 7, 1201–1217. https://doi.org/10.1039/b210932h.
(75) Ochs, T.; Turek, T. The Mechanism of Kinetic Oscillations in the Catalytic N2O Decomposition over Cu-ZSM-51. *Chem. Eng. Sci.* **1999**, *54* (20), 4513–4520. https://doi.org/10.1016/S0009-2509(98)00529-6.
(76) Ehsasi, M.; Frank, O.; Block, J. H.; Christmann, K. Coupled Chemical Oscillators in Catalytic Oxidation of CO on Pd(110) Surfaces. *Chem. Phys. Lett.* **1990**, *165* (2–3), 115–119. https://doi.org/10.1016/0009-2614(90)85414-8.
(77) Nettesheim, S.; Von Oertzen, A.; Rotermund, H. H.; Ertl, G. Reaction Diffusion Patterns in the Catalytic CO-Oxidation on Pt(110): Front Propagation and Spiral Waves. *J. Chem. Phys.* **1993**, *98* (12), 9977–9985. https://doi.org/10.1063/1.464323.
(78) Graham, M. D.; Kevrekidis, I. G.; Asakura, K.; Lauterbach, J.; Krischer, K.; Rotermund, H. H.; Ertl, G. Effects of Boundaries on Pattern Formation: Catalytic Oxidation of CO on Platinum. *Science (80-.).* **1994**, *264* (5155), 80–82. https://doi.org/10.1126/science.264.5155.80.
(79) Schüth, F.; Henry, B. E.; Schmidt, L. D. Oscillatory Reactions in Heterogeneous Catalysis. *Adv. Catal.* **1993**, *39* (C), 51–127. https://doi.org/10.1016/S0360-0564(08)60577-5.
(80) Imbihl, R.; Ertl, G. Oscillatory Kinetics in Heterogeneous Catalysis. *Chem. Rev.* **1995**, *95* (3), 697–733. https://doi.org/10.1021/cr00035a012.
(81) Takoudis, C. G.; Schmidt, L. D.; Aris, R. Isothermal Oscillations in Surface Reactions with Coverage Independent Parameters. *Chem. Eng. Sci.* **1982**, *37* (1), 69–76. https://doi.org/10.1016/0009-2509(82)80068-7.
(82) Mckarnin, M. A.; Aris, R.; Schmidt, L. D. K. Autonomous Bifurcations of a Simple Bimolecular Surface-Reaction Model. *Process Syst. Eng.* **1999**, *1* (C), 282–306. https://doi.org/10.1016/S1874-5970(99)80021-6.
(83) Sheintuch, M.; Luss, D. Application of Singularity Theory to Modelling of Steady-State Multiplicity: Propylene Oxidation on Platinum. *Ind. Eng. Chem. Res.* **1983**, *22*, 209–215.
(84) Eiswirth, M.; Krischer, K.; Ertl, G. Transition to Chaos in an Oscillating Surface Reaction. *Surf. Sci.* **1988**, *202* (3), 565–591. https://doi.org/10.1016/0039-6028(88)90053-2.
(85) Aris, R. *Mathematical Modeling: A Chemical Engineer's Perspective*; Academic Press: London, UK, 1999.
(86) Sheintucs, M.; Schmitz, H. A. Osciilations in Catalytic Reactions. *Catal. Rev.* **1977**, *15* (1), 107–172. https://doi.org/10.1080/03602457708081723.
(87) P L Silverton. *Composition Modulation of Catalytic Reactors*; CRC Press, 1998.
(88) Liu, T.; Temur, H.; Veser, G. Autothermal Reforming of Methane in a Reverse-Flow Reactor. *Chem. Eng. Technol.* **2009**, *32* (9), 1358–1366. https://doi.org/10.1002/ceat.200900203.
(89) Mitri, A.; Neumann, D.; Liu, T.; Veser, G. Reverse-Flow Reactor Operation and Catalyst Deactivation during High-Temperature Catalytic Partial Oxidation. *Chem. Eng. Sci.* **2004**, *59* (22–23), 5527–5534. https://doi.org/10.1016/j.ces.2004.07.104.
(90) Neumann, D.; Veser, G. Catalytic Partial Oxidation of Methane in a High-Temperature Reverse-Flow Reactor. *AIChE J.* **2005**, *51* (1), 210–223. https://doi.org/10.1002/aic.10284.
(91) Silveston, P. L.; Hudgins, R. R. Periodic Temperature Forcing of Catalytic Reactions. *Chem. Eng. Sci.* **2004**, *59* (19), 4043–4053. https://doi.org/10.1016/j.ces.2004.05.034.
(92) Dorawala, T. G.; Douglas, J. M. Complex Reactions in Oscillating Reactors. *AIChE J.* **1971**, *17* (4), 974–981. https://doi.org/10.1002/aic.690170434.
(93) Du, Y.; Sheng, H.; Astruc, D.; Zhu, M. Atomically Precise Noble Metal Nanoclusters as Efficient Catalysts: A

Bridge between Structure and Properties. *Chem. Rev.* **2020**, *120* (2), 526–622. https://doi.org/10.1021/acs.chemrev.8b00726.

(94) Liu, J. Catalysis by Supported Single Metal Atoms. *ACS Catal.* **2017**, *7* (1), 34–59. https://doi.org/10.1021/acscatal.6b01534.

(95) Fabbri, E.; Nachtegaal, M.; Binninger, T.; Cheng, X.; Kim, B.-J.; Durst, J.; Bozza, F.; Graule, T.; Schäublin, R.; Wiles, L.; Pertoso, M.; Danilovic, N.; Ayers, K. E.; Schmidt, T. J. Dynamic Surface Self-Reconstruction Is the Key of Highly Active Perovskite Nano-Electrocatalysts for Water Splitting. *Nat. Mater.* **2017**, *16* (9), 925–931. https://doi.org/10.1038/nmat4938.

(96) Lee, H.; Wu, X.; Sun, L. Copper-Based Homogeneous and Heterogeneous Catalysts for Electrochemical Water Oxidation. *Nanoscale* **2020**, *12* (7), 4187–4218. https://doi.org/10.1039/c9nr10437b.

(97) Montemore, M.M.; Medlin, J. W. Scaling Relations between Adsorption Energies for Computational Screening and Design of Catalysts. *Catal. Sci. Technol.* **2014**, *4*, 3748–3761. https://doi.org/10.1039/C4CY00335G.

(98) Wang, S.; Petzold, V.; Tripkovic, V.; Kleis, J.; Howalt, J. G.; Skúlason, E.; Fernández, E. M.; Hvolbæk, B.; Jones, G.; Toftelund, A.; Falsig, H.; Björketun, M.; Studt, F.; Abild-Pedersen, F.; Rossmeisl, J.; Nørskov, J. K.; Bligaard, T. Universal Transition State Scaling Relations for (de)Hydrogenation over Transition Metals. *Phys. Chem. Chem. Phys.* **2011**, *13* (46), 20760–20765. https://doi.org/10.1039/c1cp20547a.

(99) Sutton, J. E.; Vlachos, D. G. A Theoretical and Computational Analysis of Linear Free Energy Relations for the Estimation of Activation Energies. *ACS Catal.* **2012**, *2* (8), 1624–1634. https://doi.org/10.1021/cs3003269.

(100) Campbell, C. T.; Sellers, J. R. V. The Entropies of Adsorbed Molecules. *J. Am. Chem. Soc.* **2012**, *134* (43), 18109–18115. https://doi.org/10.1021/ja3080117.

(101) De Moor, B. A.; Reyniers, M. F.; Gobin, O. C.; Lercher, J. A.; Marin, G. B. Adsorption of C2-C8 n-Alkanes in Zeolites. *J. Phys. Chem. C* **2011**, *115* (4), 1204–1219. https://doi.org/10.1021/jp106536m.

(102) Eder, F.; Lercher, J. A. Alkane Sorption in Molecular Sieves: The Contribution of Ordering, Intermolecular Interactions, and Sorption on Brønsted Acid Sites. *Zeolites* **1997**, *18* (1), 75–81. https://doi.org/10.1016/S0144-2449(96)00127-3.

(103) Dauenhauer, P. J.; Abdelrahman, O. A. A Universal Descriptor for the Entropy of Adsorbed Molecules in Confined Spaces. *ACS Cent. Sci.* **2018**, *4* (9), 1235–1243. https://doi.org/10.1021/acscentsci.8b00419.

(104) Jennings, J. R. Catalytic Ammonia Synthesis. *Springer Sci. Bus. Media* **1991**, 451. https://doi.org/10.1007/978-1-4757-9592-9.

(105) Colby, J. L.; Dauenhauer, P. J.; Michael, B. C.; Bhan, A.; Schmidt, L. D. Improved Utilization of Biomass-Derived Carbon by Co-Processing with Hydrogen-Rich Feedstocks in Millisecond Reactors. *Green Chem.* **2010**, *12* (3), 378–38. https://doi.org/10.1039/b920387g.

(106) Grabow, L. C.; Mavrikakis, M. Mechanism of Methanol Synthesis on Cu through CO2 and CO Hydrogenation. *ACS Catal.* **2011**, *1* (4), 365–384. https://doi.org/10.1021/cs200055d.

(107) Pakhare, D.; Spivey, J. A Review of Dry (CO2) Reforming of Methane over Noble Metal Catalysts. *Chem. Soc. Rev.* **2014**, *43* (22), 7813–7837. https://doi.org/10.1039/c3cs60395d.

(108) Fu, Q.; Saltsburg, H.; Flytzani-Stephanopoulos, M. Active Nonmetallic Au and Pt Species on Ceria-Based Water-Gas Shift Catalysts. *Science (80-.).* **2003**, *301* (5635), 935–938. https://doi.org/10.1126/science.1085721.

(109) Ratnasamy, C.; Wagner, J. Water Gas Shift Catalysis. *Catal. Rev. - Sci. Eng.* **2009**, *51* (3), 325–440. https://doi.org/10.1080/01614940903048661.

(110) Newsome, D. S. The Water-Gas Shift Reaction. *Catal. Rev.* **1980**, *21* (2), 275–318. https://doi.org/10.1080/03602458008067535

5.
(111) Buelens, L. C.; Galvita, V. V.; Poelman, H.; Detavernier, C.; Marin, G. B. Super-Dry Reforming of Methane Intensifies CO2 Utilization via Le Chatelier's Principle. *Science (80-.).* **2016**, *354* (6311), 449–452. https://doi.org/10.1126/science.aah7161.
(112) Lin, W.; Murphy, C. J. A Demonstration of Le Chatelier's Principle on the Nanoscale. *ACS Cent. Sci.* **2017**, *3* (10), 1096–1102. https://doi.org/10.1021/acscentsci.7b00302.
(113) Suryanto, B. H. R.; Du, H.-L.; Wang, D.; Chen, J.; Simonov, A. N.; MacFarlane, D. R. Challenges and Prospects in the Catalysis of Electroreduction of Nitrogen to Ammonia. *Nat. Catal.* **2019**, *2* (4), 290–296. https://doi.org/10.1038/s41929-019-0252-4.
(114) Todd, D.; Schwager, M.; Mérida, W. Thermodynamics of High-Temperature, High-Pressure Water Electrolysis. *J. Power Sources* **2014**, *269*, 424–429. https://doi.org/10.1016/j.jpowsour.2014.06.144.
(115) Roger, I.; Shipman, M. A.; Symes, M. D. Earth-Abundant Catalysts for Electrochemical and Photoelectrochemical Water Splitting. *Nat. Rev. Chem.* **2017**, *1*. https://doi.org/10.1038/s41570-016-0003.
(116) Mehta, P.; Barboun, P.; Engelmann, Y.; Go, D. B.; Bogaerts, A.; Schneider, W. F.; Hicks, J. C. Plasma-Catalytic Ammonia Synthesis Beyond the Equilibrium Limit. *ACS Catal.* **2020**. https://doi.org/10.1021/acscatal.0c00684.
(117) Hoffmann, P. M. *Life's Ratchet. How Molecular Machines Extract Order from Chaos.*; Basic Books, 2012; Vol. 52. https://doi.org/10.1002/anie.201304031.
(118) Blackmond, D. G. "If Pigs Could Fly" Chemistry: A Tutorial on the Principle of Microscopic Reversibility. *Angew. Chemie - Int. Ed.* **2009**, *48* (15), 2648–2654. https://doi.org/10.1002/anie.200804566.
(119) Clayden, J. No Turning Back for Motorized Molecules. *Nature* **2016**, *534* (7606), 187–188. https://doi.org/10.1038/534187a.
(120) Wilson, M. R.; Solà, J.; Carlone, A.; Goldup, S. M.; Lebrasseur, N.; Leigh, D. A. An Autonomous Chemically Fuelled Small-Molecule Motor. *Nature* **2016**, *534* (7606), 235–240. https://doi.org/10.1038/nature18013.
(121) Carbonio, E. A.; Rocha, T. C. R.; Klyushin, A. Y.; Píš, I.; Magnano, E.; Nappini, S.; Piccinin, S.; Knop-Gericke, A.; Schlögl, R.; Jones, T. E. Are Multiple Oxygen Species Selective in Ethylene Epoxidation on Silver? *Chem. Sci.* **2018**, *9* (4), 990–998. https://doi.org/10.1039/c7sc04728b.
(122) Kuld, S.; Thorhauge, M.; Falsig, H.; Elkjær, C. F.; Helveg, S.; Chorkendorff, I.; Sehested, J. Quantifying the Promotion of Cu Catalysts by ZnO for Methanol Synthesis. *Science (80-.).* **2016**, *352* (6288), 969–974. https://doi.org/10.1126/science.aaf0718.
(123) Grabow, Lars C.; Gokhale, Amit A.; Evans, Steven T.; Dumesic, James A.; Mavrikakis, M. Mechanism of the Water Gas Shift Reaction on Pt: First Principles, Experiments, and Microkinetic Modeling. *J. Phys. Chem. C* **2008**, *112*, 4608–4617. https://doi.org/10.1021/jp7099702.
(124) Yoo, J. S.; Abild-Pedersen, F.; Nørskov, J. K.; Studt, F. Theoretical Analysis of Transition-Metal Catalysts for Formic Acid Decomposition. *ACS Catal.* **2014**, *4* (4), 1226–1233. https://doi.org/10.1021/cs400664z.
(125) Kandoi, S.; Greeley, J.; Sanchez-Castillo, M. A.; Evans, S. T.; Gokhale, A. A.; Dumesic, J. A.; Mavrikakis, M. Prediction of Experimental Methanol Decomposition Rates on Platinum from First Principles. *Top. Catal.* **2006**, *37* (1), 17–27. https://doi.org/10.1007/s11244-006-0001-1.
(126) Wojciechowski, B. W. The Reaction Mechanism of Catalytic Cracking: Quantifying Activity, Selectivity, and Catalyst Decay. *Catal. Rev. - Sci. Eng.* **1998**, *40* (3), 209–328. https://doi.org/10.1080/01614949808007110.
(127) Stefanidis, G. D.; Vlachos, D. G. Millisecond Methane Steam Reforming via Process and Catalyst Intensification. *Chem. Eng. Technol.* **2008**, *31* (8), 1201–1209. https://doi.org/10.1002/ceat.200800237.
(128) Ciuparu, D.; Lyubovsky, M. R.; Altman,

E.; Pfefferle, L. D.; Datye, A. Catalytic Combustion of Methane over Palladium-Based Catalysts. *Catal. Rev. - Sci. Eng.* **2002**, *44* (4), 593–649. https://doi.org/10.1081/CR-120015482.

(129) Toyao, T.; Maeno, Z.; Takakusagi, S.; Kamachi, T.; Takigawa, I.; Shimizu, K. I. Machine Learning for Catalysis Informatics: Recent Applications and Prospects. *ACS Catal.* **2020**, *10* (3), 2260–2297. https://doi.org/10.1021/acscatal.9b04186.

(130) Kitchin, J. R. Machine Learning in Catalysis. *Nat. Catal.* **2018**, *1* (4), 230–232. https://doi.org/10.1038/s41929-018-0056-y.

(131) Goyal, H.; Vlachos, D. G. Multiscale Modeling of Microwave-Heated Multiphase Systems. *Chem. Eng. J.* **2020**, *397*. https://doi.org/10.1016/j.cej.2020.125262.

(132) Stolte, J.; Özkan, L.; Thüne, P. C.; Niemantsverdriet, J. W.; Backx, A. C. P. M. Pulsed Activation in Heterogeneous Catalysis. *Appl. Therm. Eng.* **2013**, *57* (1–2), 180–187. https://doi.org/10.1016/j.applthermaleng.2012.06.035.

(133) Machado, E.; Buendia, G. M.; Rikvold, P. A.; Ziff, R. M. Response of a Catalytic Reaction to Periodic Variation of the CO Pressure: Increased CO 2 Production and Dynamic Phase Transition. *Phys. Rev. E - Stat. Nonlinear, Soft Matter Phys.* **2005**, *71* (1). https://doi.org/10.1103/PhysRevE.71.016120.

(134) Mavrikakis, M.; Hammer, B.; Nørskov, J. K. Effect of Strain on the Reactivity of Metal Surfaces. *Phys. Rev. Lett.* **1998**, *81* (13), 2819–2822. https://doi.org/10.1103/PhysRevLett.81.2819.

(135) Khorshidi, A.; Violet, J.; Hashemi, J.; Peterson, A. A. How Strain Can Break the Scaling Relations of Catalysis. *Nat. Catal.* **2018**, *1* (4), 263–268. https://doi.org/10.1038/s41929-018-0054-0.

(136) Kitchin, J. R. Correlations in Coverage-Dependent Atomic Adsorption Energies on Pd(111). *Phys. Rev. B* **2009**, *79* (20), 205412. https://doi.org/10.1103/PhysRevB.79.205412.

(137) Hwang, J.; Feng, Z.; Charles, N.; Wang, X. R.; Lee, D.; Stoerzinger, K. A.; Muy, S.; Rao, R. R.; Lee, D.; Jacobs, R.; Morgan, D.; Shao-Horn, Y. Tuning Perovskite Oxides by Strain: Electronic Structure, Properties, and Functions in (Electro)Catalysis and Ferroelectricity. *Mater. Today* **2019**, *31*, 100–118. https://doi.org/10.1016/j.mattod.2019.03.014.

(138) Kampshoff, E.; Hahn, E.; Kern, K. Correlation between Surface Stress and the Vibrational Shift of CO Chemisorbed on Cu Surfaces. *Phys. Rev. Lett.* **1994**, *73* (5), 704–707. https://doi.org/10.1103/PhysRevLett.73.704.

(139) Larsen, J. H.; Chorkendorff, I. Increased Dissociation Probability of CH4 on Co/Cu(111). *Surf. Sci.* **1998**, *405* (1), 62–73. https://doi.org/10.1016/S0039-6028(98)00045-4.

(140) Sethuraman, V. A.; Vairavapandian, D.; Lafouresse, M. C.; Adit Maark, T.; Karan, N.; Sun, S.; Bertocci, U.; Peterson, A. A.; Stafford, G. R.; Guduru, P. R. Role of Elastic Strain on Electrocatalysis of Oxygen Reduction Reaction on Pt. *J. Phys. Chem. C* **2015**, *119* (33), 19042–19052. https://doi.org/10.1021/acs.jpcc.5b06096.

(141) Schlapka, A.; Lischka, M.; Groß, A.; Käsberger, U.; Jakob, P. Surface Strain versus Substrate Interaction in Heteroepitaxial Metal Layers: Pt on Ru(0001). *Phys. Rev. Lett.* **2003**, *91* (1), 016101/1-016101/4. https://doi.org/10.1103/PhysRevLett.91.016101.

(142) Xu, Y.; Mavrikakis, M. Adsorption and Dissociation of O2 on Gold Surfaces: Effect of Steps and Strain. *J. Phys. Chem. B* **2003**, *107* (35), 9298–9307. https://doi.org/10.1021/jp034380x.

(143) Liu, F.; Wu, C.; Yang, G.; Yang, S. CO Oxidation over Strained Pt(100) Surface: A DFT Study. *J. Phys. Chem. C* **2015**, *119* (27), 15500–15505.

https://doi.org/10.1021/acs.jpcc.5b04511.
(144) Xu, Y.; Mavrikakis, M. Adsorption and Dissociation of O2 on Cu(1 1 1): Thermochemistry, Reaction Barrier and the Effect of Strain. *Surf. Sci.* **2001**, *494* (2), 131–144. https://doi.org/10.1016/S0039-6028(01)01464-9.
(145) Wang, L.; Zeng, Z.; Gao, W.; Maxson, T.; Raciti, D.; Giroux, M.; Pan, X.; Wang, C.; Greeley, J. Tunable Intrinsic Strain in Two-Dimensional Transition Metal Electrocatalysts. *Science (80-.).* **2019**, *363* (6429), 870–874. https://doi.org/10.1126/science.aat8051.
(146) Du, X.; Huang, J.; Zhang, J.; Yan, Y.; Wu, C.; Hu, Y.; Yan, C.; Lei, T.; Chen, W.; Fan, C.; Xiong, J. Modulating Electronic Structures of Inorganic Nanomaterials for Efficient Electrocatalytic Water Splitting. *Angew. Chemie - Int. Ed.* **2019**, *58* (14), 4484–4502. https://doi.org/10.1002/anie.201810104.
(147) Wang, H.; Xu, S.; Tsai, C.; Li, Y.; Liu, C.; Zhao, J.; Liu, Y.; Yuan, H.; Abild-Pedersen, F.; Prinz, F. B.; Nørskov, J. K.; Cui, Y. Direct and Continuous Strain Control of Catalysts with Tunable Battery Electrode Materials. *Science (80-.).* **2016**, *354* (6315), 1031–1036. https://doi.org/10.1126/science.aaf7680.
(148) Xu, J.; Dou, Y.; Wei, Z.; Ma, J.; Deng, Y.; Li, Y.; Liu, H.; Dou, S. Recent Progress in Graphite Intercalation Compounds for Rechargeable Metal (Li, Na, K, Al)-Ion Batteries. *Adv. Sci.* **2017**, *4* (10). https://doi.org/10.1002/advs.201700146.
(149) Muralidharan, N.; Brock, C. N.; Cohn, A. P.; Schauben, D.; Carter, R. E.; Oakes, L.; Walker, D. G.; Pint, C. L. Tunable Mechanochemistry of Lithium Battery Electrodes. *ACS Nano* **2017**, *11* (6), 6243–6251. https://doi.org/10.1021/acsnano.7b02404.
(150) Laipan, M.; Xiang, L.; Yu, J.; Martin, B. R.; Zhu, R.; Zhu, J.; He, H.; Clearfield, A.; Sun, L. Layered Intercalation Compounds: Mechanisms, New Methodologies, and Advanced Applications. *Prog. Mater. Sci.* **2020**, *109*. https://doi.org/10.1016/j.pmatsci.2019.100631.
(151) Hao, J.; Li, W.; Zhai, J.; Chen, H. Progress in High-Strain Perovskite Piezoelectric Ceramics. *Mater. Sci. Eng. R Reports* **2019**, *135*, 1–57. https://doi.org/10.1016/j.mser.2018.08.001.
(152) Zhao, Z. H.; Dai, Y.; Huang, F. The Formation and Effect of Defect Dipoles in Lead-Free Piezoelectric Ceramics: A Review. *Sustain. Mater. Technol.* **2019**, *20*. https://doi.org/10.1016/j.susmat.2019.e00092.
(153) Hu, C.; Meng, X.; Zhang, M. H.; Tian, H.; Daniels, J. E.; Tan, P.; Huang, F.; Li, L.; Wang, K.; Li, J. F.; Lu, Q.; Cao, W.; Zhou, Z. Ultra-Large Electric Field-Induced Strain in Potassium Sodium Niobate Crystals. *Sci. Adv.* **2020**, *6* (13). https://doi.org/10.1126/sciadv.aay5979.
(154) Zhang, Y.; Sun, H.; Chen, W. A Brief Review of Ba(Ti0.8Zr0.2)O3-(Ba0.7Ca0.3)TiO3 Based Lead-Free Piezoelectric Ceramics: Past, Present and Future Perspectives. *J. Phys. Chem. Solids* **2018**, *114*, 207–219. https://doi.org/10.1016/j.jpcs.2017.10.041.
(155) Wu, H.; Zhang, Y.; Wu, J.; Wang, J.; Pennycook, S. J. Microstructural Origins of High Piezoelectric Performance: A Pathway to Practical Lead-Free Materials. *Adv. Funct. Mater.* **2019**, *29* (33). https://doi.org/10.1002/adfm.201902911.
(156) Johnson, B.; Guduru, P. R.; Peterson, A. A. Strain-Induced Changes to the Methanation Reaction on Thin-Film Nickel Catalysts. *Catal. Sci. Technol.* **2019**, *9* (12), 3279–3286. https://doi.org/10.1039/c9cy00735k.
(157) Yan, K.; Kim, S. K.; Khorshidi, A.; Guduru, P. R.; Peterson, A. A. High Elastic Strain Directly Tunes the Hydrogen Evolution Reaction on Tungsten Carbide. *J. Phys. Chem. C* **2017**, *121* (11), 6177–6183. https://doi.org/10.1021/acs.jpcc.7b00281.
(158) Inoue, Y. Acoustic Enhancement of Surface Reactions. *MRS Bull.* **2019**, *44* (5), 361–371. https://doi.org/10.1557/mrs.2019.106.
(159) Nishiyama, H.; Inoue, Y. PEEM Study of Work Function Changes in Cu, Au and Pd Metal Surfaces with Surface Acoustic Wave Propagation. *Surf. Sci.* **2006**, *600*

(13), 2644–2649. https://doi.org/10.1016/j.susc.2006.03.047.
(160) Inoue, Y. Effects of Acoustic Waves-Induced Dynamic Lattice Distortion on Catalytic and Adsorptive Properties of Metal, Alloy and Metal Oxide Surfaces. *Surf. Sci. Rep.* **2007**, *62* (8), 305–336. https://doi.org/10.1016/j.surfrep.2007.01.001.
(161) Inoue, Y.; Matsukawa, M.; Sato, K. Effect of Surface Acoustic Wave Generated on Ferroelectric Support upon Catalysis. *J. Am. Chem. Soc.* **1989**, *111* (24), 8965–8966. https://doi.org/10.1021/ja00206a055.
(162) Nishiyama, H.; Saito, N.; Shima, M.; Watanabe, Y.; Inoue, Y. Effects of Acoustic Waves on Activation of Thin Film Pd and Ni Catalysts for Ethanol and CO Oxidation. *Faraday Discuss.* **1997**, *107*, 425–434. https://doi.org/10.1039/a703302h.
(163) Saito, N.; Nishiyama, H.; Sato, K.; Inoue, Y. Artificial Control of Selectivity for Ethanol Decomposition on a Ag Catalyst by Thickness-Extensional Mode Resonance Oscillation of z-Cut LiNbO3. *Chem. Phys. Lett.* **1998**, *297* (1–2), 72–76. https://doi.org/10.1016/S0009-2614(98)01095-1.
(164) Kelling, S.; Mitrelias, T.; Matsumoto, Y.; Ostanin, V. P.; King, D. A. Influence of Acoustic Wave Excitation on CO Oxidation over a Pt{110} Single Crystal. *Faraday Discuss.* **1997**, *107*, 435–444. https://doi.org/10.1039/a703246c.
(165) An, Q.; Qian, J.; Nielsen, R. R.; Sementa, L.; Barcaro, G.; Negreiros, F. R.; Fortunelli, A.; Goddard III, W. A. The Quantum Mechanics Derived Atomistic Mechanism Underlying the Acceleration of Catalytic CO Oxidation on Pt(110) by Surface Acoustic Waves. *J. Mater. Chem. A* **2016**, *4* (31), 12036–12045. https://doi.org/10.1039/c6ta03669d.
(166) Saito, N.; Ohkawara, Y.; Watanabe, Y.; Inoue, Y. Anomalous Enhancement of Catalytic Activity over a Pd Thin Film by the Effects of Resonance Oscillation Generated on a Ferroelectric Substrate. *Appl. Surf. Sci.* **1997**, *121–122*, 343–346. https://doi.org/10.1016/S0169-4332(97)00323-1.
(167) Yukawa, Y.; Saito, N.; Nishiyama, H.; Inoue, Y. Promotion of Partial Oxidation of Methanol over Thin Pt and Pd Film Catalysts by Resonance Oscillation of Acoustic Waves. *Appl. Surf. Sci.* **2005**, *250* (1–4), 104–108. https://doi.org/10.1016/j.apsusc.2004.12.038.
(168) Treacy, M. M. J.; Foster, M. D. Packing Sticky Hard Spheres into Rigid Zeolite Frameworks. *Microporous Mesoporous Mater.* **2009**, *118* (1–3), 106–114. https://doi.org/10.1016/j.micromeso.2008.08.039.
(169) Pang, S. H.; Schoenbaum, C. A.; Schwartz, D. K.; Medlin, J. W. Directing Reaction Pathways by Catalyst Active-Site Selection Using Self-Assembled Monolayers. *Nat. Commun.* **2013**, *4*. https://doi.org/10.1038/ncomms3448.
(170) Horike, S.; Shimomura, S.; Kitagawa, S. Soft Porous Crystals. *Nat. Chem.* **2009**, *1* (9), 695–704. https://doi.org/10.1038/nchem.444.
(171) Furukawa, H.; Cordova, K. E.; O'Keeffe, M.; Yaghi, O. M. The Chemistry and Applications of Metal-Organic Frameworks. *Science (80-.).* **2013**, *341* (6149). https://doi.org/10.1126/science.1230444.
(172) Férey, G.; Serre, C. Large Breathing Effects in Three-Dimensional Porous Hybrid Matter: Facts, Analyses, Rules and Consequences. *Chem. Soc. Rev.* **2009**, *38* (5), 1380–1399. https://doi.org/10.1039/b804302g.
(173) Kuznicki, S. M.; Bell, V. A.; Nair, S.; Hillhouse, H. W.; Jacubinas, R. M.; Braunbarth, C. M.; Toby, B. H.; Tsapatsis, M. A Titanosilicate Molecular Sieve with Adjustable Pores for Size-Selective Adsorption of Molecules. *Nature* **2001**, *412* (6848), 720–724. https://doi.org/10.1038/35089052.
(174) Kitagawa, S.; Kondo, M. Functional Micropore Chemistry of Crystalline Metal Complex-Assembled Compounds. *Bull. Chem. Soc. Jpn.* **1998**, *71* (8), 1739–1753. https://doi.org/10.1246/bcsj.71.1739.
(175) Evans, J. D.; Bon, V.; Senkovska, I.; Lee,

H. C.; Kaskel, S. Four-Dimensional Metal-Organic Frameworks. *Nat. Commun.* **2020**, *11* (1), 2690. https://doi.org/10.1038/s41467-020-16527-8.

(176) Schneemann, A.; Bon, V.; Schwedler, I.; Senkovska, I.; Kaskel, S.; Fischer, R. A. Flexible Metal-Organic Frameworks. *Chem. Soc. Rev.* **2014**, *43* (16), 6062–6096. https://doi.org/10.1039/c4cs00101j.

(177) Kitaura, R.; Seki, K.; Akiyama, G.; Kitagawa, S. Porous Coordination-Polymer Crystals with Gated Channels Specific for Supercritical Gases. *Angew. Chemie - Int. Ed.* **2003**, *42* (4), 428–431. https://doi.org/10.1002/anie.200390130.

(178) Chen, B.; Liang, C.; Yang, J.; Contreras, D. S.; Clancy, Y. L.; Lobkovsky, E. B.; Yaghi, O. M.; Dai, S. A Microporous Metal-Organic Framework for Gas-Chromatographic Separation of Alkanes. *Angew. Chemie - Int. Ed.* **2006**, *45* (9), 1390–1393. https://doi.org/10.1002/anie.200502844.

(179) Serre, C.; Millange, F.; Thouvenot, C.; Noguès, M.; Marsolier, G.; Louër, D.; Férey, G. Very Large Breathing Effect in the First Nanoporous Chromium(III)-Based Solids: MIL-53 or CrIII(OH)·{O2C-C6H4-CO2}·{HO2C-C6H4 -CO2H}x·H2Oy. *J. Am. Chem. Soc.* **2002**, *124* (45), 13519–13526. https://doi.org/10.1021/ja0276974.

(180) Murdock, C. R.; Hughes, B. C.; Lu, Z.; Jenkins, D. M. Approaches for Synthesizing Breathing MOFs by Exploiting Dimensional Rigidity. *Coord. Chem. Rev.* **2014**, *258–259* (1), 119–136. https://doi.org/10.1016/j.ccr.2013.09.006.

(181) Banerjee, R.; Phan, A.; Wang, B.; Knobler, C.; Furukawa, H.; O'Keeffe, M.; Yaghi, O. M. High-Throughput Synthesis of Zeolitic Imidazolate Frameworks and Application to CO2 Capture. *Science (80-.).* **2008**, *319* (5865), 939–943. https://doi.org/10.1126/science.1152516.

(182) Verploegh, R. J.; Nair, S.; Sholl, D. S. Temperature and Loading-Dependent Diffusion of Light Hydrocarbons in ZIF-8 as Predicted Through Fully Flexible Molecular Simulations. *J. Am. Chem. Soc.* **2015**, *137* (50), 15760–15771. https://doi.org/10.1021/jacs.5b08746.

(183) Coudert, F. X. Molecular Mechanism of Swing Effect in Zeolitic Imidazolate Framework ZIF-8: Continuous Deformation upon Adsorption. *ChemPhysChem* **2017**, *18* (19), 2732–2738. https://doi.org/10.1002/cphc.201700463.

(184) Haldoupis, E.; Watanabe, T.; Nair, S.; Sholl, D. S. Quantifying Large Effects of Framework Flexibility on Diffusion in MOFs: CH4 and CO2 in ZIF-8. *ChemPhysChem* **2012**, *13* (15), 3449–3452. https://doi.org/10.1002/cphc.201200529.

(185) Tan, N. Y.; Ruggiero, M. T.; Orellana-Tavra, C.; Tian, T.; Bond, A. D.; Korter, T. M.; Fairen-Jimenez, D.; Zeitler, J. A. Investigation of the Terahertz Vibrational Modes of ZIF-8 and ZIF-90 with Terahertz Time-Domain Spectroscopy. *Chem. Commun.* **2015**, *51* (89), 16037–16040. https://doi.org/10.1039/c5cc06455d.

(186) Russell, B.; Villaroel, J.; Sapag, K.; Migone, A. D. O2 Adsorption on ZIF-8: Temperature Dependence of the Gate-Opening Transition. *J. Phys. Chem. C* **2014**, *118* (49), 28603–28608. https://doi.org/10.1021/jp508382v.

(187) Zhang, L.; Hu, Z.; Jiang, J. Sorption-Induced Structural Transition of Zeolitic Imidazolate Framework-8: A Hybrid Molecular Simulation Study. *J. Am. Chem. Soc.* **2013**, *135* (9), 3722–3728. https://doi.org/10.1021/ja401129h.

(188) Gücüyener, C.; van den Bergh, J.; Gascon, J.; Kapteijn, F. Ethane/Ethene Separation Turned on Its Head: Selective Ethane Adsorption on the Metal-Organic Framework ZIF-7 through a Gate-Opening Mechanism. *J. Am. Chem. Soc.* **2010**, *132* (50), 17704–17706. https://doi.org/10.1021/ja1089765.

(189) Zhang, C.; Gee, J. A.; Sholl, D. S.; Lively, R. P. Crystal-Size-Dependent Structural Transitions in Nanoporous Crystals: Adsorption-Induced Transitions in ZIF-8. *J. Phys. Chem. C* **2014**, *118* (35), 20727–20733. https://doi.org/10.1021/jp5081466.

(190) Modrow, A.; Zargarani, D.; Herges, R.; Stock, N. The First Porous MOF with Photoswitchable Linker Molecules. *Dalt. Trans.* **2011**, *40* (16), 4217–4222.

https://doi.org/10.1039/c0dt01629b.
(191) Brown, J. W.; Henderson, B. L.; Kiesz, M. D.; Whalley, A. C.; Morris, W.; Grunder, S.; Deng, H.; Furukawa, H.; Zink, J. I.; Stoddart, J. F.; Yaghi, O. M. Photophysical Pore Control in an Azobenzene-Containing Metal-Organic Framework. *Chem. Sci.* **2013**, *4* (7), 2858–2864. https://doi.org/10.1039/c3sc21659d.
(192) Liu, Y.; Her, J. H.; Dailly, A.; Ramirez-Cuesta, A. J.; Neumann, D. A.; Brown, C. M. Reversible Structural Transition in MIL-53 with Large Temperature Hysteresis. *J. Am. Chem. Soc.* **2008**, *130* (35), 11813–11818. https://doi.org/10.1021/ja803669w.
(193) Walker, A. M.; Civalleri, B.; Slater, B.; Mellot-Draznieks, C.; Corà, F.; Zicovich-Wilson, C. M.; Román-Pérez, G.; Soler, J. M.; Gale, J. D. Flexibility in a Metal-Organic Framework Material Controlled by Weak Dispersion Forces: The Bistability of MIL-53(Al). *Angew. Chemie - Int. Ed.* **2010**, *49* (41), 7501–7503. https://doi.org/10.1002/anie.201002413.
(194) Tan, J. C.; Cheetham, A. K. Mechanical Properties of Hybrid Inorganic–Organic Framework Materials: Establishing Fundamental Structure–Property Relationships. *Chem. Soc. Rev.* **2011**, *40* (2), 1059–1080. https://doi.org/10.1039/c0cs00163e.
(195) Chapman, K. W.; Sava, D. F.; Halder, G. J.; Chupas, P. J.; Nenoff, T. M. Trapping Guests within a Nanoporous Metal–Organic Framework through Pressure-Induced Amorphization. *J. Am. Chem. Soc.* **2011**, *133* (46), 18583–18585. https://doi.org/10.1021/ja2085096.
(196) Ghoufi, A.; Benhamed, K.; Boukli-Hacene, L.; Maurin, G. Electrically Induced Breathing of the MIL-53(Cr) Metal-Organic Framework. *ACS Cent. Sci.* **2017**, *3* (5), 394–398. https://doi.org/10.1021/acscentsci.6b00392.
(197) Knebel, A.; Geppert, B.; Volgmann, K.; Kolokolov, D. I.; Stepanov, A. G.; Twiefel, J.; Heitjans, P.; Volkmer, D.; Caro, J. Defibrillation of Soft Porous Metal-Organic Frameworks with Electric Fields. *Science (80-.).* **2017**, *358* (6361), 347–351. https://doi.org/10.1126/science.aal2456.
(198) Schmid, R. An Electric Field Induced Breath for Metal-Organic Frameworks. *ACS Cent. Sci.* **2017**, *3* (5), 369–371. https://doi.org/10.1021/acscentsci.7b00162.
(199) Kolesnikov, A. L.; Budkov, Y. A.; Möllmer, J.; Kiselev, M. G.; Gläser, R. Metal–Organic Framework Breathing in the Electric Field: A Theoretical Study. *J. Phys. Chem. C* **2019**, *123* (16), 10333–10338. https://doi.org/10.1021/acs.jpcc.8b11630.
(200) Dürholt, J. P.; Jahromi, B. F.; Schmid, R. Tuning the Electric Field Response of MOFs by Rotatable Dipolar Linkers. *ACS Cent. Sci.* **2019**, *5* (8), 1440–1448. https://doi.org/10.1021/acscentsci.9b00497.
(201) Wang, X. D.; Graugnard, E.; King, J. S.; Wang, Z. L.; Summers, C. J. Large-Scale Fabrication of Ordered Nanobowl Arrays. *Nano Lett.* **2004**, *4* (11), 2223–2226. https://doi.org/10.1021/nl048589d.
(202) Ray, N. A.; Van Duyne, R. P.; Stair, P. C. Synthesis Strategy for Protected Metal Nanoparticles. *J. Phys. Chem. C* **2012**, *116* (14), 7748–7756. https://doi.org/10.1021/jp210688z.
(203) Canlas, C. P.; Lu, J.; Ray, N. A.; Grosso-Giordano, N. A.; Lee, S.; Elam, J. W.; Winans, R. E.; Van Duyne, R. P.; Stair, P. C.; Notestein, J. M. Shape-Selective Sieving Layers on an Oxide Catalyst Surface. *Nat. Chem.* **2012**, *4* (12), 1030–1036. https://doi.org/10.1038/nchem.1477.
(204) Grzybek, J.; Roth, W. J.; Gil, B.; Korzeniowska, A.; Mazur, M.; Čejka, J.; Morris, R. E. A New Layered MWW Zeolite Synthesized with the Bifunctional Surfactant Template and the Updated Classification of Layered Zeolite Forms Obtained by Direct Synthesis. *J. Mater. Chem. A* **2019**, *7* (13), 7701–7709. https://doi.org/10.1039/C8TA09826C.
(205) Marshall, S. T.; O'Brien, M.; Oetter, B.; Corpuz, A.; Richards, R. M.; Schwartz, D. K.; Medlin, J. W. Controlled Selectivity for Palladium Catalysts Using Self-Assembled Monolayers. *Nat. Mater.* **2010**, *9* (10), 853–858. https://doi.org/10.1038/nmat2849.
(206) Makosch, M.; Lin, W.-I.; Bumbálek, V.;

Sá, J.; Medlin, J. W.; Hungerbühler, K.; van Bokhoven, J. A. Organic Thiol Modified Pt/TiO2 Catalysts to Control Chemoselective Hydrogenation of Substituted Nitroarenes. *ACS Catal.* **2012**, *2* (10), 2079–2081. https://doi.org/10.1021/cs300378p.

(207) Sanchez, S.; Demain, A. L. Useful Microbial Enzymes-An Introduction. *Biotechnol. Microb. Enzym. Prod. Biocatal. Ind. Appl.* **2017**, 1–11. https://doi.org/10.1016/B978-0-12-803725-6.00001-7.

(208) Bu, Z.; Callaway, D. J. E. Proteins Move! Protein Dynamics and Long-Range Allostery in Cell Signaling. *Adv. Protein Chem. Struct. Biol.* **2011**, *83*, 163–221. https://doi.org/10.1016/B978-0-12-381262-9.00005-7.

(209) Monod, J.; Wyman, J.; Changeux, J. P. On the Nature of Allosteric Transitions: A Plausible Model. *J. Mol. Biol.* **1965**, *12* (1), 88–118. https://doi.org/10.1016/S0022-2836(65)80285-6.

(210) Koshland, D. E.; Némethy, G.; Filmer, D. Comparison of Experimental Binding Data and Theoretical Models in Proteins Containing Subunits*. *Biochemistry* **1966**, *5* (1), 365–385. https://doi.org/10.1021/bi00865a047.

(211) Cuendet, M. A.; Weinstein, H.; LeVine, M. V. The Allostery Landscape: Quantifying Thermodynamic Couplings in Biomolecular Systems. *J. Chem. Theory Comput.* **2016**, *12* (12), 5758–5767. https://doi.org/10.1021/acs.jctc.6b00841.

(212) Campbell, E.; Kaltenbach, M.; Correy, G. J.; Carr, P. D.; Porebski, B. T.; Livingstone, E. K.; Afriat-Jurnou, L.; Buckle, A. M.; Weik, M.; Hollfelder, F.; Tokuriki, N.; Jackson, C. J. The Role of Protein Dynamics in the Evolution of New Enzyme Function. *Nat. Chem. Biol.* **2016**, *12* (11), 944–950. https://doi.org/10.1038/nchembio.2175.

(213) Eisenmesser, E. Z.; Bosco, D. A.; Akke, M.; Kern, D. Enzyme Dynamics during Catalysis. *Science (80-.).* **2002**, *295* (5559), 1520–1523. https://doi.org/10.1126/science.1066176.

(214) Henzler-Wildman, K.; Kern, D. Dynamic Personalities of Proteins. *Nature* **2007**, *450* (7172), 964–972. https://doi.org/10.1038/nature06522.

(215) Henzler-Wildman, K. A.; Thai, V.; Lei, M.; Ott, M.; Wolf-Watz, M.; Fenn, T.; Pozharski, E.; Wilson, M. A.; Petsko, G. A.; Karplus, M.; Hübner, C. G.; Kern, D. Intrinsic Motions along an Enzymatic Reaction Trajectory. *Nature* **2007**, *450* (7171), 838–844. https://doi.org/10.1038/nature06410.

(216) Stiller, J. B.; Jordan Kerns, S.; Hoemberger, M.; Cho, Y.-J.; Otten, R.; Hagan, M. F.; Kern, D. Probing the Transition State in Enzyme Catalysis by High-Pressure NMR Dynamics. *Nat. Catal.* **2019**, *2* (8), 726–734. https://doi.org/10.1038/s41929-019-0307-6.

(217) Min, W.; Xie, X. S.; Bagchi, B. Two-Dimensional Reaction Free Energy Surfaces of Catalytic Reaction: Effects of Protein Conformational Dynamics on Enzyme Catalysis. *J. Phys. Chem. B* **2008**, *112* (2), 454–466. https://doi.org/10.1021/jp076533c.

(218) Kamerlin, S. C. L.; Warshel, A. At the Dawn of the 21st Century: Is Dynamics the Missing Link for Understanding Enzyme Catalysis? *Proteins Struct. Funct. Bioinforma.* **2010**, *78* (6), 1339–1375. https://doi.org/10.1002/prot.22654.

(219) Pisliakov, A. V.; Cao, J.; Kamerlin, S. C. L.; Warshel, A. Enzyme Millisecond Conformational Dynamics Do Not Catalyze the Chemical Step. *Proc. Natl. Acad. Sci. U. S. A.* **2009**, *106* (41), 17359–17364. https://doi.org/10.1073/pnas.0909150106.

(220) McGeagh, J. D.; Ranaghan, K. E.; Mulholland, A. J. Protein Dynamics and Enzyme Catalysis: Insights from Simulations. *Biochim. Biophys. Acta - Proteins Proteomics* **2011**, *1814* (8), 1077–1092. https://doi.org/10.1016/j.bbapap.2010.12.002.

(221) Hohlfeld, J.; Wellershoff, S. S.; Güdde, J.; Conrad, U.; Jähnke, V.; Matthias, E. Electron and Lattice Dynamics Following Optical Excitation of Metals. *Chem. Phys.*

2000, *251* (1–3), 237–258. https://doi.org/10.1016/S0301-0104(99)00330-4.

(222) Zhou, X. L.; Zhu, X. Y.; White, J. M. Photochemistry at Adsorbate/Metal Interfaces. *Surf. Sci. Rep.* **1991**, *13* (3–6), 73–220. https://doi.org/10.1016/0167-5729(91)90009-M.

(223) Zimmermann, F. M.; Ho, W. State Resolved Studies of Photochemical Dynamics at Surfaces. *Surf. Sci. Rep.* **1995**, *22* (4–6), 127–247. https://doi.org/10.1016/0167-5729(96)80001-X.

(224) Ho, W. Femtosecond Laser-Induced Dynamical Quantum Processes on Solid Surfaces (DQPSS). *Surf. Sci.* **1996**, *363* (1–3), 166–178. https://doi.org/10.1016/0039-6028(96)00130-6.

(225) Czyzewski, J. J.; Madey, T. E.; Yates, J. T. Angular Distributions of Electron-Stimulated-Desorption Ions: Oxygen on W(100). *Phys. Rev. Lett.* **1974**, *32* (14), 777–780. https://doi.org/10.1103/PhysRevLett.32.777.

(226) Kale, M. J.; Avanesian, T.; Xin, H.; Yan, J.; Christopher, P. Controlling Catalytic Selectivity on Metal Nanoparticles by Direct Photoexcitation of Adsorbate–Metal Bonds. *Nano Lett.* **2014**, *14* (9), 5405–5412. https://doi.org/10.1021/nl502571b.

(227) Christopher, P.; Xin, H.; Marimuthu, A.; Linic, S. Singular Characteristics and Unique Chemical Bond Activation Mechanisms of Photocatalytic Reactions on Plasmonic Nanostructures. *Nat. Mater.* **2012**, *11* (12), 1044–1050. https://doi.org/10.1038/nmat3454.

(228) Christopher, P.; Xin, H.; Linic, S. Visible-Light-Enhanced Catalytic Oxidation Reactions on Plasmonic Silver Nanostructures. *Nat. Chem.* **2011**, *3* (6), 467–472. https://doi.org/10.1038/nchem.1032.

(229) Kale, M. J.; Avanesian, T.; Christopher, P. Direct Photocatalysis by Plasmonic Nanostructures. *ACS Catal.* **2014**, *4* (1), 116–128. https://doi.org/10.1021/cs400993w.

(230) Aslam, U.; Rao, V. G.; Chavez, S.; Linic, S. Catalytic Conversion of Solar to Chemical Energy on Plasmonic Metal Nanostructures. *Nat. Catal.* **2018**, *1* (9), 656–665. https://doi.org/10.1038/s41929-018-0138-x.

(231) Linic, S.; Aslam, U.; Boerigter, C.; Morabito, M. Photochemical Transformations on Plasmonic Metal Nanoparticles. *Nat. Mater.* **2015**, *14* (6), 567–576. https://doi.org/10.1038/nmat4281.

(232) Seemala, B.; Therrien, A. J.; Lou, M.; Li, K.; Finzel, J. P.; Qi, J.; Nordlander, P.; Christopher, P. Plasmon-Mediated Catalytic O2 Dissociation on Ag Nanostructures: Hot Electrons or Near Fields? *ACS Energy Lett.* **2019**, *4* (8), 1803–1809. https://doi.org/10.1021/acsenergylett.9b00990.

(233) Mukherjee, S.; Zhou, L.; Goodman, A. M.; Large, N.; Ayala-Orozco, C.; Zhang, Y.; Nordlander, P.; Halas, N. J. Hot-Electron-Induced Dissociation of H2 on Gold Nanoparticles Supported on SiO2. *J. Am. Chem. Soc.* **2014**, *136* (1), 64–67. https://doi.org/10.1021/ja411017b.

(234) Mukherjee, S.; Libisch, F.; Large, N.; Neumann, O.; Brown, L. V.; Cheng, J.; Lassiter, J. B.; Carter, E. A.; Nordlander, P.; Halas, N. J. Hot Electrons Do the Impossible: Plasmon-Induced Dissociation of H2 on Au. *Nano Lett.* **2013**, *13* (1), 240–247. https://doi.org/10.1021/nl303940z.

(235) Ro, I.; Sener, C.; Stadelman, T. M.; Ball, M. R.; Venegas, J. M.; Burt, S. P.; Hermans, I.; Dumesic, J. A.; Huber, G. W. Measurement of Intrinsic Catalytic Activity of Pt Monometallic and Pt-MoOx Interfacial Sites over Visible Light Enhanced PtMoOx/SiO2 Catalyst in Reverse Water Gas Shift Reaction. *J. Catal.* **2016**, *344*, 784–794. https://doi.org/10.1016/j.jcat.2016.08.011.

(236) Zhou, L.; Swearer, D. F.; Zhang, C.; Robatjazi, H.; Zhao, H.; Henderson, L.; Dong, L.; Christopher, P.; Carter, E. A.; Nordlander, P.; Halas, N. J. Quantifying Hot Carrier and Thermal Contributions in Plasmonic Photocatalysis. *Science (80-.).* **2018**, *362* (6410), 69–72.

https://doi.org/10.1126/science.aat6967.
(237) Robatjazi, H.; Bao, J. L.; Zhang, M.; Zhou, L.; Christopher, P.; Carter, E. A.; Nordlander, P.; Halas, N. J. Plasmon-Driven Carbon–Fluorine (C(Sp3)–F) Bond Activation with Mechanistic Insights into Hot-Carrier-Mediated Pathways. *Nat. Catal.* **2020**. https://doi.org/10.1038/s41929-020-0466-5.
(238) Gorte, R. J.; Schmidt, L. D. Interactions between NO and CO on Pt(111). *Surf. Sci.* **1981**, *111* (2), 260–278. https://doi.org/10.1016/0039-6028(80)90708-6.
(239) Avanesian, T.; Christopher, P. Adsorbate Specificity in Hot Electron Driven Photochemistry on Catalytic Metal Surfaces. *J. Phys. Chem. C* **2014**, *118* (48), 28017–28031. https://doi.org/10.1021/jp509555m.
(240) Li, K.; Hogan, N. J.; Kale, M. J.; Halas, N. J.; Nordlander, P.; Christopher, P. Balancing Near-Field Enhancement, Absorption, and Scattering for Effective Antenna-Reactor Plasmonic Photocatalysis. *Nano Lett.* **2017**, *17* (6), 3710–3717. https://doi.org/10.1021/acs.nanolett.7b00992.
(241) Wang, J. X.; Springer, T. E.; Liu, P.; Shao, M.; Adzic, R. R. Hydrogen Oxidation Reaction on Pt in Acidic Media: Adsorption Isotherm and Activation Free Energies. *J. Phys. Chem. C* **2007**, *111* (33), 12425–12433. https://doi.org/10.1021/jp073400i.
(242) Watanabe, S.; Inukai, J.; Ito, M. Coverage and Potential Dependent CO Adsorption on Pt(1111), (711) and (100) Electrode Surfaces Studied by Infrared Reflection Absorption Spectroscopy. *Surf. Sci.* **1993**, *293* (1–2), 1–9. https://doi.org/10.1016/0039-6028(93)90237-E.
(243) Wiberg, G. K. H.; Arenz, M. Establishing the Potential Dependent Equilibrium Oxide Coverage on Platinum in Alkaline Solution and Its Influence on the Oxygen Reduction. *J. Power Sources* **2012**, *217*, 262–267. https://doi.org/10.1016/j.jpowsour.2012.06.019.
(244) Bard, A. J.; Faulkner, L. *Electrochemical Methods Fundamentals and Applications*; Wiley, 1980.
(245) Korzeniewski, C.; Pons, S.; Schmidt, P. P.; Severson, M. W. A Theoretical Analysis of the Vibrational Spectrum of Carbon Monoxide on Platinum Metal Electrodes. *J. Chem. Phys.* **1986**, *85* (7), 4153–4160. https://doi.org/10.1063/1.450888.
(246) Korzeniewski, C.; Pons, S. In Situ Infrared Spectroelectrochemistry. *J. Vac. Sci. Technol. B Microelectron. Process. Phenom.* **1985**, *3* (5), 1421–1424. https://doi.org/10.1116/1.583002.
(247) Oklejas, V.; Sjostrom, C.; Harris, J. M. SERS Detection of the Vibrational Stark Effect from Nitrile-Terminated SAMs to Probe Electric Fields in the Diffuse Double-Layer. *J. Am. Chem. Soc.* **2002**, *124* (11), 2408–2409. https://doi.org/10.1021/ja017656s.
(248) Patrow, J. G.; Sorenson, S. A.; Dawlaty, J. M. Direct Spectroscopic Measurement of Interfacial Electric Fields near an Electrode under Polarizing or Current-Carrying Conditions. *J. Phys. Chem. C* **2017**, *121* (21), 11585–11592. https://doi.org/10.1021/acs.jpcc.7b03134.
(249) Lu, G.-Q.; Crown, A.; Wieckowski, A. Formic Acid Decomposition on Polycrystalline Platinum and Palladized Platinum Electrodes. *J. Phys. Chem. B* **1999**, *103* (44), 9700–9711. https://doi.org/10.1021/jp992297x.
(250) Grozovski, V.; Solla-Gullón, J.; Climent, V.; Herrero, E.; Feliu, J. M. Formic Acid Oxidation on Shape-Controlled Pt Nanoparticles Studied by Pulsed Voltammetry. *J. Phys. Chem. C* **2010**, *114* (32), 13802–13812. https://doi.org/10.1021/jp104755b.
(251) Grozovski, V.; Climent, V.; Herrero, E.; Feliu, J. M. Intrinsic Activity and Poisoning Rate for HCOOH Oxidation on Platinum Stepped Surfaces. *Phys. Chem. Chem. Phys.* **2010**, *12* (31), 8822–8831. https://doi.org/10.1039/B925472B.
(252) Grozovski, V.; Climent, V.; Herrero, E.; Feliu, J. M. Intrinsic Activity and Poisoning Rate for HCOOH Oxidation at Pt(100) and Vicinal Surfaces Containing

Monoatomic (111) Steps. *ChemPhysChem* **2009**, *10* (11), 1922–1926. https://doi.org/10.1002/cphc.200900261.

(253) Tsiplakides, D.; Neophytides, S.; Vayenas, C. G. Investigation of Electrochemical Promotion Using Temperature-Programmed Desorption and Work Function Measurements. *Solid State Ionics* **2000**, *136–137*, 839–847. https://doi.org/10.1016/S0167-2738(00)00523-3.

(254) Neophytides, S. G.; Vayenas, C. G. TPD and Cyclic Voltammetric Investigation of the Origin of Electrochemical Promotion in Catalysis. *J. Phys. Chem.* **1995**, *99* (47), 17063–17067. https://doi.org/10.1021/j100047a001.

(255) Linic, S.; Barteau, M. A. On the Mechanism of Cs Promotion in Ethylene Epoxidation on Ag. *J. Am. Chem. Soc.* **2004**, *126* (26), 8086–8087. https://doi.org/10.1021/ja048462q.

(256) Neophytides, S. G.; Vayenas, C. G. The Effect of Catalyst-Electrode Potential and Work Function on the Chemisorptive Bond of Oxygen on Pt Interfaced with YSZ. *Ionics (Kiel).* **1995**, *1* (1), 80–84. https://doi.org/10.1007/BF02426012.

(257) Tsiplakides, D.; Neophytides, S.; Vayenas, C. G. Thermal Desorption Study of Oxygen Adsorption on Pt, Ag & Au Films Deposited on YSZ. *Ionics (Kiel).* **1997**, *3* (3), 201–208. https://doi.org/10.1007/BF02375617.

(258) Neophytides, S. G.; Tsiplakides, D.; Vayenas, C. G. Temperature-Programmed Desorption of Oxygen from Pt Films Interfaced with Y2O3-Doped ZrO2. *J. Catal.* **1998**, *178* (2), 414–428. https://doi.org/10.1006/jcat.1998.2155.

(259) Tsiplakides, D.; Vayenas, C. G. Temperature Programmed Desorption of Oxygen from Ag Films Interfaced with Y2O3-Doped ZrO2. *J. Catal.* **1999**, *185* (2), 237–251. https://doi.org/10.1006/jcat.1999.2522.

(260) Bebelis, S.; Vayenas, C. G. Non-Faradaic Electrochemical Modification of Catalytic Activity. 1. The Case of Ethylene Oxidation on Pt. *J. Catal.* **1989**, *118* (1), 125–146. https://doi.org/10.1016/0021-9517(89)90306-0.

(261) Shockley, W; Pearson, G. L. Surface States and Rectification at Metal Semiconductor Contact. *Phys. Rev* **1948**, *74* (8), 717–727. https://doi.org/10.1103/PhysRev.74.23.

(262) Sze, S.M.; Ng, K. K. *Physics of Semiconductor Devices*, 3rd Editio.; Wiley: New Jersey, 2007.

(263) Zheng, C.; Jin, X.; Li, Y.; Mei, J.; Sun, Y.; Xiao, M.; Zhang, H.; Zhang, Z.; Zhang, G. J. Sensitive Molybdenum Disulfide Based Field Effect Transistor Sensor for Real-Time Monitoring of Hydrogen Peroxide. *Sci. Rep.* **2019**, *9* (1). https://doi.org/10.1038/s41598-018-36752-y.

(264) Wang, Y.; Udyavara, S.; Neurock, M.; Daniel Frisbie, C. Field Effect Modulation of Electrocatalytic Hydrogen Evolution at Back-Gated Two-Dimensional MoS2 Electrodes. *Nano Lett.* **2019**, *19* (9), 6118–6123. https://doi.org/10.1021/acs.nanolett.9b02079.

(265) Wang, Y.; Kim, C. H.; Yoo, Y.; Johns, J. E.; Frisbie, C. D. Field Effect Modulation of Heterogeneous Charge Transfer Kinetics at Back-Gated Two-Dimensional MoS2 Electrodes. *Nano Lett.* **2017**, *17* (12), 7586–7592. https://doi.org/10.1021/acs.nanolett.7b03564.

(266) Kim, C. H.; Frisbie, C. D. Field Effect Modulation of Outer-Sphere Electrochemistry at Back-Gated, Ultrathin ZnO Electrodes. *J. Am. Chem. Soc.* **2016**, *138* (23), 7220–7223. https://doi.org/10.1021/jacs.6b02547.

(267) Stallinga, P.; Roy, V. A. L.; Xu, Z. X.; Xiang, H. F.; Che, C. M. Metal-Insulator-Metal Transistors. *Adv. Mater.* **2008**, *20* (11), 2120–2124. https://doi.org/10.1002/adma.200702525.

(268) Yajima, T.; Oike, G.; Nishimura, T.; Toriumi, A. Independent Control of Phases and Defects in TiO2 Thin Films for Functional Transistor Channels. *Phys. Status Solid Appl. Mater. Sci.* **2016**, *213* (8), 2196–2202. https://doi.org/10.1002/pssa.201600006.

(269) Wu, Y.; Ringe, S.; Wu, C. L.; Chen, W.;

Yang, A.; Chen, H.; Tang, M.; Zhou, G.; Hwang, H. Y.; Chan, K.; Cui, Y. A Two-Dimensional MoS2 Catalysis Transistor by Solid-State Ion Gating Manipulation and Adjustment (SIGMA). *Nano Lett.* **2019**, *19* (10), 7293–7300. https://doi.org/10.1021/acs.nanolett.9b02888.

(270) Yamazoe, N.; Shimanoe, K. Fundamentals of Semiconductor Gas Sensors. In *Semiconductor Gas Sensors*; Elsevier, 2019; pp 3–38. https://doi.org/10.1016/B978-0-08-102559-8.00001-X.

(271) Poghossian, A.; Abouzar, M. H.; Sakkari, M.; Kassab, T.; Han, Y.; Ingebrandt, S.; Offenhäusser, A.; Schöning, M. J. Field-Effect Sensors for Monitoring the Layer-by-Layer Adsorption of Charged Macromolecules. *Sensors Actuators, B Chem.* **2006**, *118* (1–2), 163–170. https://doi.org/10.1016/j.snb.2006.04.013.

(272) Hong, S.; Hong, Y.; Jeong, Y.; Jung, G.; Shin, W.; Park, J.; Lee, J. K.; Jang, D.; Bae, J. H.; Lee, J. H. Improved CO Gas Detection of Si MOSFET Gas Sensor with Catalytic Pt Decoration and Pre-Bias Effect. *Sensors Actuators, B Chem.* **2019**, *300*. https://doi.org/10.1016/j.snb.2019.127040.

(273) Seo, G.; Lee, G.; Kim, M. J.; Baek, S. H.; Choi, M.; Ku, K. B.; Lee, C. S.; Jun, S.; Park, D.; Kim, H. G.; Kim, S. J.; Lee, J. O.; Kim, B. T.; Park, E. C.; Kim, S. Il. Rapid Detection of COVID-19 Causative Virus (SARS-CoV-2) in Human Nasopharyngeal Swab Specimens Using Field-Effect Transistor-Based Biosensor. *ACS Nano* **2020**, *14* (4), 5135–5142. https://doi.org/10.1021/acsnano.0c02823.

(274) Yan, M.; Pan, X.; Wang, P.; Chen, F.; He, L.; Jiang, G.; Wang, J.; Liu, J. Z.; Xu, X.; Liao, X.; Yang, J.; Mai, L. Field-Effect Tuned Adsorption Dynamics of VSe2 Nanosheets for Enhanced Hydrogen Evolution Reaction. *Nano Lett.* **2017**, *17* (7), 4109–4115. https://doi.org/10.1021/acs.nanolett.7b00855.

(275) Che, F.; Ha, S.; McEwen, J. S. Elucidating the Field Influence on the Energetics of the Methane Steam Reforming Reaction: A Density Functional Theory Study. *Appl. Catal. B Environ.* **2016**, *195*, 77–89. https://doi.org/10.1016/j.apcatb.2016.04.026.

(276) Shetty, M.; Ardagh, M. A.; Pang, Y.; Abdelrahman, O. A.; Dauenhauer, P. J. Electric-Field Assisted Modulation of Surface Thermochemistry. *ChemRxiv* **2020**. https://doi.org/10.26434/chemrxiv.12127191.v1.

(277) Chen, L. D.; Urushihara, M.; Chan, K.; Nørskov, J. K. Electric Field Effects in Electrochemical CO2 Reduction. *ACS Catal.* **2016**, *6* (10), 7133–7139. https://doi.org/10.1021/acscatal.6b02299.

(278) Liu, X.; Xiao, J.; Peng, H.; Hong, X.; Chan, K.; Nørskov, J. K. Understanding Trends in Electrochemical Carbon Dioxide Reduction Rates. *Nat. Commun.* **2017**, *8*. https://doi.org/10.1038/ncomms15438.

(279) Dickens, C. F.; Kirk, C.; Nørskov, J. K. Insights into the Electrochemical Oxygen Evolution Reaction with Ab Initio Calculations and Microkinetic Modeling: Beyond the Limiting Potential Volcano. *J. Phys. Chem. C* **2019**, *123* (31), 18960–18977. https://doi.org/10.1021/acs.jpcc.9b03830.

(280) Lines, M. E.; Glass, A. M. Principles and Applications of Ferroelectrics and Related Materials. *Princ. Appl. Ferroelectr. Relat. Mater.* **2010**. https://doi.org/10.1093/acprof:oso/9780198507789.001.0001.

(281) Kakekhani, A.; Ismail-Beigi, S.; Altman, E. I. Ferroelectrics: A Pathway to Switchable Surface Chemistry and Catalysis. *Surf. Sci.* **2016**, *650*, 302–316. https://doi.org/10.1016/j.susc.2015.10.055.

(282) Parravano, G. Ferroelectric Transitions and Heterogenous Catalysis. *J. Chem. Phys.* **1952**, *20* (2), 342–343. https://doi.org/10.1063/1.1700412.

(283) Inoue, Y.; Watanabe, Y. Use of LINbO3 for Design of Device-Type Catalysts with Activity Controllable Functions. *Catal. Today* **1993**, *16* (3–4), 487–494. https://doi.org/10.1016/0920-5861(93)80089-J.

(284) Park, C.; Baker, R. T. K. Induction of an

Electronic Perturbation in Supported Metal Catalysts. *J. Phys. Chem. B* **2000**, *104* (18), 4418–4424. https://doi.org/10.1021/jp993219c.

(285) Garrity, K.; Kolpak, A. M.; Ismail-Beigi, S.; Altman, E. I. Chemistry of Ferroelectric Surfaces. *Adv. Mater.* **2010**, *22* (26–27), 2969–2973. https://doi.org/10.1002/adma.200903723.

(286) Kakekhani, A.; Ismail-Beigi, S. Polarization-Driven Catalysis: Via Ferroelectric Oxide Surfaces. *Phys. Chem. Chem. Phys.* **2016**, *18* (29), 19676–19695. https://doi.org/10.1039/c6cp03170f.

(287) Uchino, K. *Ferroelectric Devices*, 2nd ed.; CRC Press, 2018. https://doi.org/10.1201/b15852.

(288) Li, D.; Zhao, M. H.; Garra, J.; Kolpak, A. M.; Rappe, A. M.; Bonnell, D. A.; Vohs, J. M. Direct in Situ Determination of the Polarization Dependence of Physisorption on Ferroelectric Surfaces. *Nat. Mater.* **2008**, *7* (6), 473–477. https://doi.org/10.1038/nmat2198.

(289) Kolpak, A. M.; Grinberg, I.; Rappe, A. M. Polarization Effects on the Surface Chemistry of PbTiO3-Supported Pt Films. *Phys. Rev. Lett.* **2007**, *98* (16), 3–6. https://doi.org/10.1103/PhysRevLett.98.166101.

(290) Balachandran, P. V.; Xue, D.; Lookman, T. Structure-Curie Temperature Relationships in BaTiO3 -Based Ferroelectric Perovskites: Anomalous Behavior of (Ba,Cd)TiO3 from DFT, Statistical Inference, and Experiments. *Phys. Rev. B* **2016**, *93* (14), 1–12. https://doi.org/10.1103/PhysRevB.93.144111.

(291) Bhide, V. G.; Deshmukh, K. G.; Hegde, M. S. Ferroelectric Properties of PbTiO3. *Physica* **1962**, *28* (9), 871–876. https://doi.org/10.1016/0031-8914(62)90075-7.

(292) Warlimont, H.; Martienssen, W. Springer Handbook of Materials Data. **2018**, 1140. https://doi.org/10.1007/978-3-319-69743-7.

(293) Kakekhani, A.; Ismail-Beigi, S. Ferroelectric-Based Catalysis: Switchable Surface Chemistry. *ACS Catal.* **2015**, *5* (8), 4537–4545. https://doi.org/10.1021/acscatal.5b00507.

(294) Park, J. Y.; Renzas, J. R.; Contreras, A. M.; Somorjai, G. A. The Genesis and Importance of Oxide–Metal Interface Controlled Heterogeneous Catalysis; the Catalytic Nanodiode. *Top. Catal.* **2007**, *46* (1–2), 217–222. https://doi.org/10.1007/s11244-007-0331-7.

(295) Somorjai, G. A. The Catalytic Nanodiode. Its Role in Catalytic Reaction Mechanisms in a Historical Perspective. *Catal. Letters* **2005**, *101* (1–2), 1–3. https://doi.org/10.1007/s10562-005-0112-5.

(296) Somorjai, G. A.; Tao, F.; Park, J. Y. The Nanoscience Revolution: Merging of Colloid Science, Catalysis and Nanoelectronics. *Top. Catal.* **2008**, *47* (1–2), 1–14. https://doi.org/10.1007/s11244-007-9028-1.

(297) Kasap, S. O. *Principles of Electronic Materials and Devices*, 4th ed.; McGraw Hill: New York, 2018.

(298) Tung, R. T. Chemical Bonding and Fermi Level Pinning at Metal-Semiconductor Interfaces. *Phys. Rev. Lett.* **2000**, *84* (26), 7068–6081. https://doi.org/10.1103/PhysRevLett.84.6078.

(299) Lechuga, L. M.; Calle, A.; Golmayo, D.; Briones, F. Different Catalytic Metals (Pt, Pd and Ir) for GaAs Sqhottky Barrier Sensors. *Sensors and Actuators* **1992**, *7* (1–3), 614–618. https://doi.org/10.1016/0925-4005(92)80374-7.

(300) Ji, X. Z.; Somorjai, G. A. Continuous Hot Electron Generation in Pt/TiO 2, Pd/TiO 2, and Pt/GaN Catalytic Nanodiodes from Oxidation of Carbon Monoxide. *J. Phys. Chem. B* **2005**, *109* (47), 22530–22535. https://doi.org/10.1021/jp054163r.

(301) Uneus, L.; Tobias, P.; Lundstrom, I.; Spetz, A. L. Schottky Diodes with Thin Catalytic Gate Metals for Potential Use as Ammonia Sensors for Exhaust Gases. *Sensors Mater.* **1999**, *11* (5), 305–318.

(302) Park, J. Y.; Somorjai, G. A. Energy Conversion from Catalytic Reaction to Hot Electron Current with Metal-Semiconductor Schottky Nanodiodes. *J.*

Vac. Sci. Technol. B Microelectron. Nanom. Struct. **2006**, *24* (4), 1967–1971. https://doi.org/10.1116/1.2218861.

(303) Deshlahra, P.; Pfeifer, K.; Bernstein, G. H.; Wolf, E. E. CO Adsorption and Oxidation Studies on Nanofabricated Model Catalysts Using Multilayer Enhanced IRAS Technique. *Appl. Catal. A Gen.* **2011**, *391* (1–2), 22–30. https://doi.org/10.1016/j.apcata.2010.07.026.

(304) Park, J. Y.; Somorjai, G. A. The Catalytic Nanodiode: Detecting Continous Electron Flow at Oxide-Metal Interfaces Generated by a Gas-Phase Exothermic Reaction. *ChemPhysChem* **2006**, *7* (7), 1409–1413. https://doi.org/10.1002/cphc.200600056.

(305) Ji, X.; Zuppero, A.; Gidwani, J. M.; Somorjai, G. A. The Catalytic Nanodiode: Gas Phase Catalytic Reaction Generated Electron Flow Using Nanoscale Platinum Titanium Oxide Schottky Diodes. *Nano Lett.* **2005**, *5* (4), 753–756. https://doi.org/10.1021/nl050241a.

(306) Park, J. Y.; Lee, H.; Renzas, J. R.; Zhang, Y.; Somorjai, G. A. Probing Hot Electron Flow Generated on Pt Nanoparticles with Au/TiO 2 Schottky Diodes during Catalytic CO Oxidation. *Nano Lett.* **2008**, *8* (8), 2388–2392. https://doi.org/10.1021/nl8012456.

(307) Deshlahra, P.; Schneider, W. F.; Bernstein, G. H.; Wolf, E. E. Direct Control of Electron Transfer to the Surface-CO Bond on a Pt/TiO 2 Catalytic Diode. *J. Am. Chem. Soc.* **2011**, *133* (41), 16459–16467. https://doi.org/10.1021/ja2020789.

(308) Baker, L. R.; Hervier, A.; Kennedy, G.; Somorjai, G. A. Solid-State Charge-Based Device for Control of Catalytic Carbon Monoxide Oxidation on Platinum Nanofilms Using External Bias and Light. *Nano Lett.* **2012**, *12* (5), 2554–2558. https://doi.org/10.1021/nl3007787.

(309) Wilamowski, B. M. Schottky Diodes with High Breakdown Voltages. *Solid-State Electron* **1983**, *26* (5), 491493. https://doi.org/10.1016/0038-1101(83)90106-5.

(310) Yang, J.; Ahn, S.; Ren, F.; Pearton, S. J.; Jang, S.; Kim, J.; Kuramata, A. High Reverse Breakdown Voltage Schottky Rectifiers without Edge Termination on Ga2O3. *Appl. Phys. Lett.* **2017**, *110* (19). https://doi.org/10.1063/1.4983203.

(311) Liu, F.; Xue, T.; Wu, C.; Yang, S. Coadsorption of CO and O over Strained Metal Surfaces. *Chem. Phys. Lett.* **2019**, *722*, 18–25. https://doi.org/10.1016/j.cplett.2019.03.010.

(312) Ford, D. C.; Xu, Y.; Mavrikakis, M. Atomic and Molecular Adsorption on Pt(1 1 1). *Surf. Sci.* **2005**, *587* (3), 159–174. https://doi.org/10.1016/j.susc.2005.04.028.

(313) Herron, J. A.; Tonelli, S.; Mavrikakis, M. Atomic and Molecular Adsorption on Pd(111). *Surf. Sci.* **2012**, *606* (21–22), 1670–1679. https://doi.org/10.1016/j.susc.2012.07.003.

(314) Santiago-Rodríguez, Y.; Herron, J. A.; Curet-Arana, M. C.; Mavrikakis, M. Atomic and Molecular Adsorption on Au(111). *Surf. Sci.* **2014**, *627*, 57–69. https://doi.org/10.1016/j.susc.2014.04.012.

(315) Krekelberg, W. P.; Greeley, J.; Mavrikakis, M. Atomic and Molecular Adsorption on Ir(111). *J. Phys. Chem. B* **2004**, *108* (3), 987–994. https://doi.org/10.1021/jp035786c.

(316) Chen, B. W. J.; Kirvassilis, D.; Bai, Y.; Mavrikakis, M. Atomic and Molecular Adsorption on Ag(111). *J. Phys. Chem. C* **2019**, *123* (13), 7551–7566. https://doi.org/10.1021/acs.jpcc.7b11629.

(317) Bai, Y.; Kirvassilis, D.; Xu, L.; Mavrikakis, M. Atomic and Molecular Adsorption on Ni(111). *Surf. Sci.* **2019**, *679*, 240–253. https://doi.org/10.1016/j.susc.2018.08.004.

(318) Che, F.; Gray, J. T.; Ha, S.; McEwen, J. S. Improving Ni Catalysts Using Electric Fields: A DFT and Experimental Study of the Methane Steam Reforming Reaction. *ACS Catal.* **2017**, *7* (1), 551–562. https://doi.org/10.1021/acscatal.6b02318.

(319) Moulijn, J. A.; Van Diepen, A. E.; Kapteijn, F. Catalyst Deactivation: Is It Predictable? What to Do? *Appl. Catal. A Gen.* **2001**, *212*, 3–16. https://doi.org/10.1016/S0926-860X(00)00842-5.

(320) Bartholomew, C. H. Mechanisms of Catalyst Deactivation. *Appl. Catal. A Gen.* **2001**, *212*, 17–60. https://doi.org/10.1016/S0926-860X(00)00843-7.
(321) Mao, Z.; Campbell, C. T. Apparent Activation Energies in Complex Reaction Mechanisms: A Simple Relationship via Degrees of Rate Control. *ACS Catal.* **2019**, *9* (10), 9465–9473. https://doi.org/10.1021/acscatal.9b02761.
(322) Nørskov, J. K.; Bligaard, T.; Logadottir, A.; Kitchin, J. R.; Chen, J. G.; Pandelov, S.; Stimming, U. Trends in the Exchange Current for Hydrogen Evolution. *J. Electrochem. Soc.* **2005**, *152* (3), J23. https://doi.org/10.1149/1.1856988.
(323) Man, I. C.; Su, H. Y.; Calle-Vallejo, F.; Hansen, H. A.; Martínez, J. I.; Inoglu, N. G.; Kitchin, J.; Jaramillo, T. F.; Nørskov, J. K.; Rossmeisl, J. Universality in Oxygen Evolution Electrocatalysis on Oxide Surfaces. *ChemCatChem* **2011**, *3* (7), 1159–1165. https://doi.org/10.1002/cctc.201000397.
(324) Latimer, A. A.; Kakekhani, A.; Kulkarni, A. R.; Nørskov, J. K. Direct Methane to Methanol: The Selectivity-Conversion Limit and Design Strategies. *ACS Catal.* **2018**, *8* (8), 6894–6907. https://doi.org/10.1021/acscatal.8b00220.
(325) Foster, S. L.; Bakovic, S. I. P.; Duda, R. D.; Maheshwari, S.; Milton, R. D.; Minteer, S. D.; Janik, M. J.; Renner, J. N.; Greenlee, L. F. Catalysts for Nitrogen Reduction to Ammonia. *Nat. Catal.* **2018**, *1* (7), 490–500. https://doi.org/10.1038/s41929-018-0092-7.